

Supporting information for:

A neutral cyclic aluminium (I) trimer

Imogen Squire[‡], Matthew de Vere-Tucker[‡], Michelangelo Tritto, Lygia Silva de Moraes, Tobias
Krämer* and Clare Bakewell*

[‡]Authors contributed equally

Table of contents

- 1. General Experimental Section**
- 2. Synthetic Procedures**
- 3. Supporting Figures**
- 4. X-ray Crystallographic Data**
- 5. Computational Details**
- 6. Multinuclear NMR Data**
- 7. References**

1. General Experimental Section

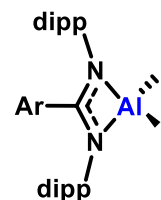
All manipulations were carried out using standard Schlenk-line and glovebox techniques under an inert atmosphere. An MBraun Labmaster glovebox with an atmosphere of N₂ was employed, operating at < 0.1 ppm O₂ and < 0.1 ppm H₂O. Glassware was dried for at least 12 h at 125 °C prior to use. Toluene and hexane were dried over activated alumina from an SPS (solvent purification system) based upon the Grubbs design, pentane was distilled over CaH₂ and all solvents were stored over activated 3 Å molecular sieves and degassed via the freeze-pump-thaw method prior to use. Benzene-*d*₆ and cyclohexane-*d*₆ were purchased dry and stored over activated 3 Å molecular sieves. Ethene gas was purchased from CK isotopes. Dihydrogen gas was obtained from a PEAK Scientific hydrogen generator. NMR-scale reactions were conducted in J Young tap tubes and prepared in a glovebox. NMR tubes were heated using a DrySyn NMR tube heating block or a Julabo Corio CD-BC4 oil bath. Capillary internal standards of mesitylene in benzene-*d*₆ and cyclohexane-*d*₆ were used to obtain NMR yields where appropriate. ¹H (tetramethylsilane; 0 ppm) and ¹³C (tetramethylsilane; 0 ppm) NMR spectra were obtained on BRUKER 400 MHz, 700 MHz or 800 MHz (with cryoprobe) instruments; all chemical shift values are quoted in ppm. Data was processed using MestReNova software. Elemental analysis was conducted by Orfhlait McCullough at London Metropolitan University and has been obtained to the best of our abilities given the extremely air and moisture sensitive nature of the compounds. UV spectra were acquired using an Agilent Cary100 UV-Vis spectrometer. EPR spectra were obtained using a Magnettech ESR5000 at the PEPR facility (Imperial College London). Aluminium dihydride complexes, compounds **II**, **A**, [(^{Mes}BDIMg)₂], and ^{dipp/p-tol}AlAlMe₂ were synthesised *via* modified literature procedures.^{1–5}

2. Synthetic procedures

Precursor synthesis

Compound 1

Aluminium dihydride complex (1 equiv.) was dissolved in hexane (20 mL) and a solution of iodine (1 equiv.) in hexane was added dropwise with stirring until suspension remained light yellow. The mixture was then stirred for a further hour, during which time the colour disappeared. The solvent was removed *in vacuo* and the solid crystallised from toluene, giving the product as a colourless crystalline solid.



1^{p-tol}

600 mg aluminium dihydride, 315.5 mg iodine, yield: 687.2 mg (75%). Isolated as powder, washed with hexane.

¹H NMR (400 MHz, benzene-*d*₆, 298 K): δ_{H} 0.89 (d, 12H, CH(CH₃)₂, ³*J*_{HH} = 6.8 Hz), 1.38 (d, 12H, CH(CH₃)₂, ³*J*_{HH} = 6.8 Hz), 1.58 (s, 3H, *p*-CH₃), 3.72 (hept, 4H, CH(CH₃)₂, ³*J*_{HH} = 6.8 Hz), 6.32 (d, 2H, *p*-tol-*m*-H, ³*J*_{HH} = 8.1 Hz), 6.95 – 7.04 (m, ArH, 6H), 7.05 – 7.10 (m, ArH, 2H). **¹³C{¹H} NMR** (101 MHz, benzene-*d*₆, 298 K): δ_{C} 21.0 (*p*-CH₃), 23.1 (CH(CH₃)₂), 27.3 (CH(CH₃)₂), 29.1 (CH(CH₃)₂), 124.7 (ArC), 127.5 (ArC), 129.0 (ArC), 131.0 (ArC), 135.9 (C^{IV}), 143.3 (C^{IV}-*p*-CH₃), 144.6 (C^{IV}), 176.9 (NC(Ar)N).

Elemental analysis calculated for C₃₂H₄₁AlI₂N₄: C, 52.33; H, 5.63; N, 3.81. Found: C, 52.98; H, 5.71; N, 3.74.

1^{m-xyl}

591 mg aluminium dihydride, 293.2 mg iodine, yield: 542.4 mg (63%).

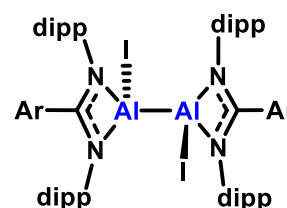
¹H NMR (400 MHz, benzene-*d*₆, 298 K): δ_{H} 0.92 (d, 12H, CH(CH₃)₂, ³*J*_{HH} = 6.8 Hz), 1.38 (d, 12H, CH(CH₃)₂, ³*J*_{HH} = 6.7 Hz), 1.70 (dd, 6H, *m*-Xyl-CH₃, ⁴*J*_{HH} = 0.7 Hz), 3.72 (hept, 4H, CH(CH₃)₂, ³*J*_{HH} = 6.8 Hz), 6.41 (dq, 1H, *m*-Xyl-*p*-H, ³*J*_{HH} = 0.8, 1.6 Hz), 6.75 – 6.81 (qd, 2H, *m*-Xyl-*o*-H, ³*J*_{HH} = 1.6, 0.8 Hz), 6.95 – 7.09 (m, 6H, ArH). **¹³C{¹H} NMR** (101 MHz, benzene-*d*₆, 298 K): δ_{C} 20.7 (*m*-Xyl-CH₃), 23.1 (CH(CH₃)₂), 27.4 (CH(CH₃)₂), 29.1 (CH(CH₃)₂), 124.5 (ArC), 127.5 (*m*-Xyl-C), 128.9 (*m*-Xyl-C), 133.6 (*m*-Xyl-C), 135.8 (ArC), 138.0 (ArC), 144.7 (ArC), 177.5 (NC(Ar)N).

Elemental analysis calculated for C₃₃H₄₃AlI₂N₂·0.1(C₇H₈): C 53.42, H 5.83, N 3.70. Found: C 53.79, H 6.05, N 3.43

Compound 5

Route 1: Potassium (1 equiv.) and **1^{p-tol}** (1 equiv.) were stirred vigorously in hexane (15 mL) for 8 days. The solvent was removed *in vacuo* and the product was extracted into toluene, then recrystallised at –30 °C. The product was isolated as a colourless crystalline solid.*

Route 2: To a J Young NMR tube charged with a solution of **1** (2 equiv.) in benzene-*d*₆ (0.6 mL) was added **II** (1 equiv.). The resultant solution was heated to 80 °C for 3 hours and allowed to cool slowly to room temperature. The solution was decanted, affording **5** as colourless crystals suitable for single-crystal X-ray diffraction.



*The low solubility of **5^{p-tol}** in hexane, toluene and benzene makes isolating the product from the finely divided KI challenging, decreasing the isolated yield.

5^{p-tol}

Route 1: 5 mg potassium, 100 mg **1^{p-tol}**, yield 10.5 mg (13%).

Route 2: 97.5 mg **1^{p-tol}**, 29 mg **II**, yield 42.6 mg (68%).

¹H NMR (400 MHz, benzene-*d*₆, 298 K): δ_{H} 1.02 (d, 12H, CH(CH₃)₂, ³*J*_{HH} = 6.8 Hz), 1.06 (d, 12H, CH(CH₃)₂, ³*J*_{HH} = 6.8 Hz), 1.11 (d, 12H, CH(CH₃)₂, ³*J*_{HH} = 6.8 Hz), 1.57 (s, 6H, *p*-CH₃), 1.59 (d, 12H, CH(CH₃)₂, ³*J*_{HH} = 6.8 Hz), 4.00 (hept, 4H, CH(CH₃)₂, ³*J*_{HH} = 6.8 Hz), 4.10 (hept, 4H, CH(CH₃)₂, ³*J*_{HH} = 6.8 Hz), 6. (d, 4H, *p*-tol-*m*-H, ³*J*_{HH} = 8.0 Hz), 6.96 (m, ArH, 4H), 7.02 – 7.11 (m, ArH, 12H). **¹³C NMR** (101 MHz, benzene-*d*₆, 298 K): δ_{C} 20.9 (*p*-CH₃), 23.2 (CH(CH₃)₂), 23.9 (CH(CH₃)₂), 26.9 (CH(CH₃)₂), 27.5 (CH(CH₃)₂), 28.7 (CH(CH₃)₂), 28.8 (CH(CH₃)₂), 124.4 (ArC), 124.6 (ArC), 126.1 (ArC), 126.9 (ArC), 128.6 (ArC), 130.8 (ArC), 137.8 (C^V), 141.9 (C^V), 144.1 (C^V), 145.3 (C^V), 172.5 (C^V-*p*-CH₃), 175.2 (NC(Ar)N).

5^{m-xy}

Route 2: 10 mg **1^{m-xy}**, 2.7 mg **II**, yield 5 mg (65%).

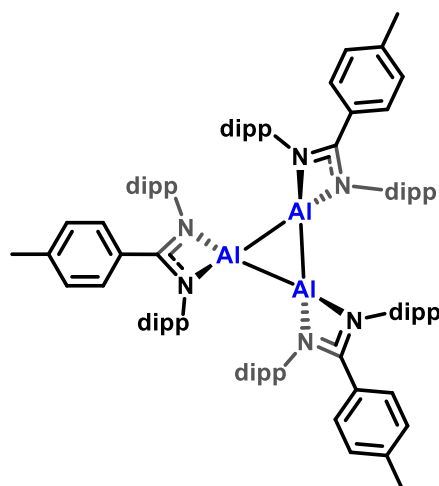
¹H NMR (400 MHz, benzene-*d*₆, 298 K): δ_{H} 1.04 (d, 12H, CH(CH₃)₂, ³*J*_{HH} = 6.7 Hz), 1.11 (d, 12H, CH(CH₃)₂, ³*J*_{HH} = 6.8 Hz), 1.12 (d, 12H, CH(CH₃)₂, ³*J*_{HH} = 6.8 Hz), 1.60 (d, 12H, CH(CH₃)₂, ³*J*_{HH} = 6.6 Hz), 1.71 (s, 12H *m*-Xyl-CH₃), 4.02 (hept, 4H, CH(CH₃)₂), 4.10 (hept, 4H, CH(CH₃)₂), 6.37 (s, 2H, *m*-Xyl-*p*-H), 6.85 (d, 4H, *m*-Xyl-*o*-H, ⁴*J*_{HH} = 1.6 Hz), 6.93 (dd, ArH, 4H), 7.00 – 7.08 (m, ArH, 8H). **¹³C{¹H} NMR** (101 MHz, benzene-*d*₆, 353 K) δ 20.6 (*m*-Xyl-CH₃), 23.2(CH(CH₃)₂), 23.8(CH(CH₃)₂), 27.1(CH(CH₃)₂), 27.7(CH(CH₃)₂), 28.7 (CH(CH₃)₂), 28.8 (CH(CH₃)₂), 124.4 (ArC), 124.4 (ArC), 126.8 (ArC), 128.9 (ArC), 132.6 (ArC), 137.4 (ArC), 138.0 (ArC), 144.5 (ArC), 145.7 (ArC), 175.8 (NC(Ar)N).

Synthesis of compound **2^{p-tol} and **2^{m-xy}** (cyclotrialumanes)**

2^{p-tol}

Route 1: Aluminium diiodide **1^{p-tol}** (200 mg, 0.27 mmol) and potassium (42 mg, 1.1 mmol) were stirred vigorously in pentane (15 mL) for 24 hours[†], during which time the solution turned dark red-black (Figure S 2). The mixture was filtered and stored at –30 °C overnight, affording the product as a black crystalline solid (37.8 mg, 29 %).

Further crops were obtained by concentrating and cooling the filtrate to –30 °C, although these are contaminated with a mixture of **5^{p-tol}** and **A**. The yield of total crude material is generally around 60%, and several small crystalline crops of **2^{p-tol}** can be obtained from this in varying yields. Doing the reactions on smaller scale (100 mg) leads to higher yields, likely due to the low solubility of **5^{p-tol}** limiting reaction efficiency on larger scale. This could be surmounted by working at higher dilution.



†As the reduction is heterogeneous, the rate of reaction depends on the efficiency of stirring and consequently reaction times can vary.⁶ Generally, the rate of reduction of **1^{m-xyI}** is faster than **1^{p-tol}** (reactions generally complete at 16 hours and 24 hours respectively from ¹H NMR of aliquots). However, the first reduction product (**5^{m-xyI/p-tol}**) is essentially insoluble in the reaction solvent so it is difficult to determine when this has been fully consumed by aliquot.

Route 2: Compound **II** (4.3 mg, 0.009 mmol) and compound **A** (9.4 mg, 0.009 mmol) were combined in cyclohexane-*d*₁₂ (0.6 mL) and heated at 80 °C for 1 hour, at which point a mixture of all four species were observed in solution (Figure S 11). The resonances of **2^{p-tol}** match those observed when synthesised independently *via* route 1, but it does not appear possible to push the equilibrium of the reaction far enough to allow isolation of the products.

¹H NMR (400 MHz, benzene-*d*₆, 298 K): δ_H 0.43 (d, 18H, CH(CH)₃, ³J_{HH} = 6.8 Hz), 0.44 (d, 18H, CH(CH)₃, ³J_{HH} = 6.8 Hz), 1.37 (d, 18H, CH(CH)₃, ³J_{HH} = 6.8 Hz), 1.56 (d, 18H, CH(CH)₃, ³J_{HH} = 6.8 Hz), 1.66 (s, 9H, *p*-CH₃), 3.33 (hept, 6H, CH(CH₃)₂, ³J_{HH} = 6.8 Hz), 4.01 (hept, 6H, CH(CH₃)₂, ³J_{HH} = 6.8 Hz), 6.42 (d, 6H, ArH, ³J_{HH} = 8.1 Hz), 6.98 – 7.07 (m, 12H, ArH), 7.08 – 7.15 (m, 12H, ArH). **¹³C{¹H} NMR** (101 MHz, benzene-*d*₆, 298 K): δ_C 21.0 (*p*-CH₃), 23.1 (CH(CH₃)₂), 23.3 (CH(CH₃)₂), 24.0 (CH(CH₃)₂), 28.0 (CH(CH₃)₂), 28.6 (CH(CH₃)₂), 29.1 (CH(CH₃)₂), 123.4 (CH), 124.4 (CH), 125.4 (CH), 128.5 (CH), 131.4 (CH), 140.1 (C^{IV}), 140.7 (C^{IV}), 143.7 (C^{IV}), 144.7 (C^{IV}), 164.7 (NC(Ar)N).

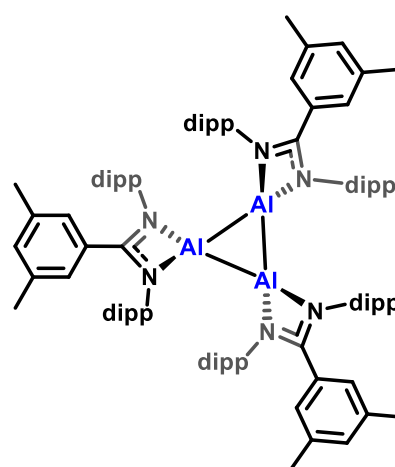
¹H NMR (400 MHz, cyclohexane-*d*₁₂, 298 K): δ_H 0.06 (d, 18H, CH(CH)₃, ³J_{HH} = 6.8 Hz), 0.15 (d, 18H, CH(CH)₃, ³J_{HH} = 6.8 Hz), 1.03 (d, 18H, CH(CH)₃, ³J_{HH} = 6.8 Hz), 1.27 (d, 18H, CH(CH)₃, ³J_{HH} = 6.8 Hz), 2.02 (s, 9H, *p*-CH₃), 3.00 (hept, 6H, CH(CH₃)₂, ³J_{HH} = 6.8 Hz), 3.66 (hept, 6H, CH(CH₃)₂, ³J_{HH} = 6.8 Hz), 6.59 (d, 6H, ArH, ³J_{HH} = 8.2 Hz), 6.73 – 6.77 (m, 6H, ArH), 6.79-6.83 (m, 6H, ArH), 6.87 – 6.94 (m, 12H, ArH). **¹³C{¹H} NMR** (101 MHz, cyclohexane-*d*₁₂, 298 K): δ_C 21.3 (*p*-CH₃), 22.9 (CH(CH₃)₂), 23.3 (CH(CH₃)₂), 24.1 (CH(CH₃)₂), 28.2 (CH(CH₃)₂), 28.8 (CH(CH₃)₂), 29.2 (CH(CH₃)₂), 123.5 (CH), 124.4 (CH), 125.4 (CH), 127.9 (CH), 128.5 (CH), 132.0 (CH), 139.9 (C^{IV}), 140.9 (C^{IV}), 143.8 (C^{IV}), 145.0 (C^{IV}), 164.7 (NC(Ar)N).

UV/Vis (cyclohexane): λ_{max} 434 nm and 311 nm.

2^{m-xyI}

A vial charged with aluminium diiodide complex **1^{m-xyI}** (1 equiv.), finely divided potassium (4 equiv.) and hexane (*ca.* 15 mL) was vigorously stirred at room temperature for 16 hours, affording a deep red-black solution. The mixture was allowed to settle, filtered, concentrated and stored at -40 °C overnight to afford **2^{m-xyI}** as a black crystalline solid. Further crops were obtained by the same method to afford pure **2^{m-xyI}** (54 mg, 82%).

The yield of total crude material is as high as 95%, although in all cases crystalline crops were used for onward reactivity.



¹H NMR (400 MHz, benzene-*d*₆, 298 K): δ_H 0.38 (d, CH(CH)₃, ³J_{HH} = 6.7 Hz, 18H), 0.46 (d, CH(CH)₃, ³J_{HH} = 6.8 Hz, 18H), 1.38 (d, CH(CH)₃, ³J_{HH} = 6.8 Hz, 18H), 1.57 (d, CH(CH)₃, ³J_{HH} = 6.6 Hz, 18H), 1.80 (s, *m*Xyl-*m*-CH₃, 18H), 3.33 (hept, CH(CH₃)₂, ³J_{HH} = 6.3 Hz, 6H), 4.00 (hept, CH(CH₃)₂, ³J_{HH} = 6.8 Hz, 6H), 6.44 (s, *m*Xyl-*p*-H, 3H), 6.79 (s, *m*Xyl-*o*-H, 6H), 6.98 (dd, *Ar*H, *J* = 2.2, 7.1 Hz, 6H), 7.06 – 7.13 (m, *Ar*H, 12H). **¹³C{¹H} NMR** (101 MHz, benzene-*d*₆, 298 K): δ_C 20.9 (*m*Xyl-CH₃), 23.1 (CH(CH₃)₂), 23.3 (CH(CH₃)₂), 24.3 (CH(CH₃)₂), 28.0 (CH(CH₃)₂), 28.6 (CH(CH₃)₂), 28.9 (CH(CH₃)₂), 123.2 (ArC), 124.3 (ArC), 125.4 (ArC), 129.6 (ArC), 130.5 (ArC), 131.2 (ArC), 137.0 (ArC), 140.6 (ArC), 143.8 (ArC), 144.9 (ArC), 164.8 (NC(Ar)N).

¹H NMR (400 MHz, cyclohexane-*d*₁₂, 298 K): δ_H 0.04 (d, CH(CH)₃, ³J_{HH} = 6.7 Hz, 18H), 0.17 (d, CH(CH)₃, ³J_{HH} = 6.7 Hz, 18H), 1.06 (d, CH(CH)₃, ³J_{HH} = 6.8 Hz, 18H), 1.28 (d, CH(CH)₃, ³J_{HH} = 6.6 Hz, 18H), 1.82 (s, *m*Xyl-*m*-CH₃, 18H), 3.01 (hept, CH(CH₃)₂, ³J_{HH} = 6.9 Hz, 6H), 3.68 (hept, CH(CH₃)₂, ³J_{HH} = 6.7 Hz, 6H), 6.49 (s, *m*Xyl-*o*-H, 6H), 6.56 (s, *m*Xyl-*p*-H, 3H), 6.79 – 6.93 (m, *Ar*H, 18H). **¹³C{¹H} NMR** (101 MHz, cyclohexane-*d*₁₂): δ_C 20.9 (*m*-Xyl-CH₃), 22.9 (CH(CH₃)₂), 23.3 (CH(CH₃)₂), 23.5 (CH(CH₃)₂), 24.3 (CH(CH₃)₂), 28.3 (CH(CH₃)₂), 28.8 (CH(CH₃)₂), 29.1 (CH(CH₃)₂), 123.3 (ArC), 124.3 (ArC), 125.3 (ArC), 130.1 (ArC), 130.9 (ArC), 131.0 (ArC), 137.1 (ArC), 140.9 (ArC), 144.0 (ArC), 145.1 (ArC), 164.9 (NC(Ar)N).

Elemental analysis calculated for C₁₀₇H₁₅₃Al₃N₆O₂Si₃ (**2^{m-xyl}**·(Si₃O₂C₈H₂₄): C 74.69, H 8.96, N 4.88. Found: C 74.12, H 8.57, N 4.68.

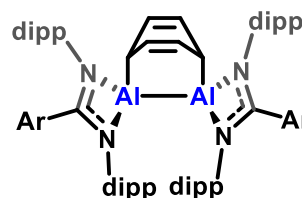
UV/Vis (cyclohexane): λ_{max} 478 nm and 315 nm.

Note: Several aliphatic solvents have been tested for the reaction, and generally the reactions have been found to proceed similarly in pentane, hexane and cyclohexane for **1^{p-tol}**, however **1^{m-xyl}** appears more sensitive to the reaction solvent, with lower yields obtained from attempted reductions in pentane, and notably larger quantities of the apparent decomposition product [(^{Dip}Am^{m-xyl}AlH)₂] (dihydrodialane) (as verified *via* comparison with independently synthesised **8^{m-xyl}**).

Reactivity studies with **2^{p-tol}** and **2^{m-xyl}**

Compound 3

Route 1: A J Young NMR tube charged with a dark red-black solution of **2** (1 equiv.) in excess benzene (0.6 mL) was heated to 80 °C for three hours. The resultant red-orange solution was dried *in vacuo* and redissolved in benzene-*d*₆. ¹H NMR spectroscopic analysis showed full conversion of **2** to **3**.



Route 2: A vial containing **1^{p-tol}** (1 equiv.) and KC₈ (2 equiv.)* in benzene (15 mL) was stirred vigorously for 5 days. The solution was allowed to settle and filtered before concentrating to an oil and adding pentane, to afford the product as a red crystalline solid.

*The route 2 reaction was also attempted with K as the reducing agent, but although the starting material was consumed, very little of **3** was formed. This may be in part due to difficulties finely dividing K in benzene, which results in a reduced surface area and precludes effective reduction.

3^{p-tol}

Route 1: 34.8 mg **2^{p-tol}**, 0.6 mL benzene, yield: 29.5 mg (78%).

Route 2: 200 mg **1^{p-tol}**, 74 mg KC₈, yield 103 mg (72%).

Characterisation has been previously reported.^{7,8}

3^{m-xyl}

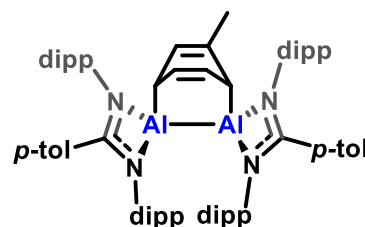
Route 1: 26.4 mg **2^{m-xyl}**, 0.6 mL benzene, yield: 21.4 mg (75%).

¹H NMR (400 MHz, benzene-*d*₆, 298 K): δ_H 0.42 (d, 6H, CH(CH₃)₂, ³J_{HH} = 6.8 Hz), 0.54 (d, 6H, CH(CH₃)₂, ³J_{HH} = 6.7 Hz), 0.84 (d, 6H, CH(CH₃)₂, ³J_{HH} = 6.7 Hz), 1.24 (d, 6H, CH(CH₃)₂, ³J_{HH} = 6.6 Hz), 1.35 (d, 6H, CH(CH₃)₂, ³J_{HH} = 6.9 Hz), 1.40 (d, 6H, CH(CH₃)₂, ³J_{HH} = 6.8 Hz), 1.50 (d, 12H, CH(CH₃)₂, ³J_{HH} = 6.8 Hz), 1.74 (s, 12H, *m*-Xyl-CH₃), 2.75 (tt, 2H, AlCH, ³J_{HH} = 6.3 Hz, ⁴J_{HH} = 1.3 Hz), 3.23 (v. dhept, 4H, CH(CH₃)₂, ³J_{HH} = 6.8 Hz), 3.94 (hept, 2H, CH(CH₃)₂, ³J_{HH} = 5.9 Hz), 4.05 (hept, 2H, CH(CH₃)₂, ³J_{HH} = 6.8 Hz), 5.40 (dd, 2H, AlCH-CH=CH, ⁴J_{HH} = 6.3 Hz, ³J_{HH} = 8.4 Hz), 6.09 (dd, 2H, AlCH-CH=CH, ⁴J_{HH} = 6.4 Hz, ³J_{HH} = 8.3 Hz), 6.40 (s, 2H, *m*-Xyl-*p*-H), 6.73 (s, 4H, *m*-Xyl-*o*-H), 6.83 (m, 2H, ArH), 6.96 – 7.13 (m, 8H, ArH), 7.18 – 7.25 (m, 4H, ArH). **¹³C{¹H} NMR** (101 MHz, Benzene-*d*₆, 298 K): δ_C 20.8 (*m*-Xyl-CH₃), 22.7 (CH(CH₃)₂), 22.7 (CH(CH₃)₂), 23.2 (CH(CH₃)₂), 23.8 (CH(CH₃)₂), 24.1 (CH(CH₃)₂), 24.7 (CH(CH₃)₂), 25.5 (CH(CH₃)₂), 26.0 (CH(CH₃)₂), 26.5 (CH(CH₃)₂), 28.1 (CH(CH₃)₂), 28.4 (CH(CH₃)₂), 28.6 (CH(CH₃)₂), 28.7 (CH(CH₃)₂), 38.6 (AlCH), 119.7 (AlCHCH), 123.3 (ArC), 123.7 (ArC), 124.3 (ArC), 124.3 (ArC), 125.8 (ArC), 126.2 (AlCHCH), 126.6 (ArC), 128.3 (ArC), 128.6 (*m*-Xyl-*o*-CH), 129.5 (ArC), 131.8 (*m*-Xyl-*p*-CH), 137.2 (*m*-Xyl-*m*-C), 139.3 (ArC), 139.4 (ArC), 143.4 (ArC), 143.7 (ArC), 144.5 (ArC), 145.3 (ArC), 172.5 (NC(*m*-Xyl)N).

Compound 4^{p-tol}

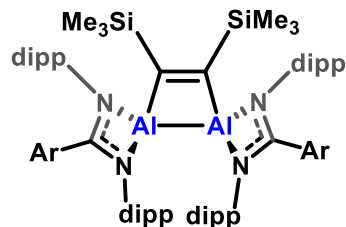
A vial containing **1^{p-tol}** (200 mg, 1 equiv.) and KC₈ (74 mg, 2 equiv.) in toluene (15 mL) was stirred vigorously for 6 days. The solution was allowed to settle and filtered before concentrating to approximately 5 mL and storing at -40 °C to afford the product as a red crystalline solid (85 mg, 44%)

Characterisation has been previously reported.⁸



Compound 6

To a J Young NMR tube charged with a solution of **2** (1 equiv.) in cyclohexane-*d*₁₂ (0.6 mL) was added *bis*(trimethylsilyl)acetylene (3 equiv.). This was heated to 80 °C for 6 hours, at which point complete conversion was confirmed *via* ¹H NMR spectroscopic analysis. **6** could be isolated following the removal of solvent *in vacuo* and subsequent extraction into pentane.



6^{p-tol}

8.9 mg **2^{p-tol}**, 3.2 mg *bis*(trimethylsilyl)acetylene, yield: 5.8 mg (55%).

¹H NMR (400 MHz, benzene-*d*₆, 298 K): δ_H 0.39 (s, 18H, Si(CH₃)₃), 1.32 (d, 12H, CH(CH₃)₂, ³J_{HH} = 6.7 Hz), 1.67 (s, 6H, *p*-CH₃), 3.48 (br s, 8H, CH(CH₃)₂), 6.38 (d, 4H, ArH, ³J_{HH} = 8.1 Hz), 6.91 (d, 4H, ArH, ³J_{HH} = 8.1 Hz), 7.08 (m, 12H, ArH). Some resonances corresponding to diisopropyl groups are missing, but spectrum is broad suggesting restricted rotation. **¹³C{¹H} NMR** (101 MHz, benzene-*d*₆, 298 K): δ_C 3.0 (Si(CH₃)₃), 21.0 (*p*-CH₃), 22.8 (CH(CH₃)₂), 23.1 (CH(CH₃)₂), 24.3 (CH(CH₃)₂), 28.7 (CH(CH₃)₂), 28.7 (CH(CH₃)₂), 124.2 (CH), 124.4 (CH), 125.7 (CH), 127.7 (CH), 128.8 (CH), 131.6 (CH), 139.7 (C^{IV}), 140.8 (C^{IV}), 143.2 (C^{IV}), 171.2 (NC(Ar)N), 243.4 (AlCSiMe₃).

6^{m-xyl}

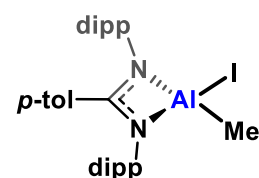
7.2 mg **2^{m-xyl}**, 2.5 mg bis(trimethylsilyl)acetylene, yield: 5.5 mg (65%).

¹H NMR (400 MHz, benzene-*d*₆, 298 K): δ_H 0.40 (s, 18H, Si(CH₃)₃), 1.32 (d, 12H, CH(CH₃)₂, ³J_{HH} = 6.7 Hz), 1.77 (s, 12H, *m*Xyl-*m*-CH₃), 3.34 – 3.65 (br. m, 8H, CH(CH₃)₂), 6.37 – 6.49 (s, 2H, *m*Xyl-*p*-H), 6.65 (s, 4H, *m*Xyl-*o*-H), 7.06 (m, 12H, ArH). Some resonances correspond to diisopropyl groups are missing, but broadened spectrum indicates restricted rotation. **¹H NMR** (400 MHz, benzene-*d*₆, 353 K): δ_H 0.35 (s, 18H, Si(CH₃)₃), 0.71 (d, 12H, CH(CH₃)₂, ³J_{HH} = 6.7 Hz), 0.82 (br. d, 12H, CH(CH₃)₂, ³J_{HH} = 6.5 Hz), 1.05 (d, CH(CH₃)₂, 12H, ³J_{HH} = 6.7 Hz), 1.29 (d, CH(CH₃)₂, 12H, ³J_{HH} = 6.7 Hz), 1.79 (s, 12H, *m*-Xyl-CH₃), 3.34 – 3.61 (m, 8H, CH(CH₃)₂), 6.50 (s, 2H, *m*-Xyl-*p*-H), 6.62 (s, 4H, *m*-Xyl-*o*-H), 7.02 – 7.07 (m, 10H, ArH). **¹³C{¹H} NMR** (101 MHz, benzene-*d*₆, 298 K): δ_C 3.0 (Si(CH₃)₃), 20.9 (*m*-Xyl-*m*-CH₃), 22.7 (CH(CH₃)₂), 22.8 (CH(CH₃)₂), 24.2 (CH(CH₃)₂), 28.6 (CH(CH₃)₂), 28.8 (CH(CH₃)₂), 124.1 (ArC), 125.6 (ArC), 129.7 (ArC), 130.3 (ArC), 131.7 (ArC), 137.4 (ArC), 139.6 (ArC), 143.2 (ArC), 171.4 (NC(Ar)N), 230.6 (AlCSiMe₃).

Elemental analysis calculated for C₇₄H₁₀₄Al₂N₄Si₂ (**6^{m-xyl}**·2.5(toluene)): C 79.06 H 8.99 N 4.03. Found: C 79.23, H 9.53, N 4.57

Compound 7^{p-tol}

Route 1: To an J Young NMR tube containing a solution of **2^{p-tol}** (37.5 mg, 1 equiv.) in benzene-*d*₆ (0.6 mL) was added methyl iodide (11.1 mg, 4.8 μL, 3 equiv.) and a colour change to very light brown was observed over the course of two minutes. The product was isolated as a white solid by removal of solvent *in vacuo* and washing with pentane (34.2 mg, 70 %).



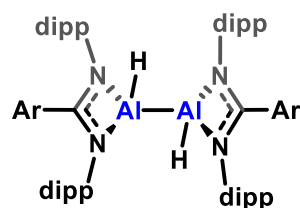
Route 2: To a J Young NMR tube containing a solution of *p*-tolAmAlMe₂ (50.0 mg, 1 equiv.) in benzene-*d*₆ (0.6 mL) was added iodine (24.8 mg, 1 equiv.). The product was dried *in vacuo* to remove the solvent and methyl iodide side-product and washed with pentane to obtain a white solid (51.9 mg, 85%).

¹H NMR (400 MHz, benzene-*d*₆, 298 K): δ_H 0.23 (s, 3H, AlCH₃), 0.91 (d, 6H, CH(CH₃)₂, ³J_{HH} = 6.8 Hz), 0.95 (d, 6H, CH(CH₃)₂, ³J_{HH} = 6.8 Hz), 1.18 (d, 6H, CH(CH₃)₂, ³J_{HH} = 6.8 Hz), 1.46 (d, 6H, CH(CH₃)₂, ³J_{HH} = 6.8 Hz), 1.61 (s, 9H, *p*-CH₃), 3.45 (hept, 2H, CH(CH₃)₂, ³J_{HH} = 6.8 Hz), 3.87 (hept, 2H, CH(CH₃)₂, ³J_{HH} = 6.8 Hz), 6.35 (d, 2H, ArH, ³J_{HH} = 8.2 Hz), 6.95 – 7.11 (m, 8H, ArH). **¹³C{¹H} NMR** (101 MHz, benzene-*d*₆, 298 K): δ_C 21.0 (*p*-CH₃), 23.0 (CH(CH₃)₂), 23.1 (CH(CH₃)₂), 25.7 (CH(CH₃)₂), 27.3 (CH(CH₃)₂), 28.9 (CH(CH₃)₂), 29.0 (CH(CH₃)₂), 124.0 (ArC), 124.8 (ArC), 125.5 (C^{IV}), 126.9 (ArC), 128.9 (ArC), 130.8 (C^{IV}), 137.1 (C^{IV}), 142.3 (C^{IV}), 143.7 (C^{IV}), 144.8 (C^{IV}), 175.6 (NC(Ar)N).

Compound 8

Route 1: To a J Young NMR tube charged with a degassed solution of **2** (1 equiv.) in benzene-*d*₆ (0.6 mL) was added an excess of H₂ gas (approx. 1 atm.). A rapid decolouration is observed. The product may be isolated *via* extraction into pentane to afford compound **8**.

Route 2: To a flask charged with aluminium dihydride (1 equiv.) and [(^{Mes}BDIMg)₂] (0.55 equiv.) was added toluene. The resultant reaction was stirred overnight at room temperature, filtered from toluene and extracted into benzene to afford **8** as a colourless solid.



A

Route 1: 17 mg **2^{p-tol}**, yield: 11.0 mg (65%). Characterisation has been previously reported.³

8^{m-xyI}

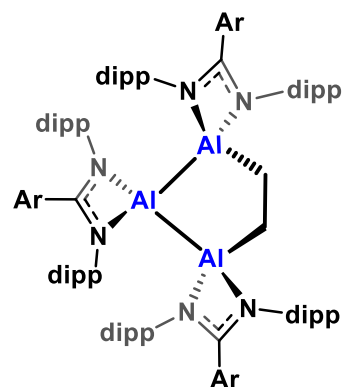
Route 1: 12 mg **2^{m-xyI}**, yield: 5.4 mg (45%).

Route 2: 100 mg aluminium dihydride, 79.2 mg [(^{Mes}BDIMg)₂], yield: 73.6 mg (74%).

¹H NMR (400 MHz, benzene-*d*₆, 298 K): δ_H 1.09 (d, 12H, CH(CH₃)₂, ³J_{HH} = 6.8 Hz), 1.14 (d, 12H, CH(CH₃)₂, ³J_{HH} = 6.9 Hz), 1.19 (d, 12H, CH(CH₃)₂, ³J_{HH} = 6.8 Hz), 1.42 (d, 12H, CH(CH₃)₂, ³J_{HH} = 6.8 Hz), 1.77 (s, 12H, *m*-Xyl-CH₃), 3.88 (v. dh, 8H, CH(CH₃)₂, ³J_{HH} = 6.7 Hz), 5.68 (s, 2H, AlH), 6.39 (s, 2H, *m*-Xyl-*p*-H), 6.87 (s, 4H, *m*-Xyl-*o*-H), 6.98 – 7.03 (m, 12H, ArH). **¹³C{¹H} NMR** (101 MHz, benzene-*d*₆, 298 K): δ_C 20.8 (*m*-Xyl-CH₃), 21.4 (CH(CH₃)₂), 23.1 (CH(CH₃)₂), 23.1 (CH(CH₃)₂), 25.8 (CH(CH₃)₂), 26.0 (CH(CH₃)₂), 28.8 (CH(CH₃)₂), 28.9 (CH(CH₃)₂), 123.6 (ArC), 123.8 (ArC), 125.7 (ArC), 126.0 (ArC), 128.6 (ArC), 129.3 (ArC), 131.7 (ArC), 137.1 (ArC), 139.3 (ArC), 144.0 (ArC), 144.3 (ArC), 171.8 (NC(Ar)N).

Compound 9

To a J Young NMR tube charged with a frozen degassed solution of **2** (1 equiv.) in cyclohexane (0.6 mL) was added ethene gas (1 atm.). The solution was allowed to thaw, instantaneously affording a red-orange solution. The solvent was immediately removed *in vacuo* and the red-orange solid redissolved in cyclohexane-*d*₁₂ or benzene-*d*₆ to afford a red-orange solution of **9^{p-tol}** or **9^{m-xyI}**, which was stable at room temperature. Crystals were afforded *via* the storage of concentrated pentane, hexane or heptane solutions at room temperature for several days.



9^{p-tol}

47 mg **2^{p-tol}**, 95% NMR conversion versus a mesitylene internal standard.

¹H NMR (700 MHz, benzene-*d*₆, 298 K): δ_H 0.29 (d, 6H, CH(CH₃)₂, ³J_{HH} = 6.8 Hz), 0.32 (br, 2H, AlCH₂), 0.44 (d, 6H, CH(CH₃)₂, ³J_{HH} = 6.8 Hz), 0.48 (d, 6H, CH(CH₃)₂, ³J_{HH} = 6.8 Hz), 0.63 (d, 6H, CH(CH₃)₂, ³J_{HH} = 6.8 Hz), 0.77 (d, 6H, CH(CH₃)₂, ³J_{HH} = 6.8 Hz), 1.21 (d, 6H, CH(CH₃)₂, ³J_{HH} = 6.8 Hz), 1.32 (d, 6H, CH(CH₃)₂, ³J_{HH} = 6.8 Hz), 1.33 (d, 6H, CH(CH₃)₂, ³J_{HH} = 6.8 Hz), 1.38 (br, 2H, AlCH₂), 1.45 (d, 6H, CH(CH₃)₂, ³J_{HH} = 6.8 Hz), 1.52 (d, 6H, CH(CH₃)₂, ³J_{HH} = 6.8 Hz), 1.62 – 1.67 (9H, *p*-CH₃ and CH(CH₃)₂), 3.21 (hept, 2H, CH(CH₃)₂, ³J_{HH} = 6.8 Hz), 3.32 (hept, 2H, CH(CH₃)₂, ³J_{HH} = 6.8 Hz), 3.36 (hept, 2H, CH(CH₃)₂, ³J_{HH} = 6.8 Hz), 3.94 (hept, 2H, CH(CH₃)₂, ³J_{HH} = 6.8 Hz), 4.05 (hept, 2H, CH(CH₃)₂, ³J_{HH} = 6.8 Hz), 4.14 (hept, 2H, CH(CH₃)₂, ³J_{HH} = 6.8 Hz), 6.37 (d, 4H, ArH, ³J_{HH} = 8.3 Hz), 6.40 (d, 2H, ArH, ³J_{HH} = 8.0 Hz), 6.97 (dd, *J* = 11.0, 7.9 Hz, 8H), 7.01 – 7.12 (m, 8H), 7.13 – 7.26 (m, 8H). **¹³C{¹H} NMR** (176 MHz, benzene-*d*₆, 298 K): δ_C 8.8 (AlCH₂), 20.9 (*p*-CH₃), 22.7 (CH(CH₃)₂), 23.4 (CH(CH₃)₂), 23.7 (CH(CH₃)₂), 23.8 (CH(CH₃)₂), 24.0 (CH(CH₃)₂), 24.2 (CH(CH₃)₂), 24.5 (CH(CH₃)₂), 25.9 (CH(CH₃)₂), 26.3 (CH(CH₃)₂), 26.4 (CH(CH₃)₂), 27.1 (CH(CH₃)₂), 28.2 (CH(CH₃)₂), 28.5 (CH(CH₃)₂), 28.5 (CH(CH₃)₂), 28.6 (CH(CH₃)₂), 28.7 (CH(CH₃)₂), 28.8 (CH(CH₃)₂), 123.2 (CH), 123.8 (CH), 124.0 (CH), 124.4 (CH), 124.6 (CH), 124.7 (CH), 125.2 (CH), 125.8 (CH), 125.9 (CH), 127.6 (CH), 128.4 (CH), 128.5 (CH), 130.9 (CH), 140.1 (C^{IV}), 140.4 (C^{IV}), 140.6 (C^{IV}), 140.8 (C^{IV}), 143.0 (C^{IV}), 144.0 (C^{IV}), 144.2 (C^{IV}), 144.4 (C^{IV}), 145.3 (C^{IV}), 145.5 (C^{IV}), 167.2 (NC(Ar)N), 170.4 (NC(Ar)N).

g^{m-xy}l

20 mg **2^{m-xy}l**, 95% NMR conversion versus a mesitylene internal standard.

¹H NMR (400 MHz, benzene-*d*₆, 298 K): δ_H 0.28 (d, 6H, CH(CH₃)₂, ³J_{HH} = 6.8 Hz), 0.31 (br. t, 2H, AlCH₂, ³J_{HH} = 13.3 Hz), 0.49 (d, 6H, CH(CH₃)₂, ³J_{HH} = 6.6 Hz), 0.51 (d, 6H, CH(CH₃)₂, ³J_{HH} = 6.8 Hz), 0.61 (d, 6H, CH(CH₃)₂, ³J_{HH} = 6.8 Hz), 0.76 (d, 6H, CH(CH₃)₂, ³J_{HH} = 6.8 Hz), 1.20 (d, 6H, CH(CH₃)₂, *J* = 6.9 Hz), 1.32 (d, 6H, CH(CH₃)₂, ³J_{HH} = 6.9 Hz), 1.33 (d, 6H, CH(CH₃)₂, ³J_{HH} = 7.0 Hz), 1.40 (d, 6H, CH(CH₃)₂, ³J_{HH} = 6.7 Hz), 1.41 (t, 2H, AlCH₂), 1.44 (d, 6H, CH(CH₃)₂, ³J_{HH} = 6.8 Hz), 1.52 (d, 6H, CH(CH₃)₂, ³J_{HH} = 6.5 Hz), 1.63 (d, 6H, CH(CH₃)₂, ³J_{HH} = 6.7 Hz), 1.76 (s, 12H, *m*-Xyl-CH₃), 1.78 (s, 6H, *m*-Xyl-CH₃), 3.20 (hept, 2H, CH(CH₃)₂, ³J_{HH} = 6.6 Hz), 3.32 (hept, 2H, CH(CH₃)₂, ³J_{HH} = 6.6 Hz), 3.39 (hept, 2H, CH(CH₃)₂, ³J_{HH} = 7.0 Hz), 3.92 (hept, 2H, CH(CH₃)₂, ³J_{HH} = 6.8 Hz), 4.03 (hept, 2H, CH(CH₃)₂, ³J_{HH} = 6.8 Hz), 4.14 (hept, 2H, CH(CH₃)₂, ³J_{HH} = 6.8 Hz), 6.40 (dq, 4H, *m*-Xyl-CH, ³J_{HH} = 0.8, 1.6 Hz), 6.70 (s, 4H, *m*-Xyl-CH), 6.74 (s, 2H, *m*-Xyl-CH), 6.91 – 7.24 (m, 18H, ArH).

¹H NMR (800 MHz, benzene-*d*₆, 298 K): δ_H 0.28 (d, 6H, CH(CH₃)₂, ³J_{HH} = 6.9 Hz), 0.30 – 0.34 (m, 2H, AlCH₂), 0.49 (d, 6H, CH(CH₃)₂, ³J_{HH} = 6.8 Hz), 0.51 (d, 6H, CH(CH₃)₂, ³J_{HH} = 6.9 Hz), 0.61 (d, 6H, CH(CH₃)₂, ³J_{HH} = 6.7 Hz), 0.76 (d, 6H, CH(CH₃)₂, ³J_{HH} = 6.8 Hz), 1.20 (d, 6H, CH(CH₃)₂, ³J_{HH} = 6.9 Hz), 1.32 (d, 6H, CH(CH₃)₂, ³J_{HH} = 6.8 Hz), 1.33 (d, 6H, CH(CH₃)₂, ³J_{HH} = 7.1 Hz), 1.35 – 1.38 (m, 2H, AlCH₂), 1.40 (d, 6H, CH(CH₃)₂, ³J_{HH} = 6.9 Hz), 1.44 (d, CH(CH₃)₂, 6H, ³J_{HH} = 6.6 Hz), 1.52 (d, CH(CH₃)₂, 6H, ³J_{HH} = 6.6 Hz), 1.63 (d, 6H, CH(CH₃)₂, ³J_{HH} = 6.7 Hz), 1.76 (s, 12H, *m*-Xyl-CH₃), 1.78 (s, 6H, *m*-Xyl-CH₃), 3.19 (hept, 2H, CH(CH₃)₂, ³J_{HH} = 6.9 Hz), 3.32 (hept, 2H, CH(CH₃)₂, ³J_{HH} = 7.2 Hz), 3.38 (hept, 2H, CH(CH₃)₂, ³J_{HH} = 6.8 Hz), 3.92 (hept, 2H, CH(CH₃)₂, ³J_{HH} = 6.7 Hz), 4.03 (hept, 2H, CH(CH₃)₂, ³J_{HH} = 6.8 Hz), 4.14 (hept, 2H, CH(CH₃)₂, ³J_{HH} = 6.9 Hz), 6.40 (s, 4H, *m*-Xyl-CH), 6.70 (s, 4H, *m*-Xyl-CH), 6.74 (s, 2H, *m*-Xyl-CH), 6.78 – 6.79 (m, 1H, *m*-Xyl-CH), 6.81 – 7.15 (m, 16H, ArH), 7.20 (d, 2H, ArH, ³J_{HH} = 7.7 Hz).

$^{13}\text{C}\{^1\text{H}\}$ NMR (201 MHz, benzene- d_6 , 298 K): δ_{C} 8.6 (AlCH₂), 20.8 (*m*-Xyl-CH₃), 20.9 (*m*-Xyl-CH₃), 22.7 (CH(CH₃)₂), 23.4 (CH(CH₃)₂), 23.6 (CH(CH₃)₂), 23.6 (CH(CH₃)₂), 23.9 (CH(CH₃)₂), 24.3 (CH(CH₃)₂), 24.5 (CH(CH₃)₂), 26.1 (CH(CH₃)₂), 26.4 (CH(CH₃)₂), 27.1 (CH(CH₃)₂), 28.1 (CH(CH₃)₂), 28.5 (CH(CH₃)₂), 28.5 (CH(CH₃)₂), 28.7 (CH(CH₃)₂), 28.8 (CH(CH₃)₂), 123.0 (ArC), 123.6 (ArC), 123.8 (ArC), 124.3 (ArC), 124.4 (ArC), 124.6 (ArC), 125.1 (ArC), 125.7 (ArC), 125.9 (ArC), 129.0 (ArC), 130.2 (ArC), 131.2 (ArC), 137.0 (ArC), 137.0 (ArC), 140.2 (ArC), 140.5 (ArC), 140.7 (ArC), 143.1 (ArC), 144.1 (ArC), 144.3 (ArC), 144.5 (ArC), 145.4 (ArC), 145.5 (ArC), 170.8 (NC(Ar)N).

Synthesis of compounds **10**, **11** and **12**

To a J Young NMR tube charged with a frozen degassed solution of **2** (1 equiv.) in cyclohexane- d_{12} (0.6 mL) was added ethene gas (1 atm.). The frozen solution was allowed to thaw, affording a red-orange solution, which over the course of approximately 10 hours lost intensity, eventually affording a colourless solution. Product distribution could be worked out *via* ^1H NMR spectroscopy versus a mesitylene internal standard.

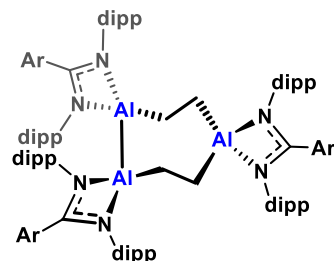
For assignment of **10**^{*p-tol*} and **10**^{*m-xy*} in both cases, due to the number of resonances and overlapping crosspeaks assignment of ^{13}C resonances is tentative; unfortunately it proved impossible to completely separate **10** from **11** and **12**, nevertheless acquiring ^1H spectra on an 800 MHz spectrometer allowed for ^1H NMR assignment (Figure S 86).

Again, for assignment of **12**^{*p-tol*} and **12**^{*m-xy*} due to the number of resonances and overlapping crosspeaks assignment of aromatic and all ^{13}C resonances is not possible, but tentative assignment of ^1H resonances is possible using an 800 MHz spectrometer (Figure S 92).

10^{*p-tol*}

19 mg **2**^{*p-tol*}, 45% conversion by ^1H NMR spectroscopy.

^1H NMR (700 MHz, benzene- d_6 , 298 K): δ_{H} 0.27 (d, 6H, CH(CH₃)₂, $^3J_{\text{HH}} = 6.8$ Hz), 0.48 (d, 6H, CH(CH₃)₂, $^3J_{\text{HH}} = 6.8$ Hz), 0.63 (br, AlCH₂, 4H), 0.69 (d, 6H, CH(CH₃)₂, $^3J_{\text{HH}} = 6.8$ Hz), 0.94 (br, AlCH₂, 2H), 0.98 – 1.04 (m, 6H, CH(CH₃)₂), 1.11 (br, CH(CH₃)₂, 2H), 1.18 (d, 6H, CH(CH₃)₂, $^3J_{\text{HH}} = 6.8$ Hz), 1.23 (d, 6H, CH(CH₃)₂, $^3J_{\text{HH}} = 6.8$ Hz), 1.24 – 1.29 (m, 6H, CH(CH₃)₂), 1.31 (m, 6H, CH(CH₃)₂), 1.37 (d, 12H, CH(CH₃)₂, $^3J_{\text{HH}} = 6.8$ Hz), 1.45 (d, 6H, CH(CH₃)₂, $^3J_{\text{HH}} = 6.8$ Hz), 1.47 (d, 6H, CH(CH₃)₂, $^3J_{\text{HH}} = 6.8$ Hz), 1.62 (s, 9H, *p*-CH₃), 3.20 (hept, 2H, CH(CH₃)₂, $^3J_{\text{HH}} = 6.8$ Hz), 3.32 (hept, 2H, CH(CH₃)₂, $^3J_{\text{HH}} = 6.8$ Hz), 3.46 (hept, 2H, CH(CH₃)₂, $^3J_{\text{HH}} = 6.8$ Hz), 3.80 (hept, 2H, CH(CH₃)₂, $^3J_{\text{HH}} = 6.8$ Hz), 3.99 (hept, 2H, CH(CH₃)₂, $^3J_{\text{HH}} = 6.8$ Hz), 4.24 (hept, 2H, CH(CH₃)₂, $^3J_{\text{HH}} = 6.8$ Hz), 6.23 – 6.49 (m, 6H, ArH), 6.88 – 7.14 (m, 20H, ArH), 7.21 – 7.35 (m, 4H, ArH). **$^{13}\text{C}\{^1\text{H}\}$ NMR** (176 MHz, benzene- d_6 , 298 K): δ_{C} -1.7 (AlCH₂), 8.1 (AlCH₂), 20.9 (*p*-CH₃), 22.8 (CH(CH₃)₂), 22.9 (CH(CH₃)₂), 23.1 (CH(CH₃)₂), 23.2 (CH(CH₃)₂), 23.3 (CH(CH₃)₂), 23.8 (CH(CH₃)₂), 23.9 (CH(CH₃)₂), 25.0 (CH(CH₃)₂), 25.5 (CH(CH₃)₂), 25.7 (CH(CH₃)₂), 26.0 (CH(CH₃)₂), 26.2 (CH(CH₃)₂), 26.9 (CH(CH₃)₂), 27.5 (CH(CH₃)₂), 28.3 (CH(CH₃)₂), 28.5 (CH(CH₃)₂), 28.7 (CH(CH₃)₂), 28.8 (CH(CH₃)₂), 29.0 (CH(CH₃)₂), 123.1 (CH), 123.4 (CH), 124.0 (CH), 124.4 (CH), 125.1 (CH), 125.2 (CH), 125.6 (CH), 125.9 (CH), 126.2 (CH), 126.3 (CH), 130.3 (CH), 130.5 (CH), 137.8 (CH), 138.4 (CH), 140.1 (C^{IV}), 140.2 (C^{IV}), 140.4 (C^{IV}), 143.3 (C^{IV}), 143.6 (C^{IV}), 143.7 (C^{IV}), 143.9 (C^{IV}), 144.3 (C^{IV}), 145.3 (C^{IV}), 146.1 (C^{IV}), 170.8 (NC(Ar)N), 172.2 (NC(Ar)N).



10^{m-xyl}

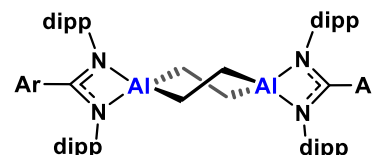
20 mg **2^{m-xyl}**, 42% conversion by ¹H NMR spectroscopy.

¹H NMR (800 MHz, benzene-*d*₆, 298 K): δ_H 0.23 (d, 6H, CH(CH₃)₂, ³J_{HH} = 6.8 Hz), 0.57 (d, 6H, CH(CH₃)₂, ³J_{HH} = 6.8 Hz), 0.59 (d, 2H, AlCH₂, ³J_{HH} = 14.2 Hz), 0.65 (d, 2H, AlCH₂, ³J_{HH} = 12.8 Hz), 0.73 (d, 6H, CH(CH₃)₂, ³J_{HH} = 6.8 Hz), 0.85 (d, 2H, AlCH₂, ³J_{HH} = 13.4 Hz), 1.00 (d, 6H, CH(CH₃)₂, ³J_{HH} = 6.8 Hz), 1.13 – 1.17 (m, 2H, AlCH₂), 1.20 (d, 6H, CH(CH₃)₂, ³J_{HH} = 6.9 Hz), 1.22 (d, 6H, CH(CH₃)₂, ³J_{HH} = 6.8 Hz), 1.23 (d, 6H, CH(CH₃)₂, ³J_{HH} = 6.8 Hz), 1.39 (v. dd, 12H, CH(CH₃)₂, ³J_{HH} = 6.6, 6.6 Hz), 1.42 (d, 6H, CH(CH₃)₂, ³J_{HH} = 6.7 Hz), 1.46 (d, 6H, CH(CH₃)₂, ³J_{HH} = 6.8 Hz), 1.75 (s, 6H, *m*-Xyl-CH₃), 1.78 (s, 12H, *m*-Xyl-CH₃), 3.16 (hept, 2H, CH(CH₃)₂, ³J_{HH} = 6.8 Hz), 3.38 (hept, 2H, CH(CH₃)₂, ³J_{HH} = 6.8 Hz), 3.48 (hept, 2H, CH(CH₃)₂, ³J_{HH} = 6.6 Hz), 3.80 (hept, 2H, CH(CH₃)₂, ³J_{HH} = 6.5 Hz), 3.96 (hept, 2H, CH(CH₃)₂, ³J_{HH} = 6.8 Hz), 4.24 (hept, 2H, CH(CH₃)₂, ³J_{HH} = 6.7 Hz), 6.39 (s, 1H, *m*-Xyl-*p*-H), 6.42 (s, 2H, *m*-Xyl-*p*-H), 6.71 (s, 4H, *m*-Xyl-*o*-H), 6.74 (a, 2H, *m*-Xyl-*o*-H), 6.91 (dd, 2H, ArH, ³J_{HH} = 1.6, 7.4 Hz), 6.94 (dd, 2H, ArH, ³J_{HH} = 1.6, 7.6 Hz), 6.98 (d, 1H, ArH, ³J_{HH} = 7.5 Hz), 7.03 (t, 4H, ArH, ³J_{HH} = 7.6 Hz), 7.06 (dd, 2H, ArH, ³J_{HH} = 1.7, 7.6 Hz), 7.08 (dd, 2H, ArH, ³J_{HH} = 1.5, 7.8 Hz), 7.14 (dd, 2H, ArH, ³J_{HH} = 1.5, 7.8 Hz), 7.20 (t, 2H, ArH, ³J_{HH} = 7.7 Hz), 7.26 (dd, 2H, ArH, ³J_{HH} = 1.6, 7.9 Hz). **¹³C{¹H} NMR** (201 MHz, benzene-*d*₆): δ_C -1.9 (AlCH₂), 7.9 (AlCH₂), 20.8 (*m*-Xyl-CH₃), 20.8 (*m*-Xyl-CH₃), 22.7 (CH(CH₃)₂), 22.9 (CH(CH₃)₂), 23.1 (CH(CH₃)₂), 23.2 (CH(CH₃)₂), 23.4 (CH(CH₃)₂), 23.7 (CH(CH₃)₂), 24.1 (CH(CH₃)₂), 25.1 (CH(CH₃)₂), 25.3 (CH(CH₃)₂), 25.9 (CH(CH₃)₂), 26.0 (CH(CH₃)₂), 26.2 (CH(CH₃)₂), 28.3 (CH(CH₃)₂), 28.4 (CH(CH₃)₂), 28.5 (CH(CH₃)₂), 28.7 (CH(CH₃)₂), 28.8 (CH(CH₃)₂), 29.0 (CH(CH₃)₂), 123.0 (ArC), 123.2 (ArC), 123.8 (ArC), 123.8 (ArC), 123.9 (ArC), 124.3 (ArC), 124.4 (ArC), 125.0 (ArC), 125.1 (ArC), 125.6 (ArC), 125.7 (ArC), 126.0 (ArC), 128.9 (ArC), 129.3 (ArC), 130.4 (ArC), 131.2 (ArC), 139.2 (ArC), 139.9 (ArC), 140.4 (ArC), 143.3 (ArC), 143.7 (ArC), 143.8 (ArC), 144.0 (ArC), 144.2 (ArC), 144.5 (ArC), 146.1 (ArC), 171.2 (NC(Ar)N), 172.8 (NC(Ar)N).

11^{p-tol}

27% conversion *via* ¹H NMR spectroscopy

¹H NMR (400 MHz, benzene-*d*₆, 298 K): δ_H 1.01 (d, 24H, CH(CH₃)₂, ³J_{HH} = 6.8 Hz), 1.20 (s, 8H, AlCH₂), (d, 24H, CH(CH₃)₂, ³J_{HH} = 6.7 Hz), 1.62 (s, 6H, *p*-CH₃), 3.71 (hept, 4H, CH(CH₃)₂, ³J_{HH} = 6.8 Hz), 6.35 – 6.41 (m, 4H, ArH), 6.97 – 7.08 (m, 32H, ArH). **¹³C{¹H} NMR** (101 MHz, benzene-*d*₆, 298 K): δ_C 2.6 (AlCH₂), 20.9 (*p*-CH₃), 23.1 (CH(CH₃)₂), 25.7 (CH(CH₃)₂), 28.8 (CH(CH₃)₂), 124.0 (CH), 125.9 (CH), 130.5 (CH), 139.2 (CH), 144.0 (C^{IV}), 173.1 (NC(Ar)N).

**11^{m-xyl}**

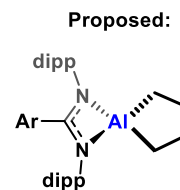
32% conversion *via* ¹H NMR spectroscopy

¹H NMR (400 MHz, benzene-*d*₆, 298 K): δ_H 1.04 (d, 24H, CH(CH₃)₂, ³J_{HH} = 6.9 Hz), 1.21 (s, 8H, AlCH₂), 1.31 (d, 24H, CH(CH₃)₂, ³J_{HH} = 6.7 Hz), 1.76 (s, 12H, *m*-Xyl-CH₃), 3.72 (hept, 8H, CH(CH₃)₂, ³J_{HH} = 6.8 Hz), 6.40 (m, 4H, ArH), 6.68 – 6.75 (m, 2H, ArH), 6.99 (s, 24H, ArH). **¹³C{¹H} NMR** (101 MHz, benzene-*d*₆, 298 K): δ_C 2.5 (AlCH₂), 14.3 (*m*-Xyl-CH₃), 20.8 (CH(CH₃)₂), 23.1 (CH(CH₃)₂), 25.9 (CH(CH₃)₂), 28.8 (CH(CH₃)₂), 123.8 (ArC), 125.9 (ArC), 137.1 (ArC), 139.1 (ArC), 144.2 (ArC), 173.7 (NC(Ar)N).

12^{p-tol}

28% conversion *via* ¹H NMR spectroscopy

¹H NMR (400 MHz, benzene-*d*₆, 298 K): δ_H 0.55 (br, 4H, Al-(CH₂-CH₂)₂), 0.87 (d, 12H, CH(CH₃)₂, ³J_{HH} = 6.8 Hz), 1.29 (d, 12H, CH(CH₃)₂, ³J_{HH} = 6.8 Hz), 1.62 (s, 9H, *p*-CH₃), 2.06 (br, 4H, Al-(CH₂-CH₂)₂), 3.70 (hept, 4H, CH(CH₃)₂, ³J_{HH} = 6.8 Hz).

**12^{m-xyl}**

26% conversion *via* ¹H NMR spectroscopy

¹H NMR (800 MHz, Benzene-*d*₆, 298 K) δ 0.55 (t, 4H, AlCH₂CH₂, ³J_{HH} = 6.9 Hz), 1.04 (d, 12H, CH(CH₃)₂, ³J_{HH} = 7.0 Hz), 1.29 (d, 12H, CH(CH₃)₂, ³J_{HH} = 6.9 Hz), 1.78 (s, 6H, *m*-Xyl-CH₃), 2.05 (p, 4H, AlCH₂CH₂, ³J_{HH} = 3.8 Hz), 3.65 (hept, 4H, CH(CH₃)₂, ³J_{HH} = 6.9 Hz).

3. Supporting figures

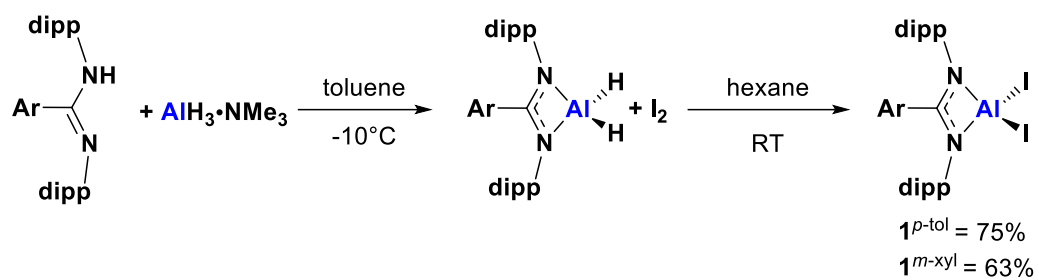


Figure S 1: Reaction scheme for the formation of complexes **1** from amidine proligands.



Figure S 2: Colour of reaction mixture for route 1 synthesis of **2^{p-tol}**.

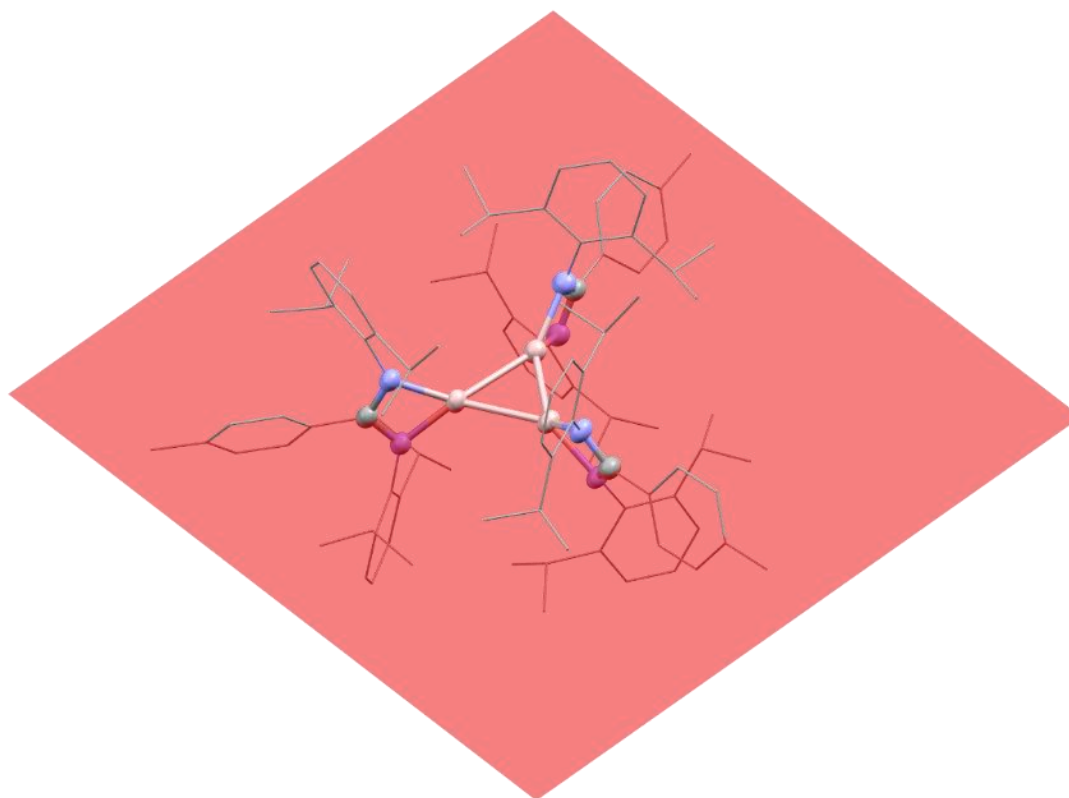


Figure S 3: Plane through Al_3 core of **2^{p-tol}** approximately bisecting the NCN backbone of the ligand.

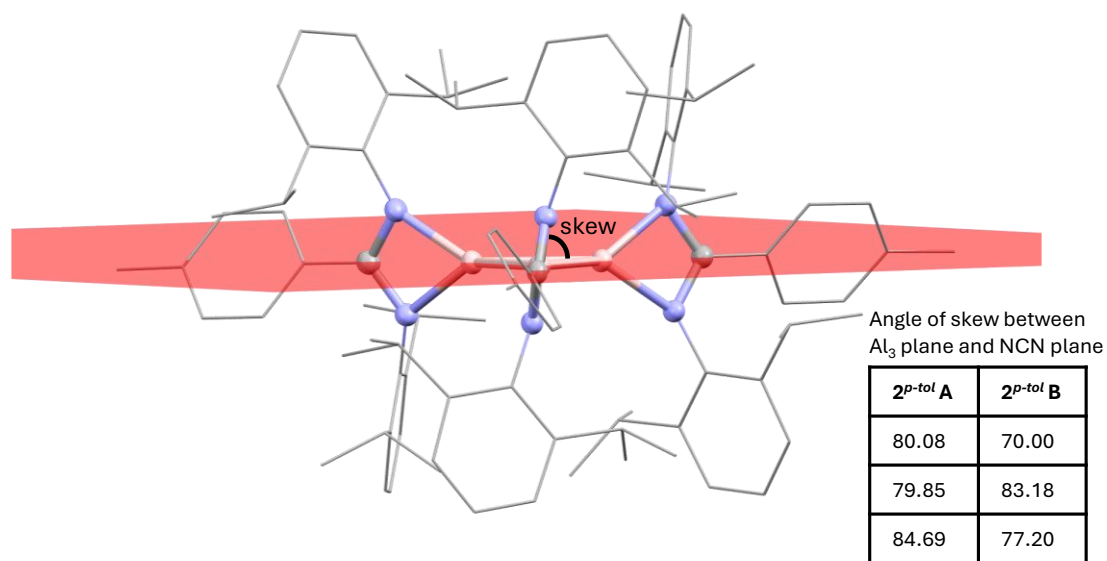


Figure S 4: Angle of skew between Al_3 and NCN planes, forming concentric pinwheel structure.

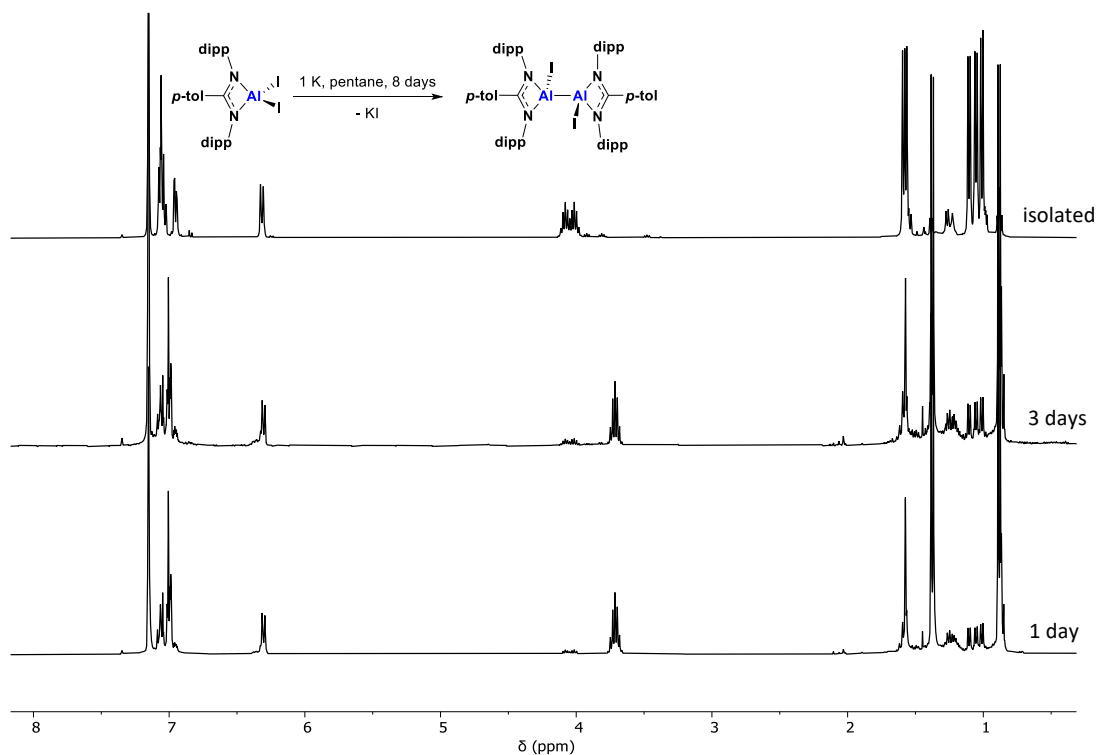


Figure S 5: ^1H NMR spectra showing reaction progress for reducing $1^{p\text{-tol}}$ to make the singly reduced diiododialane $5^{p\text{-tol}}$.

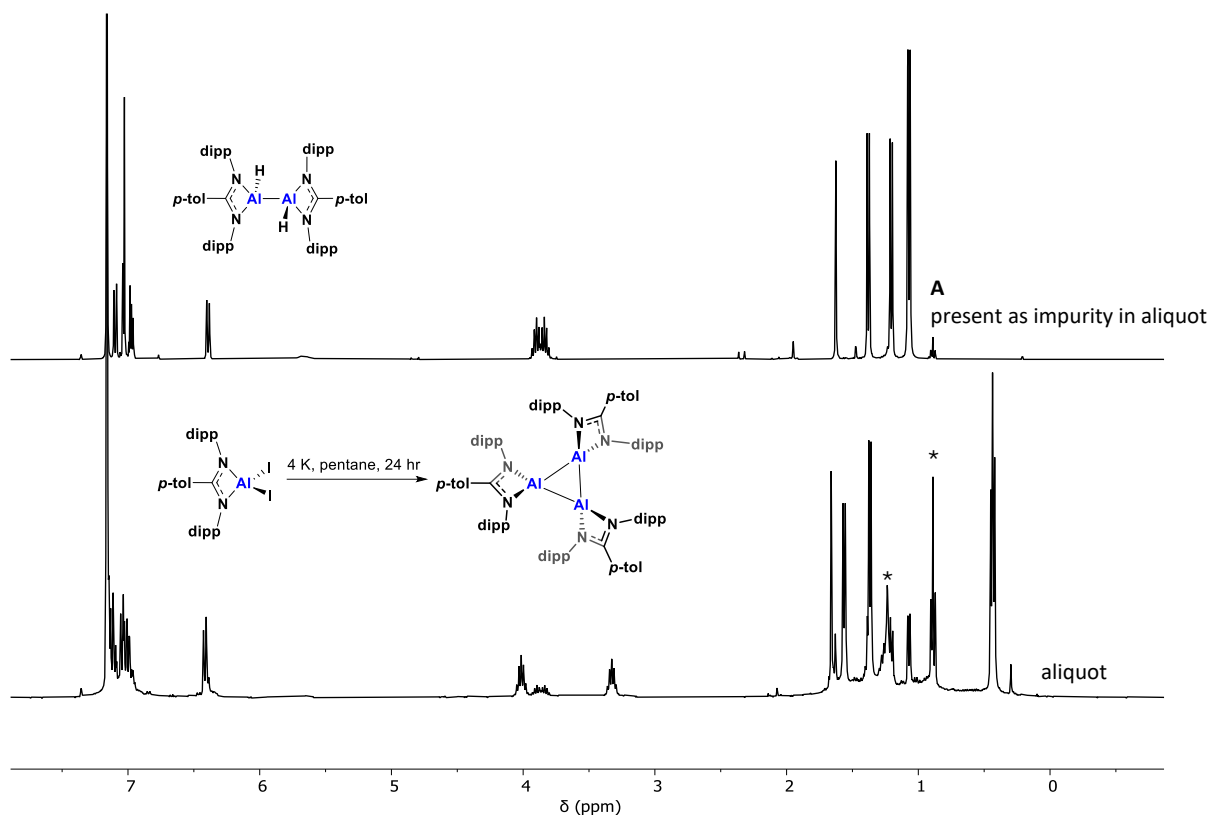


Figure S 6: ^1H NMR spectra showing aliquot from route 1 synthesis of **2^{p-tol}** containing **A** (*pentane).

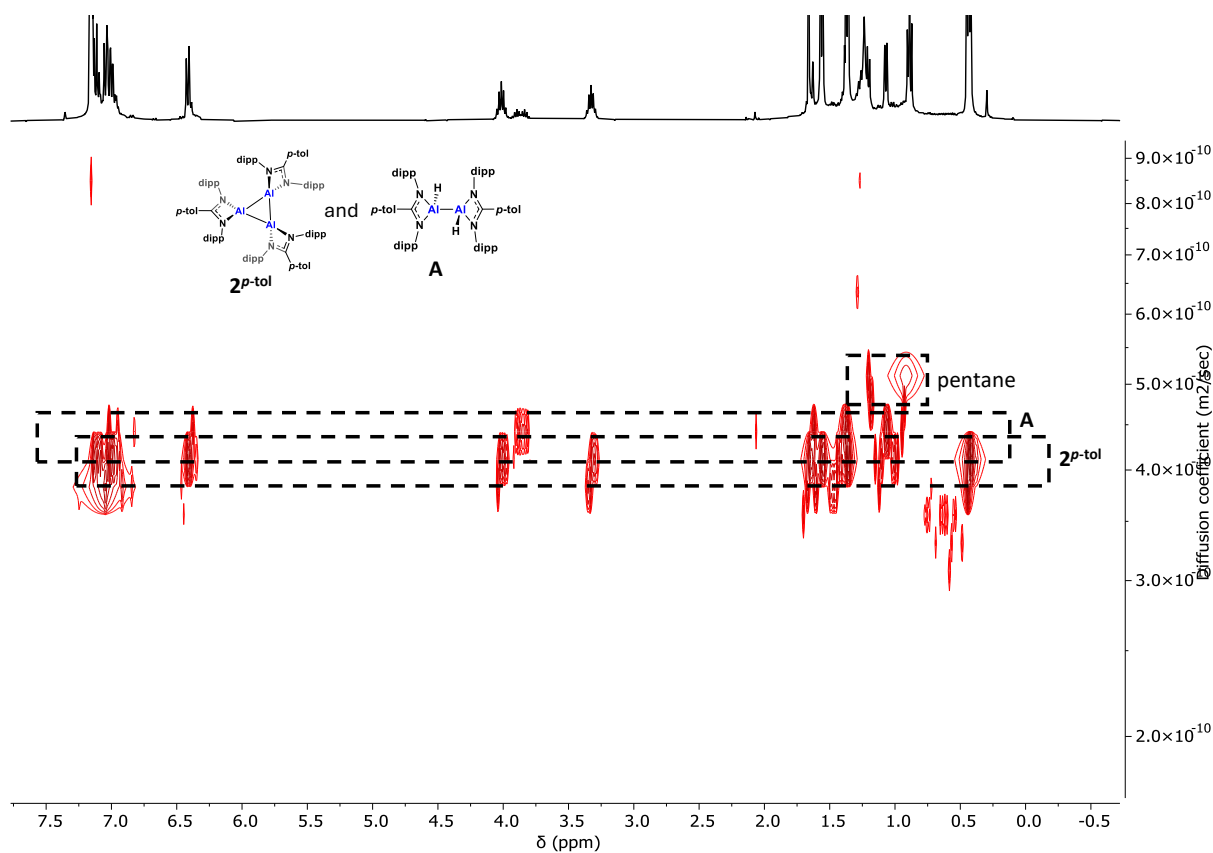


Figure S 7: DOSY NMR spectrum showing a larger diffusion coefficient for **2^{p-tol}** than **A**.

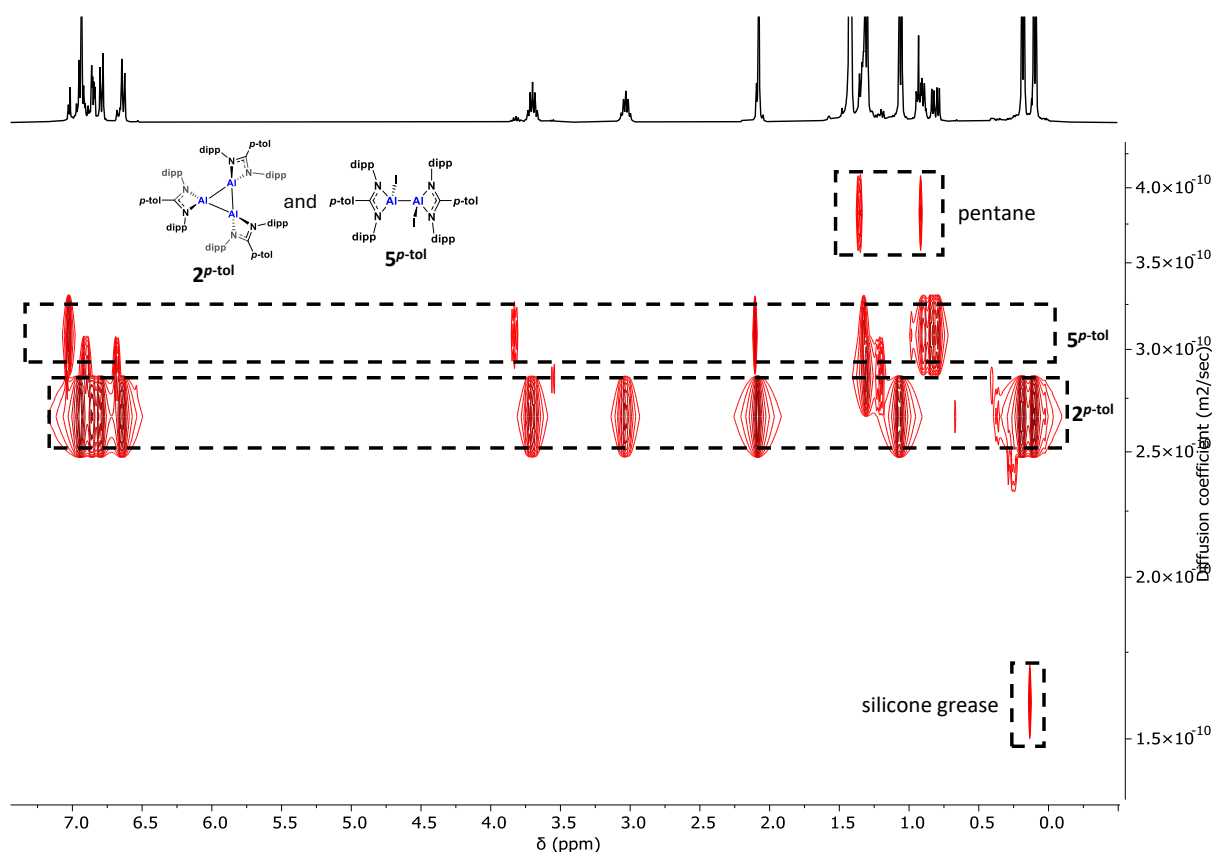


Figure S 8: DOSY NMR spectrum showing a larger diffusion coefficient for **2^{p-tol}** than **5^{p-tol}**.

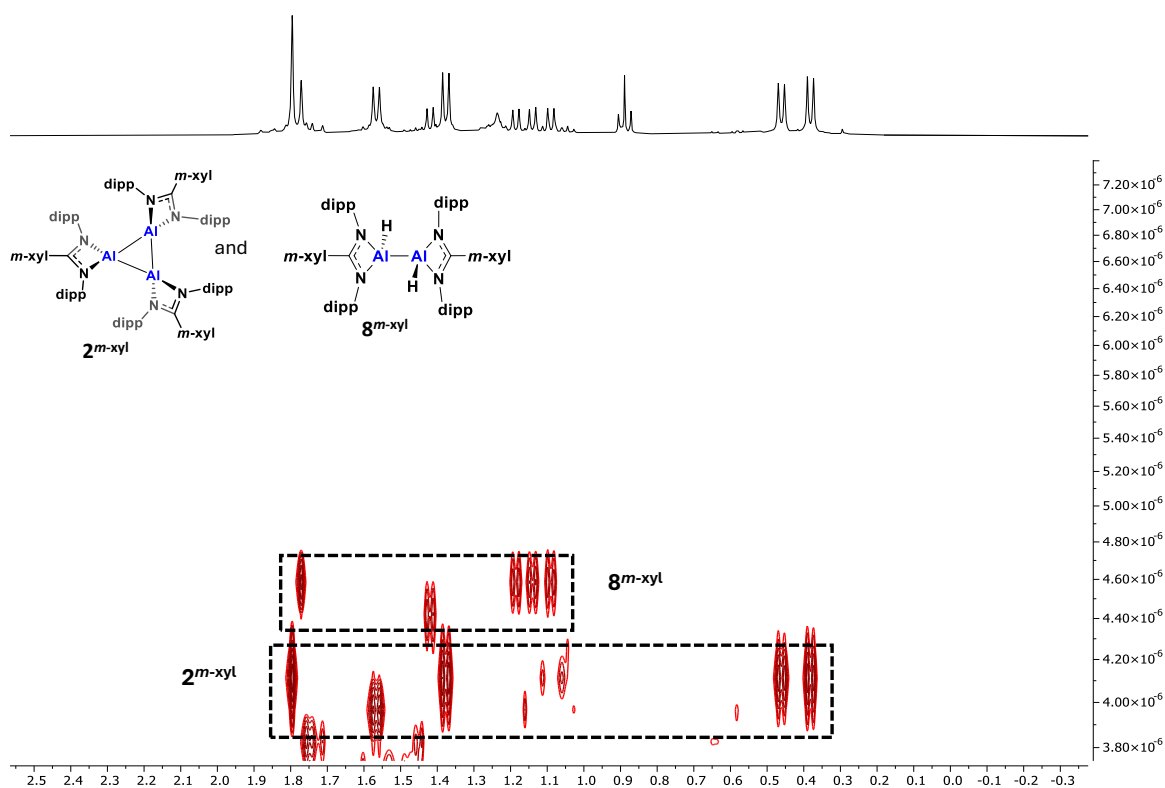


Figure S 9: DOSY NMR spectrum at 25 °C in benzene-*d*₆ of **2^{m-xyl}** and **8^{m-xyl}** showing differing diffusion coefficients.

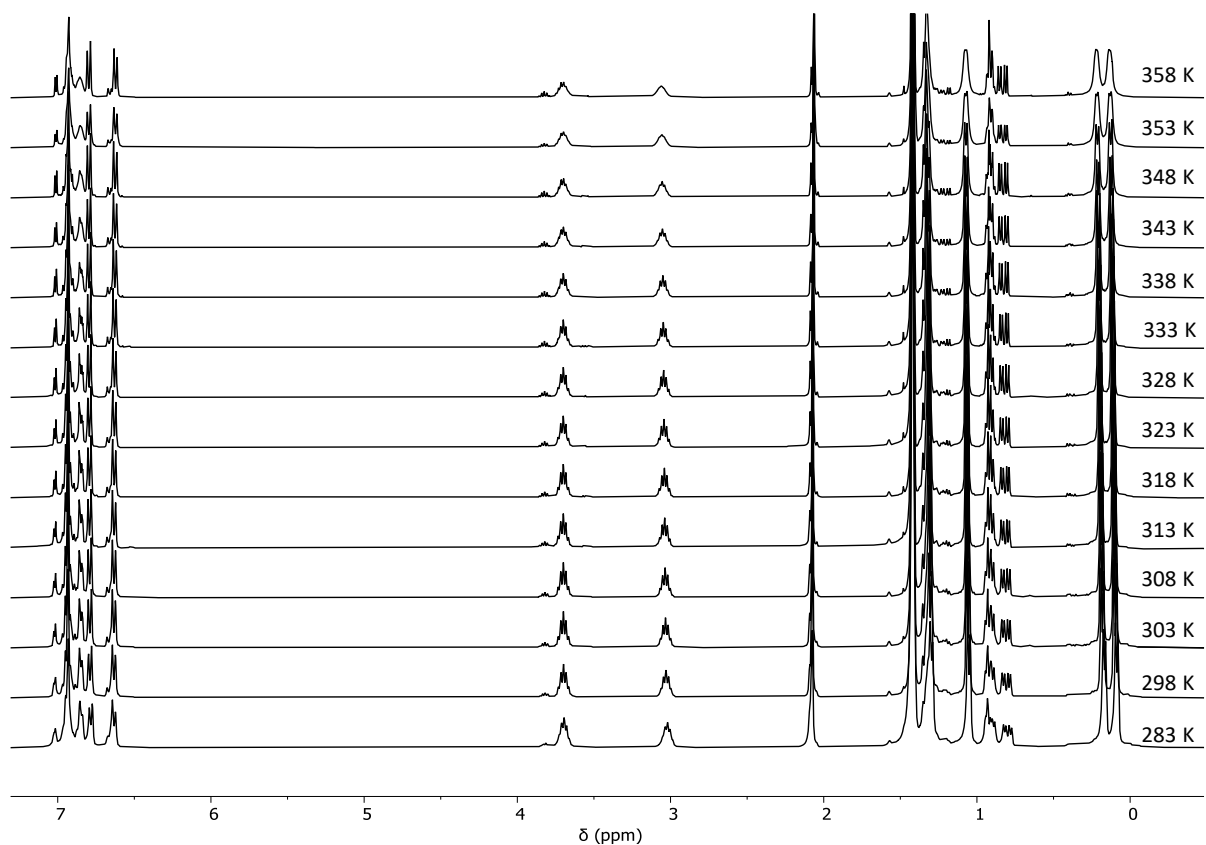


Figure S 10: ^1H VT-NMR experiment of $2^{p\text{-tol}}$ in C_6D_6 (283–358 K) showing no evidence of dissociation of the trimer up to 358 K.

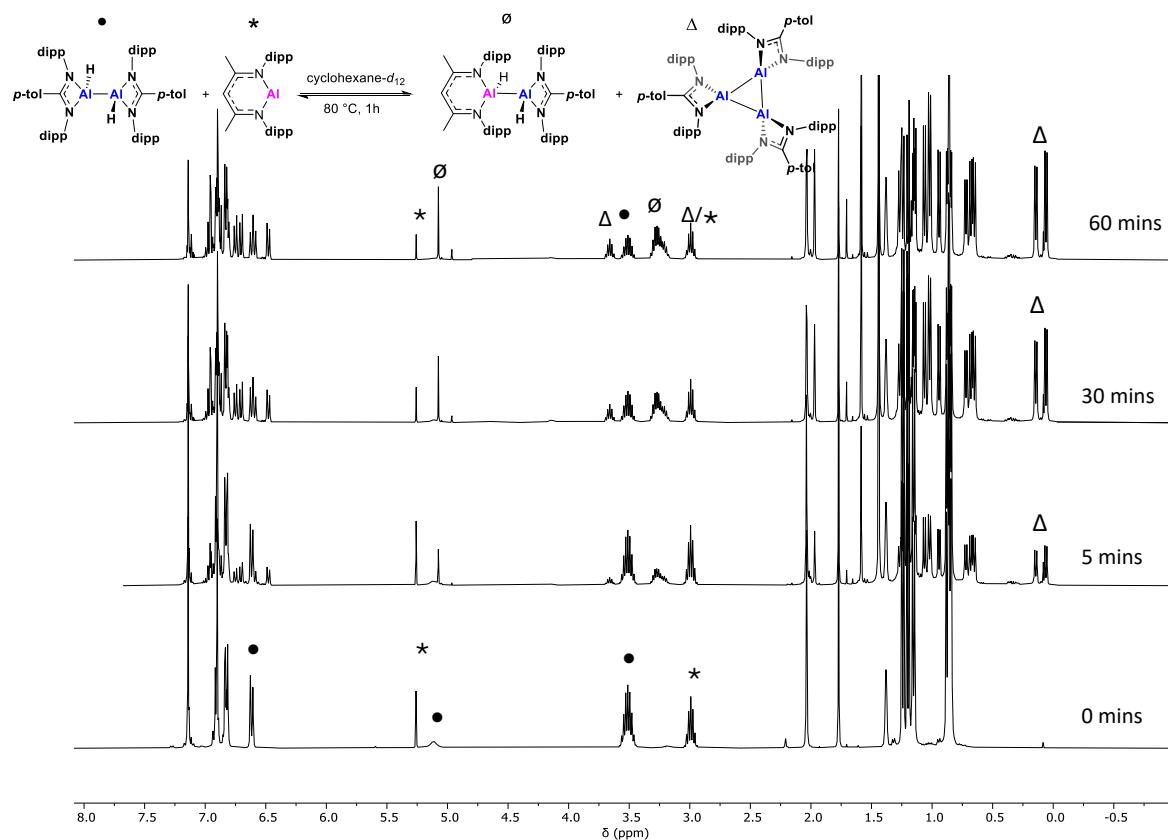


Figure S 11: ^1H NMR spectra showing reaction progress for route 2 synthesis of $2^{p\text{-tol}}$.

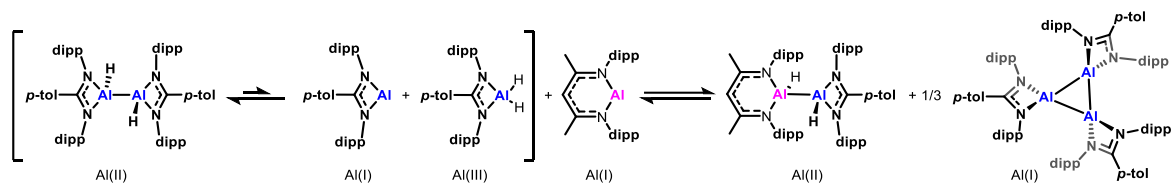


Figure S 12: Reaction scheme showing putative disproportionation of **A** and subsequent trimerisation forming **2^{*p-tol*}**.

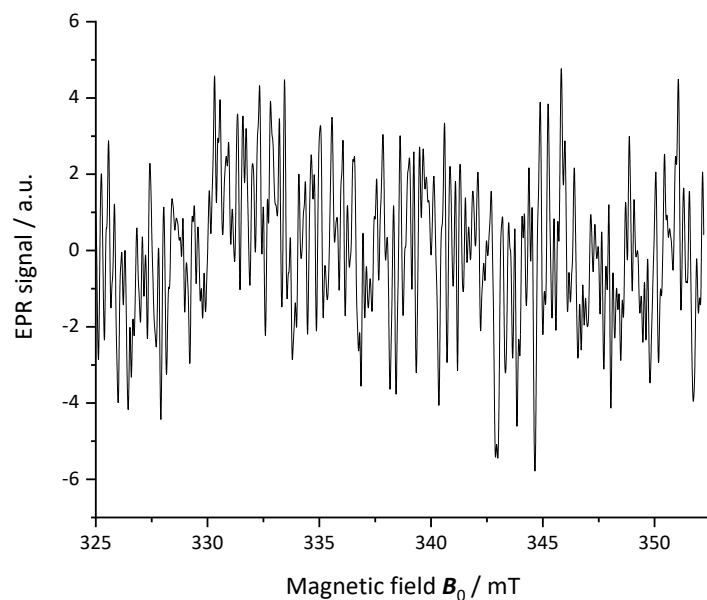


Figure S 13: EPR spectrum of **2^{*p-tol*}** in 3-methylcyclopentane, RT, 1 mW, 0.02 mT, showing no signal.

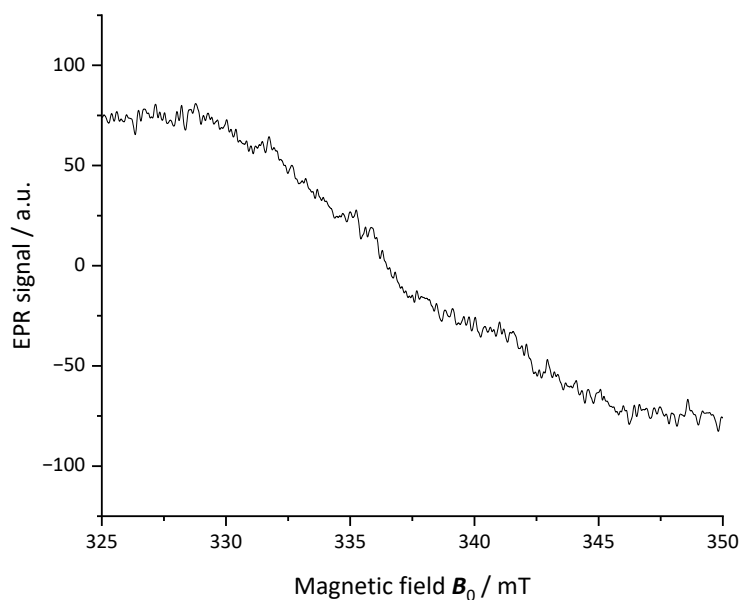


Figure S 14: EPR spectrum of **2^{*p-tol*}** in 3-methylcyclopentane, RT, 10mW, 1mT, showing no signal.

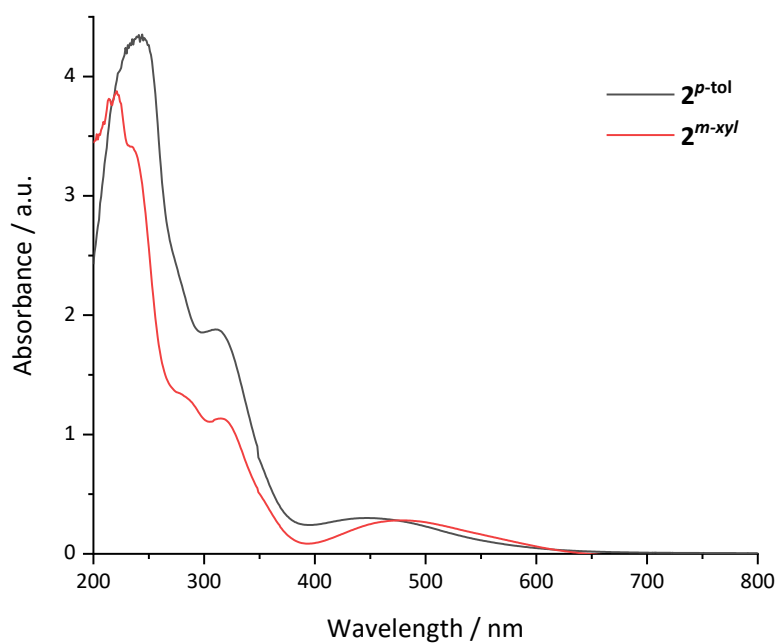


Figure S 15: Experimental UV-vis of **2^{p-tol}** and **2^{m-xyI}** (cyclohexane solution).

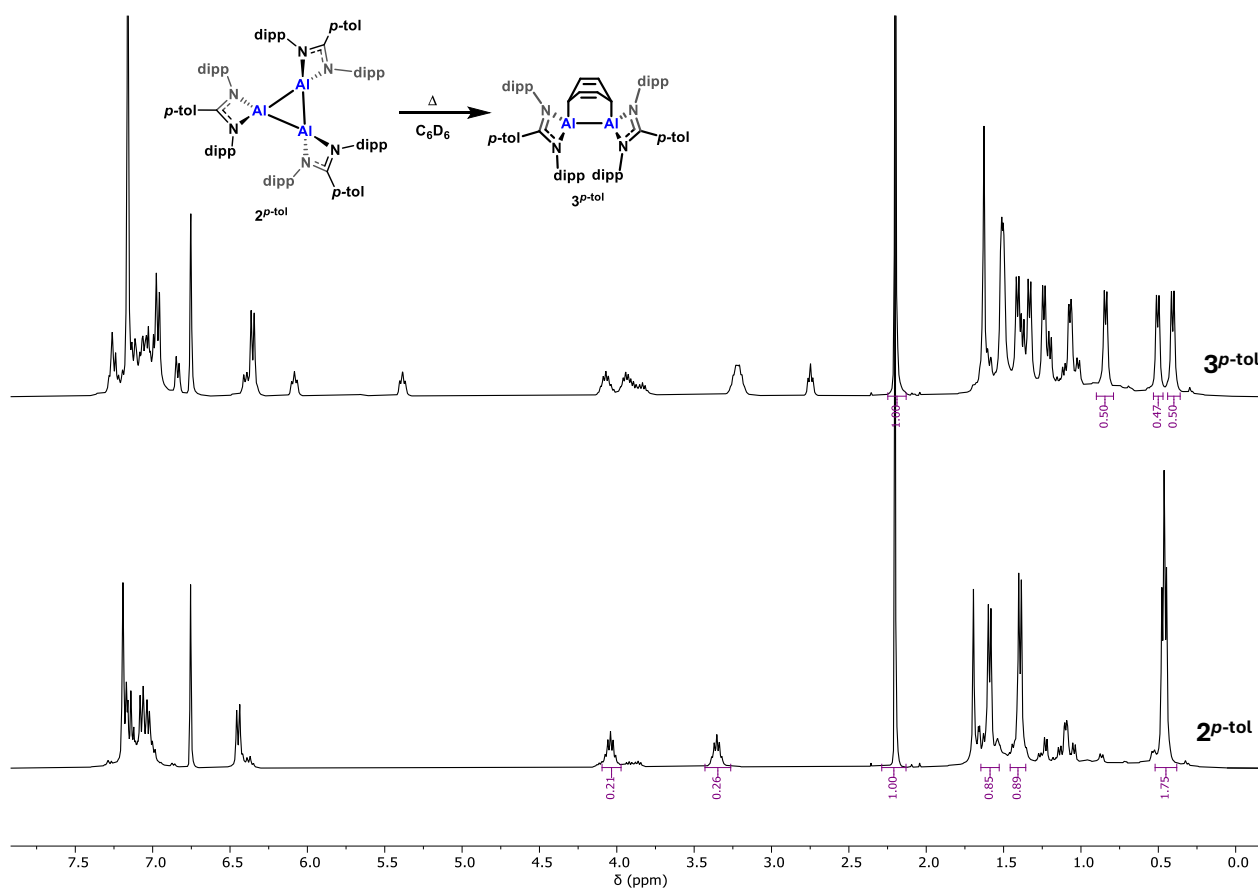


Figure S 16: ^1H NMR spectra showing **2^{p-tol}** before and after heating in benzene (non-deuterated) for 2 hours at 80 °C.

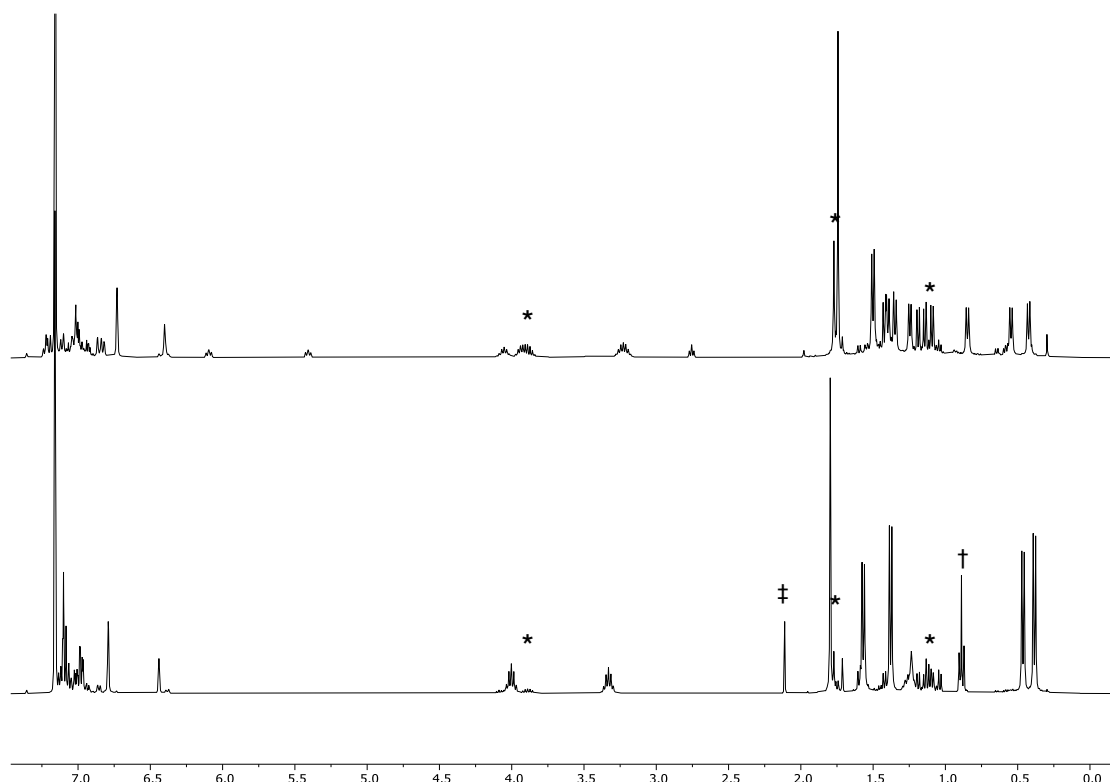


Figure S 17: ^1H NMR spectra showing $2^{\text{m-xyly}}$ prior to treatment with C_6H_6 (below, some $8^{\text{m-xyly}}$ impurity, marked with stars, and pentane (†) and toluene (‡) impurities) and subsequent to heating to $80\text{ }^\circ\text{C}$ for 2 hours (above, some $8^{\text{m-xyly}}$ impurity, marked with stars).

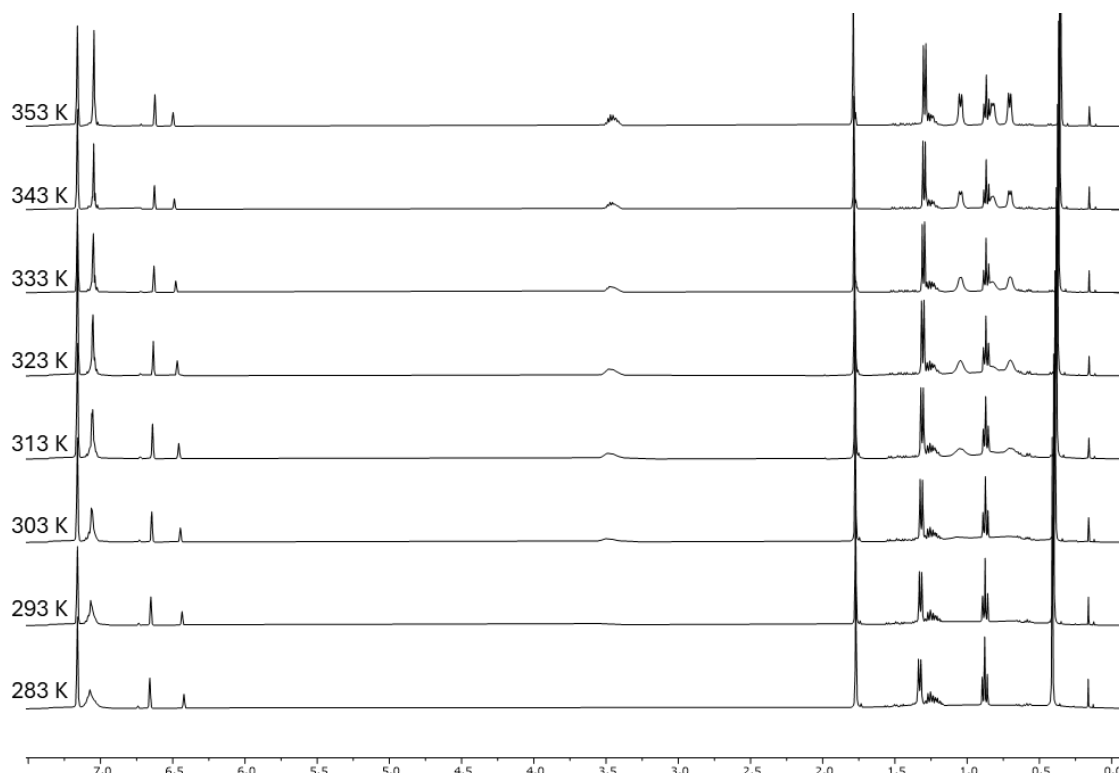


Figure S 18: ^1H VT NMR experiment of $6^{\text{m-xyly}}$ in benzene- d_6 (283-353 K) showing resolution of broad resonances corresponding to the iso-propyl protons.

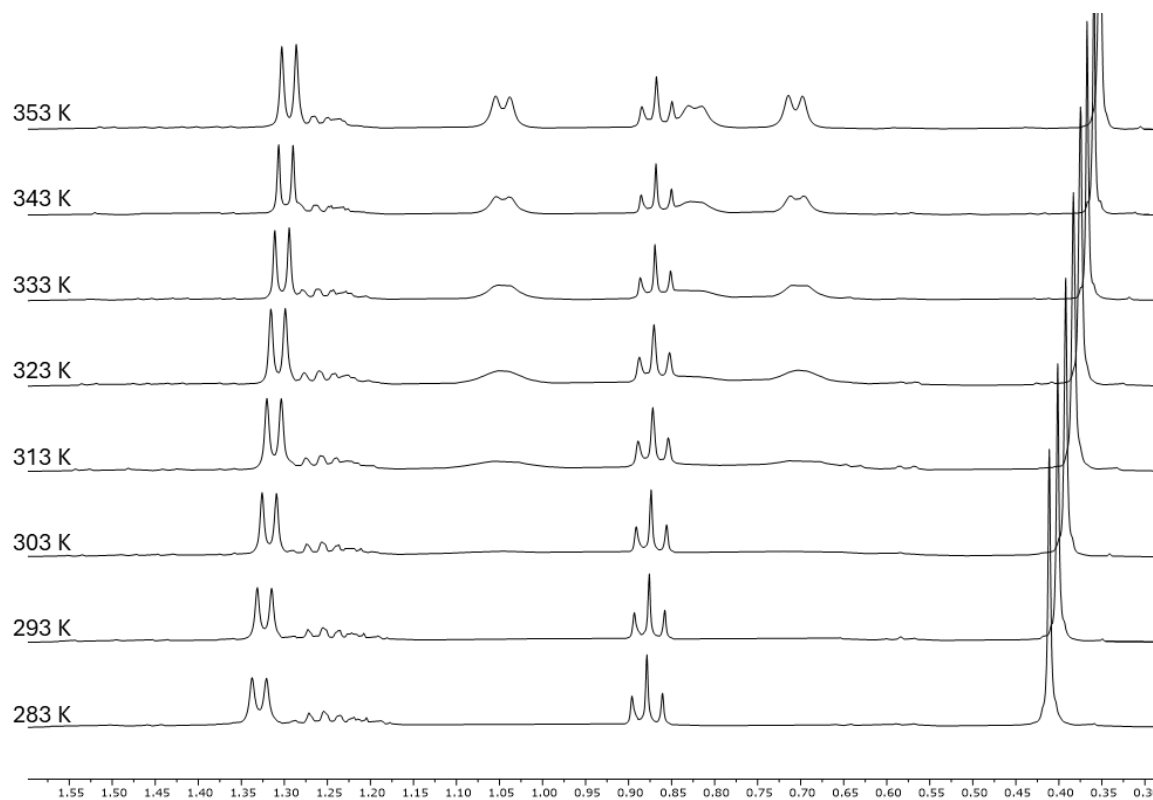


Figure S 19: ^1H VT NMR experiment of $6^{m\text{-xyI}}$ in benzene- d_6 (283-353 K) the region 0.30-1.60 ppm showing resolution of broad resonances corresponding to the iso-propyl protons.

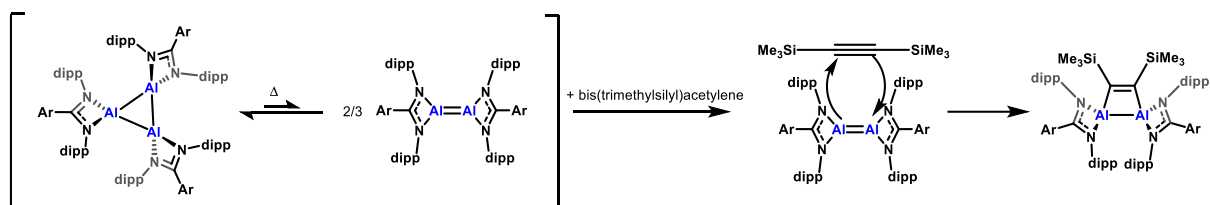


Figure S 20: Proposed [2+2] cycloaddition of a transiently formed dialumene from dissociated trimer and TMS acetylene.

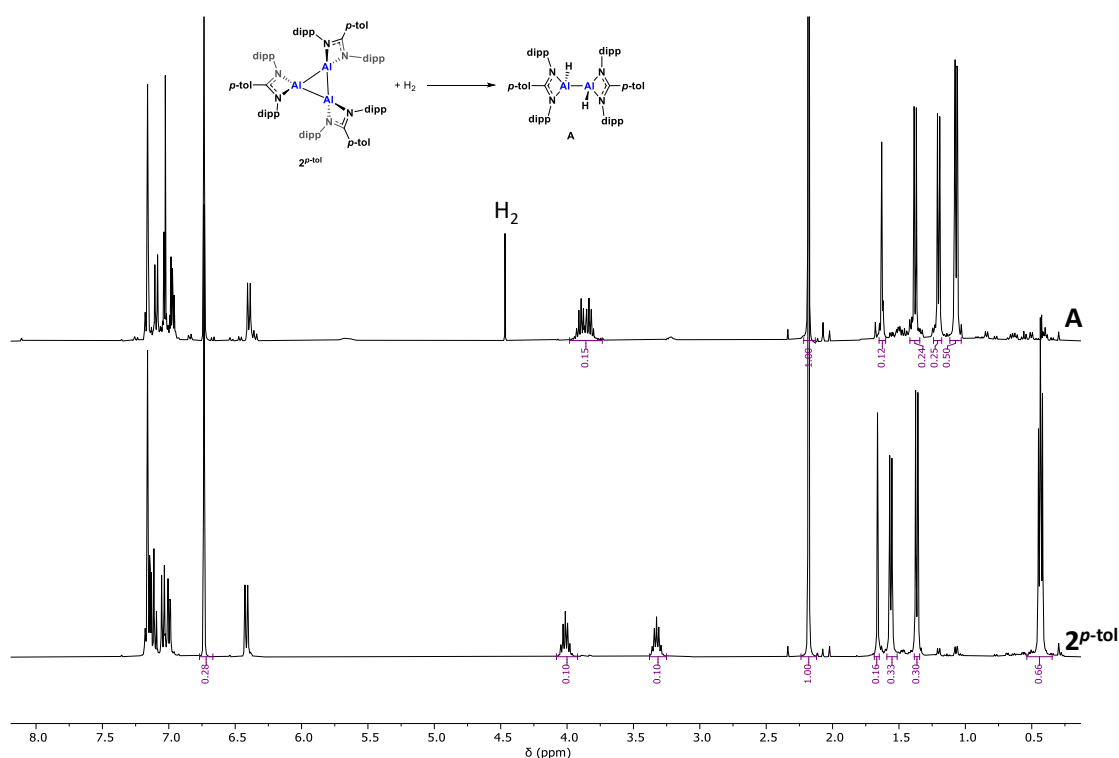


Figure S 21: ^1H NMR spectra with mesitylene internal standard of reaction from $2^{p\text{-tol}}$ to form A.

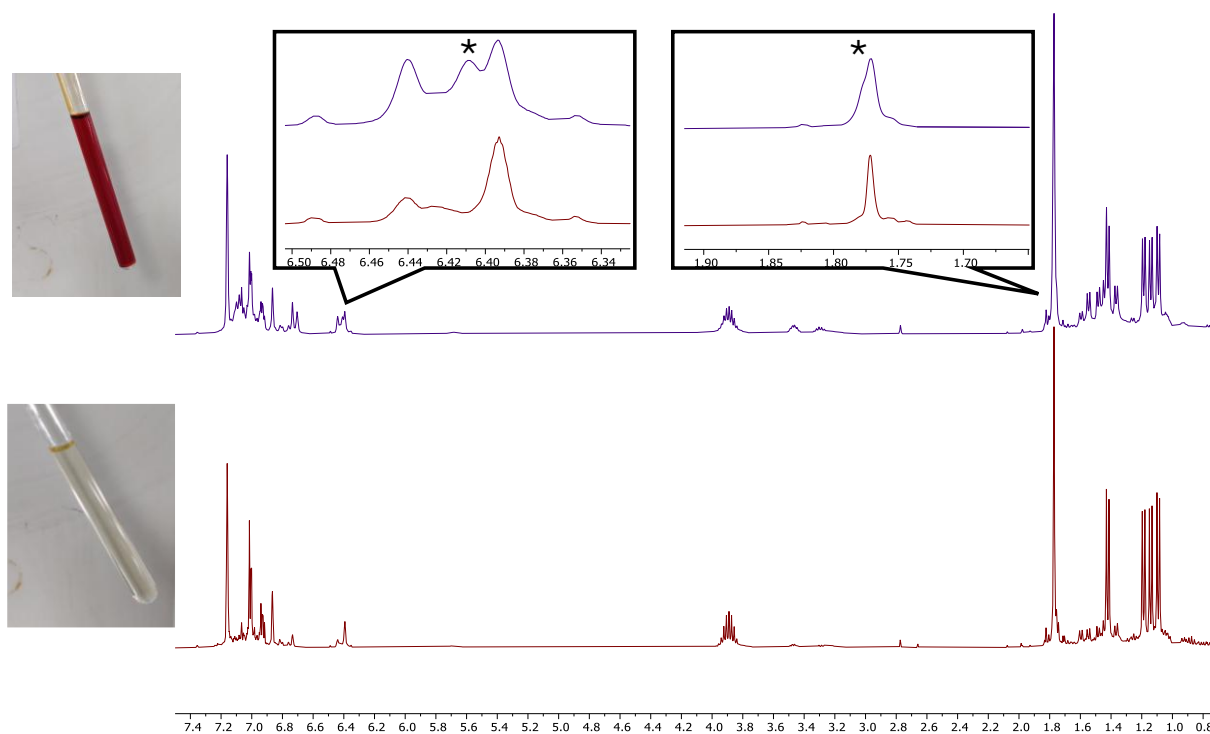


Figure S 22: Stacked ^1H NMR (500 MHz, 298 K) spectra of $8^{m\text{-xyl}}$ (bottom) and $8^{m\text{-xyl}}$ immediately subsequent to H_2 addition to $2^{m\text{-xyl}}$ showing evidence of intermediate species (inset, top, starred resonances). It is notable that only resonances corresponding to meta-xylyl protons are observed, potentially indicating a cluster-type species. Images of NMR tubes showing notable red colour where intermediate species is present.

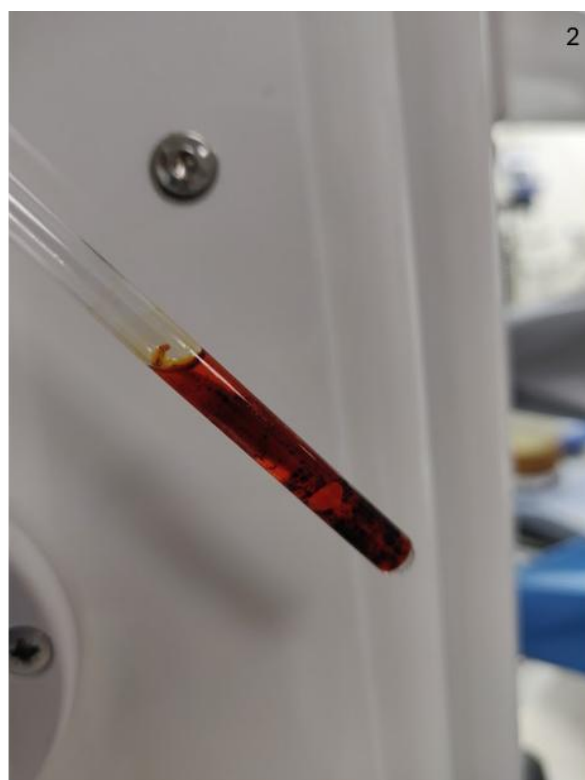


Figure S 23: Colour progression of the reaction of 2^{m-xyI} immediately subsequent to the addition of 1 bar of ethylene gas to afford 9^{m-xyI} .

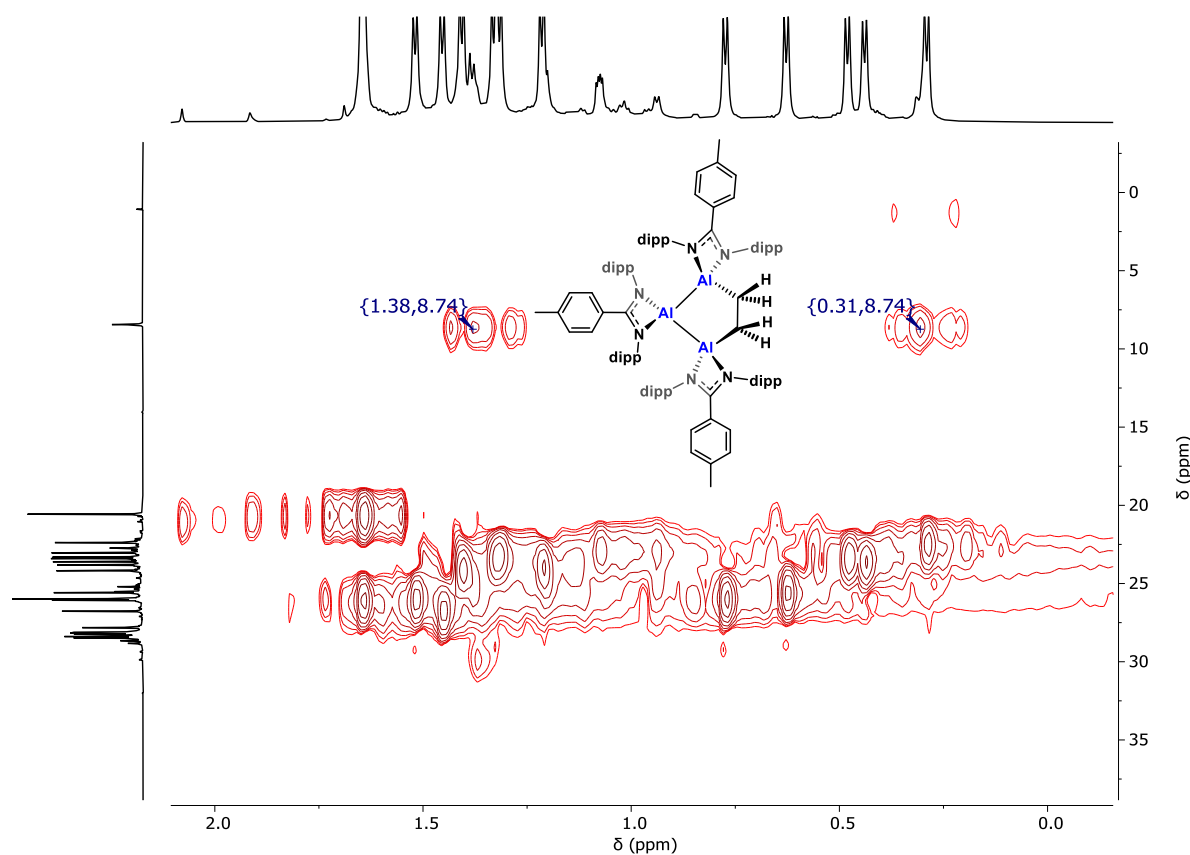


Figure S 24: HSQC of compound **9^{p-tol}** with C-H resonances from ethylene fragment marked.

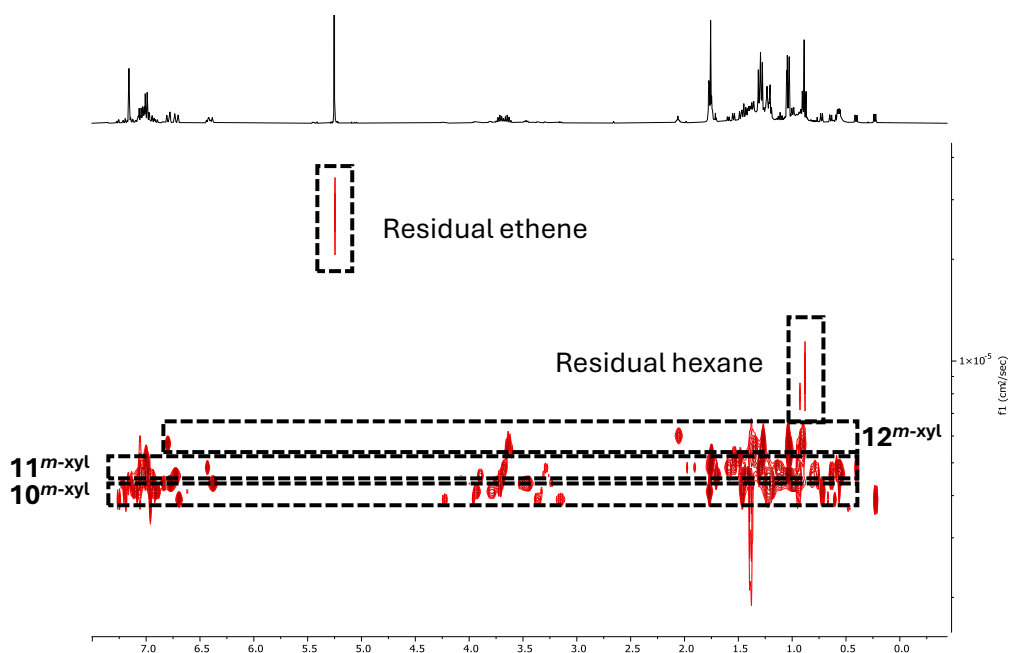


Figure S 25: DOSY NMR spectrum at 25 °C in benzene- d_6 of **10**, **11** and **12^{m-xyl}** showing differing diffusion coefficients for all three species.

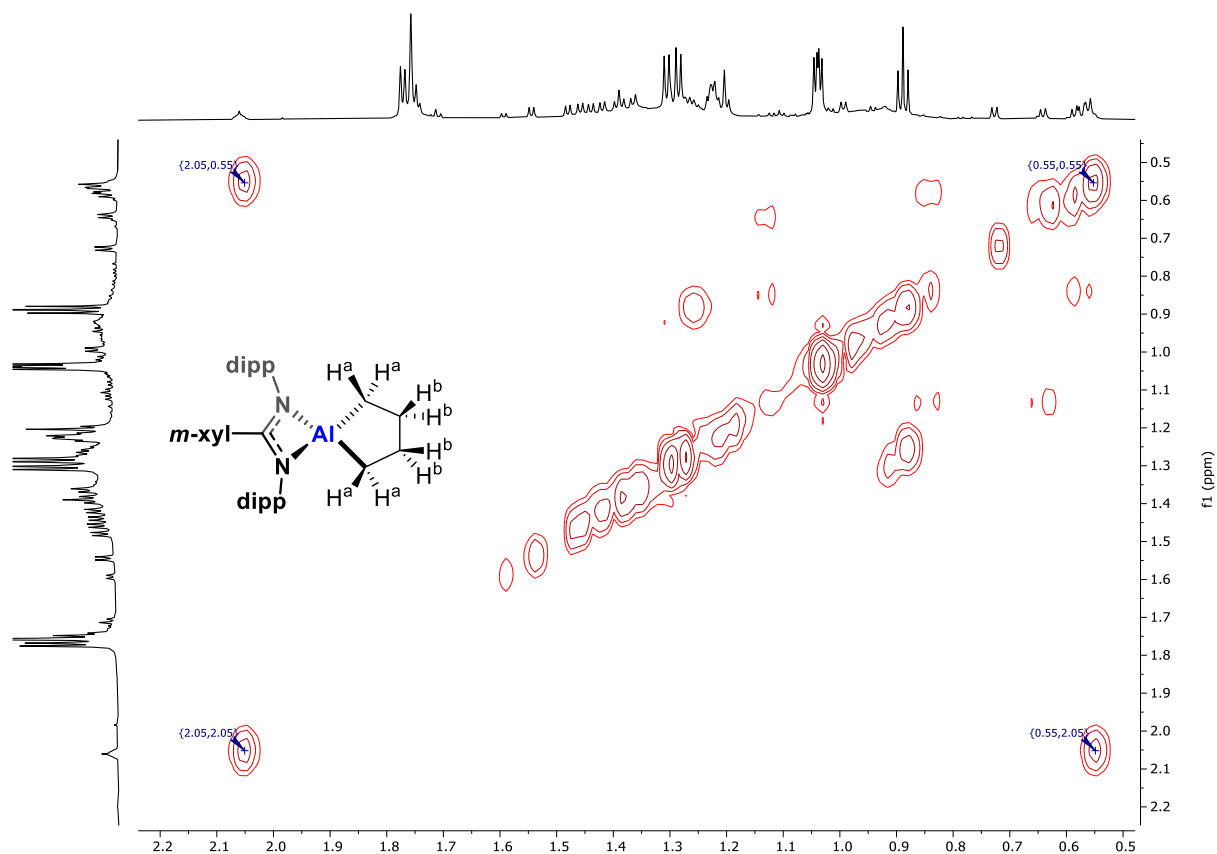


Figure S 26: ^1H - ^1H COSY NMR spectrum showing crosspeaks indicating coupling between resonances at 0.55 and 2.05 ppm, corresponding to the AlCH_2CH_2 and AlCH_2CH_2 protons, respectively, from a mixture of **10**, **11** and **12^{m-xyl}**.

4. X-ray crystallographic data

All experiments were performed at 150 K or 120 K using a Cu K α radiation source ($\lambda = 1.54184$ Å) or at 100 K using Mo K α ($\lambda = 0.7107$ Å) radiation. Measurements on compounds **2^{m-xyI}**-**1**, **9^{m-xyI}** and **10^{m-xyI}** were made using a twin-source Agilent Oxford Diffraction SuperNova diffractometer with a micro-focus Cu K α X-ray beam (50 kV, 0.8 mA) and an Atlas CCD detector. Measurements on **2^{p-tol}** were performed using a twin-source Oxford Xcalibur Gemini diffractometer with a Sapphire 3 CCD plate. The crystal structures of **1^{p-tol}**, **2^{p-tol}**-**1**, **5^{p-tol}**, **5^{m-xyI}**, **2^{m-xyI}**, **8^{m-xyI}** and **11^{m-xyI}** were obtained using a Synergy-S diffractometer equipped with a Dectris Eiger2 1M detector. Cell refinement, data collection and data reduction for all experiments were performed using Rigaku CrysAlisPro.⁹ All structures were solved with ShelXT¹⁰ and ShelXL¹¹, both programs implemented within the Olex2¹² suite. All atoms, except hydrogen, had atomic coordinates and anisotropic thermal parameters refined to convergence using least-square methods on F². Only hydrogen atoms bound to carbons are present, and they were placed in geometric positions and refined with riding modes.

Single crystal X-ray data for 1^{p-tol}

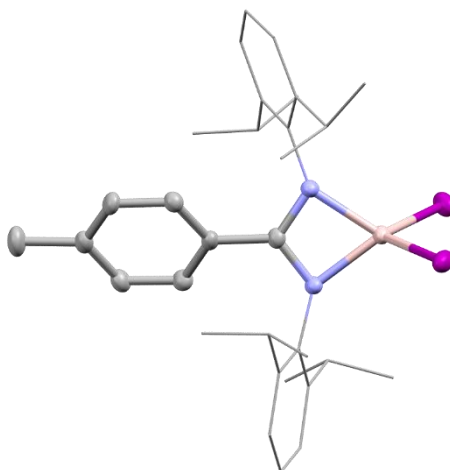


Figure S 27: The solid-state structure of **1^{p-tol}**. Hydrogen atoms omitted for clarity, key atoms shown as thermal ellipsoids at 50% probability.

Single crystals of **1^{p-tol}** were grown from slow evaporation of a saturated toluene solution. **1^{p-tol}** was found to crystallise in the $P2_1/c$ space group. The unit cell contained four molecules of toluene. $C_{39}H_{49}AlI_2N_2$ ($M = 826.58$ g/mol): monoclinic, space group $P2_1/c$ (no. 14), $a = 13.4874(5)$ Å, $b = 18.0877(5)$ Å, $c = 16.4750(4)$ Å, $\beta = 104.851(3)^\circ$, $V = 3884.9(2)$ Å³, $Z = 4$, $T = 100.0(5)$ K, $\mu(\text{Mo K}\alpha) = 1.669$ mm⁻¹, $D_{\text{calc}} = 1.413$ g/cm³, 28221 reflections measured ($4.504^\circ \leq 2\theta \leq 61.866^\circ$), 9424 unique ($R_{\text{int}} = 0.0479$, $R_{\text{sigma}} = 0.0521$) which were used in all calculations. The final R_1 was 0.0371 ($I > 2\sigma(I)$) and wR_2 was 0.0981 (all data). CCDC deposition number 2469911.

Table S 1: Selected bond lengths (Å) for **1^{p-tol}**

Al(1)-I(1)	Al(1)-I(2)	Al(1)-N(1)	Al1-N2
2.4934(8)	2.4903(8)	1.890(2)	1.898(2)

Table S 2: Selected angles (°) for **1^{p-tol}**

N(1)-Al(1)-N(2)	N(1)-C(1)-N(2)
70.78(9)	35.52(13)

Single crystal X-ray data for **2^{p-tol} – first polymorph**

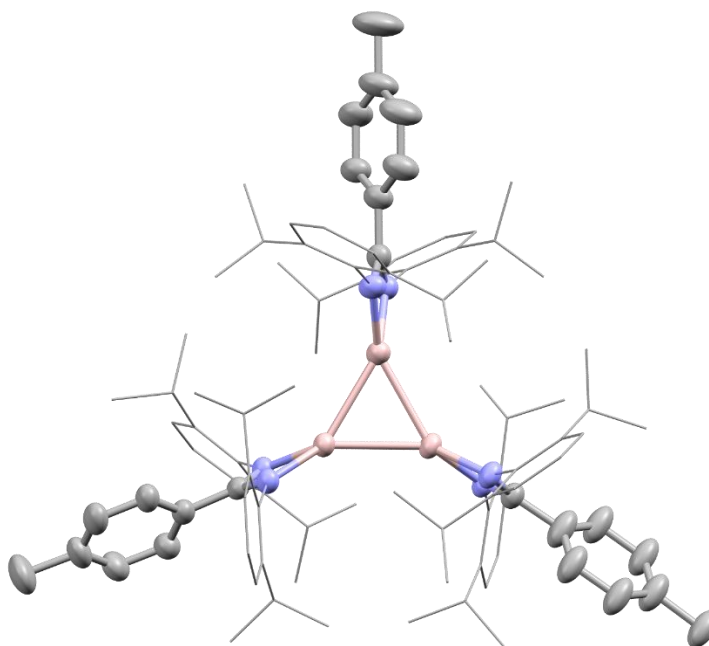


Figure S 28: The solid-state structure of **2^{p-tol}-A**. Hydrogen atoms, second molecule **2^{p-tol}-B** and disorder omitted for clarity, key atoms shown as thermal ellipsoids at 50% probability.

Single crystals of **2^{p-tol}** were grown by cooling a saturated hexane solution. **2^{p-tol}** was found to crystallise in the $P\bar{1}$ space group, with two molecules in the unit cell (**2^{p-tol}-A** and **2^{p-tol}-B**). A solvent mask (SQUEEZE) was applied to remove the electron density of 4 hexanes per unit cell. There was disorder across 4 diisopropyl groups, each of which were modelled across two positions.

There is residual electron density located off the Al-Al bonds in both molecules, corresponding to an average weight of 0.48 for **2^{p-tol}-A** and 0.42 for **2^{p-tol}-B**. This density is also seen when the solvent mask (SQUEEZE) is removed. While modelling this density as a hydride can lead to a stable refinement, the density is better explained by the electron rich Al-Al bonding interactions (see Section 5).

C₂₁₆H₃₀₂Al₆N₁₂ (*M* = 3228.56 g/mol): triclinic, space group $P\bar{1}$ (no. 2), *a* = 14.7364(4) Å, *b* = 24.9378(6) Å, *c* = 30.9657(8) Å, α = 70.319(2)°, β = 76.958(2)°, γ = 76.507(2)°, *V* = 10283.8(5) Å³, *Z* = 2, *T* = 150.00(10) K, μ (Cu K α) = 0.681 mm⁻¹, *D*_{calc} = 1.043 g/cm³, 154881 reflections measured (6.506° ≤ 2 θ ≤ 144.986°), 39700 unique (*R*_{int} = 0.0603, *R*_{sigma} = 0.0602) which were used in all calculations. The final *R*₁ was 0.0706 (*I* > 2 σ (*I*)) and *wR*₂ was 0.2160 (all data). CCDC deposition number 2469912.

Table S 3: Selected bond lengths (Å) for **2^{p-tol}-A**

Al(1)-Al(2)	Al(2)-Al(3)	Al(3)-Al(1)			
2.6575(10)	2.6530(12)	2.6308(11)			
Al(1)-N(1)	Al(1)-N(2)	Al(2)-N(3)	Al(2)-N(4)	Al(3)-N(5)	Al(3)-N(6)
1.983(3)	1.960(2)	1.969(2)	1.974(2)	1.977(2)	1.970(2)

Table S 4: Selected bond lengths (Å) for **2^{p-tol}-B**

Al(4)-Al(5)	Al(5)-Al(6)	Al(6)-Al(4)			
2.6641(12)	2.6553(11)	2.6604(10)			
Al(4)-N(7)	Al(4)-N(8)	Al(5)-N(9)	Al(5)-N(10)	Al(6)-N(11)	Al(6)-N(12)
1.992(3)	1.975(2)	1.983(2)	1.980(1)	1.980(2)	1.975(2)

Table S 5: Selected angles (°) for **2^{p-tol}-A**

Al(1)-Al(2)-Al(3)	Al(2)-Al(3)-Al(1)	Al(3)-Al(1)-Al(2)
59.39(3)	60.39(3)	60.22(3)
N(1)-Al(1)-N(2)	N(3)-Al(2)-N(4)	N(5)-Al(3)-N(6)
67.51(10)	67.51(10)	67.35(10)

Table S 6: Selected angles (°) for **2^{p-tol}-B**

Al(4)-Al(6)-Al(5)	Al(4)-Al(5)-Al(6)	Al(5)-Al(4)-Al(6)
60.16(3)	60.02(3)	59.83(3)
N(7)-Al(4)-N(8)	N(9)-Al(5)-N(10)	N(11)-Al(6)-N(12)
67.27(10)	67.12(9)	67.35(10)

Single crystal X-ray data for **2^{p-tol}-1** – second polymorph

A second polymorph of **2^{p-tol}** was observed when growing crystals by fractionally crystallising away from the products of route 2 in hexane (see Figure S 11). **2^{p-tol}-1** crystallised in the $P\bar{1}$ space group, with two molecules in the unit cell. The structure contained disordered hexane, and an attempt was made to apply a solvent mask (SQUEEZE) to remove this, with two voids containing 3.6 and 3.2 molecules of hexane per unit cell. However, due to an issue with the data collection there were 11 missing reflections below Theta(min), which may affect how reliable the mask is. Therefore, the data is included for completeness but is not discussed in detail in the main manuscript.

$C_{212.4}H_{293.6}Al_6N_{12}$ ($M=3176.86$ g/mol): triclinic, space group $P\bar{1}$ (no. 2), $a = 14.6503(2)$ Å, $b = 27.1548(4)$ Å, $c = 28.0602(4)$ Å, $\alpha = 111.6180(10)^\circ$, $\beta = 103.1750(10)^\circ$, $\gamma = 92.5320(10)^\circ$, $V = 10002.9(3)$ Å³, $Z = 2$, $T = 150.0(4)$ K, $\mu(\text{Cu K}\alpha) = 0.693$ mm⁻¹, $D_{\text{calc}} = 1.055$ g/cm³, 126761 reflections measured ($7.074^\circ \leq 2\theta \leq 157.278^\circ$), 40462 unique ($R_{\text{int}} = 0.0467$, $R_{\text{sigma}} = 0.0516$) which were used in all calculations. The final R_1 was 0.0788 ($I > 2\sigma(I)$) and wR_2 was 0.1833 (all data). CCDC deposition number 2469920.

Single crystal X-ray data for $2^{m\text{-xyl}}$

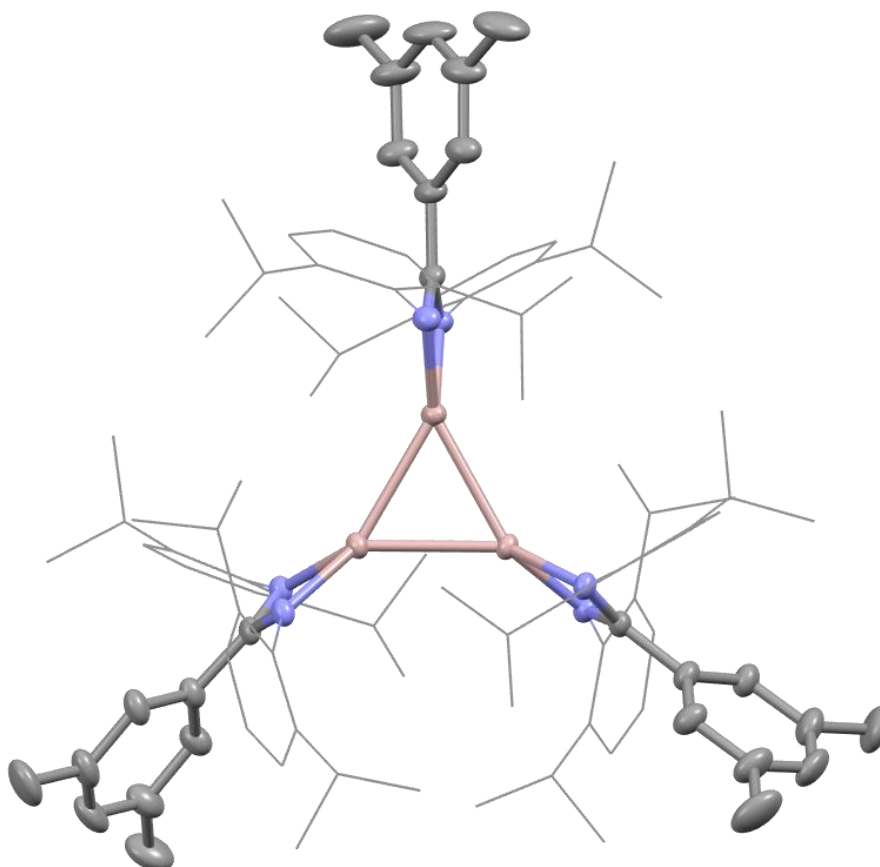


Figure S 29: The solid-state structure of $2^{m\text{-xyl}}$ (Solvent molecules and hydrogen atoms omitted, dipp groups wireframe for clarity, thermal ellipsoids 50% probability).

Single crystals of $2^{m\text{-xyl}}$ were grown from cooling of a saturated toluene solution. $2^{m\text{-xyl}}$ was found to crystallise in the $P2_1/n$ space group. The unit cell contained two molecules of toluene per asymmetric unit.

$C_{113}H_{145}Al_3N_6$ ($M=1668.28$ g/mol): monoclinic, space group $P2_1/n$ (no. 14), $a = 15.42790(10)$ Å, $b = 23.6186(2)$ Å, $c = 28.0831(3)$ Å, $\beta = 96.7170(10)^\circ$, $V = 10162.83(15)$ Å³, $Z = 4$, $T = 100.0(4)$ K, $\mu(\text{Mo K}\alpha) = 0.086$ mm⁻¹, $D_{\text{calc}} = 1.090$ g/cm³, 187504 reflections measured ($5.376^\circ \leq 2\theta \leq 54.204^\circ$), 22378 unique ($R_{\text{int}} = 0.0869$, $R_{\text{sigma}} = 0.0387$) which were used in all calculations. The final R_1 was 0.0668 ($I > 2\sigma(I)$) and wR_2 was 0.1895 (all data). CCDC deposition number 2469913.

Table S 7: Selected bond lengths (Å) for **2^{m-xyI}**

Al(1)-Al(2)	Al(2)-Al(3)	Al(1)-Al(3)			
2.6404(8)	2.6184(8)	2.6502(8)			
Al(1)-N(1)	Al(1)-N(2)	Al(2)-N(3)	Al(2)-N(4)	Al(3)-N(5)	Al(3)-N(6)
1.9744(16)	1.9729(16)	1.9767(16)	1.9605(16)	1.9670(17)	1.9767(16)

Table S 8: Selected angles (°) for **2^{m-xyI}**

Al(1)-Al(2)-Al(3)	Al(2)-Al(3)-Al(1)	Al(3)-Al(1)-Al(2)
60.52(2)	60.15(2)	59.33(2)
N(1)-Al(1)-N(2)	N(3)-Al(2)-N(4)	N(5)-Al(3)-N(6)
67.56(7)	67.70(7)	67.46(6)

Single crystal X-ray data for 2^{m-xyI}-1 – second polymorph

Single crystals of **2^{m-xyI}-1** were grown from the addition of pentane to a saturated toluene solution of **2^{m-xyI}** and subsequent storage at room temperature overnight. **2^{m-xyI}-1** crystallised in the *P*2₁/*n* space group with 2 molecules of pentane in the asymmetric unit, which were modelled using a solvent mask (SQUEEZE). There was disorder over three isopropyl groups, which were modelled over two positions, and one *meta*-xylyl group, which was modelled over two positions.

C₁₀₉H₁₅₃Al₃N₆ (*M* = 1628.30 g/mol): monoclinic, space group *P*2₁/*n* (no. 14), *a* = 15.5037(3) Å, *b* = 23.5791(4) Å, *c* = 27.8912(8) Å, *β* = 96.740(2)°, *V* = 10125.5(4) Å³, *Z* = 4, *T* = 120.00(10) K, *μ*(Cu Kα) = 0.695 mm⁻¹, *D*_{calc} = 1.068 g/cm³, 92142 reflections measured (6.856° ≤ 2θ ≤ 158.454°), 20800 unique (*R*_{int} = 0.1174, *R*_{sigma} = 0.1067) which were used in all calculations. The final *R*₁ was 0.0918 (*I* > 2σ(*I*)) and *wR*₂ was 0.2686 (all data). CCDC deposition number 2469921.

Table S 9: Selected bond lengths (Å) for **2^{m-xyI}-1**

Al(1)-Al(2)	Al(2)-Al(3)	Al(1)-Al(3)			
2.5963(15)	2.6413(17)	2.6046(17)			
Al(1)-N(1)	Al(1)-N(2)	Al(2)-N(3)	Al(2)-N(4)	Al(3)-N(5)	Al(3)-N(6)
1.976(3)	1.955(3)	1.964(3)	1.980(3)	1.964(3)	1.973(3)

Table S 10: Selected angles (°) for **2^{m-xyI}-1**

Al(1)-Al(2)-Al(3)	Al(2)-Al(3)-Al(1)	Al(3)-Al(1)-Al(2)
59.63(4)	59.32(4)	61.04(4)
N(1)-Al(1)-N(2)	N(3)-Al(2)-N(4)	N(5)-Al(3)-N(6)
67.94(13)	67.40(12)	67.32(14)

Single crystal X-ray data for $5^{p\text{-tol}}$

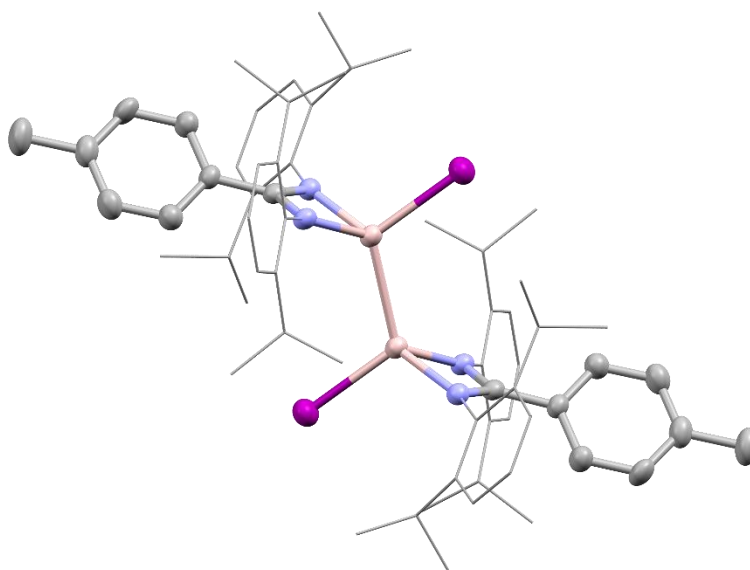


Figure S 30: The solid-state structure of $5^{p\text{-tol}}$. Hydrogen atoms and solvent omitted for clarity, key atoms shown as thermal ellipsoids at 50% probability.

Single crystals of $5^{p\text{-tol}}$ were grown from cooling of a saturated toluene solution. $5^{p\text{-tol}}$ was found to crystallise in the $P2_1/n$ space group. The unit cell contained 4 molecules of toluene per unit cell.

$C_{78}H_{98}N_4Al_2I_2$ ($M = 1399.36$ g/mol): monoclinic, space group $P2_1/n$ (no. 14), $a = 10.49250(10)$ Å, $b = 18.2327(2)$ Å, $c = 19.1795(2)$ Å, $\beta = 98.4090(10)^\circ$, $V = 3629.72(7)$ Å³, $Z = 2$, $T = 151(2)$ K, $\mu(\text{Cu K}\alpha) = 7.362$ mm⁻¹, $D_{\text{calc}} = 1.280$ g/cm³, 71485 reflections measured ($6.724^\circ \leq 2\theta \leq 157.962^\circ$), 7519 unique ($R_{\text{int}} = 0.0948$, $R_{\text{sigma}} = 0.0484$) which were used in all calculations. The final R_1 was 0.0581 ($I > 2\sigma(I)$) and wR_2 was 0.1674 (all data). CCDC deposition number 2469914.

Table S 11: Selected bond lengths (Å) and angles ($^\circ$) for $5^{p\text{-tol}}$

Al(1)-Al(1')	Al(1)-N(1)	Al(1)-N(2)	Al(1)-I(1)
2.604(2)	1.915(3)	1.952(3)	2.5483(10)

Table S 12: Selected bond angles ($^\circ$) for $5^{p\text{-tol}}$

N(1)-Al(1)-N(2)	Al(1')-Al(1)-I(1)
69.15(13)	114.95(6)

Single crystal X-ray data for $5^{m\text{-xyl}}$

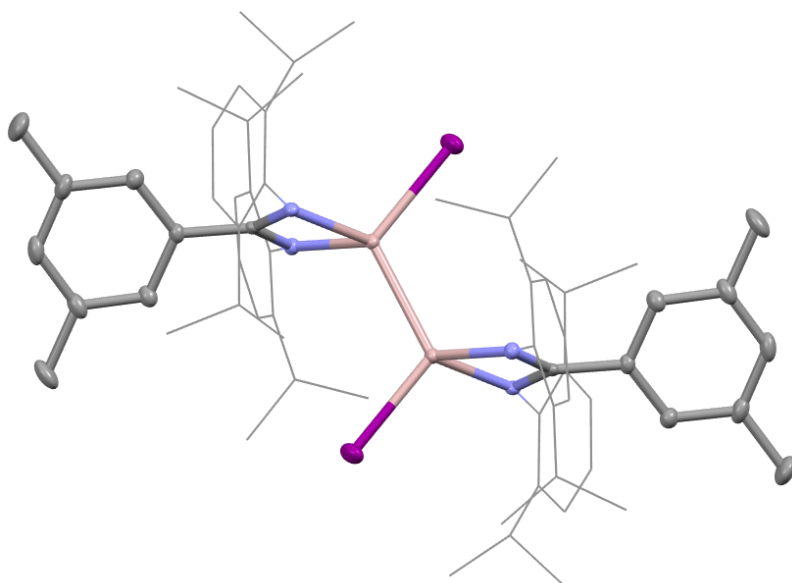


Figure S 31: The solid-state of $5^{m\text{-xyl}}$ (Solvent molecules and hydrogen atoms omitted, dipp groups wireframe for clarity, thermal ellipsoids 50% probability).

Single crystals of $5^{m\text{-xyl}}$ were grown from a benzene solution. $5^{m\text{-xyl}}$ was found to crystallise in the $P\bar{1}$ space group, with half a molecule in the asymmetric unit. The unit cell contained 1 benzene molecule per unit cell.

$C_{72}H_{92}N_4Al_2I_2$ ($M = 1321.25$ g/mol): triclinic, space group $P\bar{1}$ (no. 2), $a = 10.69630(10)$ Å, $b = 12.3546(2)$ Å, $c = 14.0145(2)$ Å, $\alpha = 67.7240(10)^\circ$, $\beta = 77.7910(10)^\circ$, $\gamma = 87.4630(10)^\circ$, $V = 1673.70(4)$ Å³, $Z = 1$, $T = 100.0(5)$ K, $\mu(\text{Mo K}\alpha) = 1.009$ mm⁻¹, $D_{\text{calc}} = 1.311$ g/cm³, 27224 reflections measured ($4.5^\circ \leq 2\theta \leq 61.906^\circ$), 8463 unique ($R_{\text{int}} = 0.0511$, $R_{\text{sigma}} = 0.0409$) which were used in all calculations. The final R_1 was 0.0335 ($I > 2\sigma(I)$) and wR_2 was 0.0928 (all data). CCDC deposition number 2469915.

Table S 13: Selected bond lengths (Å) and angles (°) for $5^{m\text{-xyl}}$

Al(1)-Al(1')	Al(1)-N(1)	Al(1)-N(2)	Al(1)-I(1)
2.5832(12)	1.9540(17)	1.9272(18)	2.5353(6)

Table S 14: Selected bond angles (°) for $5^{m\text{-xyl}}$

N(1)-Al(1)-N(2)	Al(1')-Al(1)-I(1)
68.82(7)	115.15(3)

Single crystal X-ray data for $6^{m\text{-xyl}}$

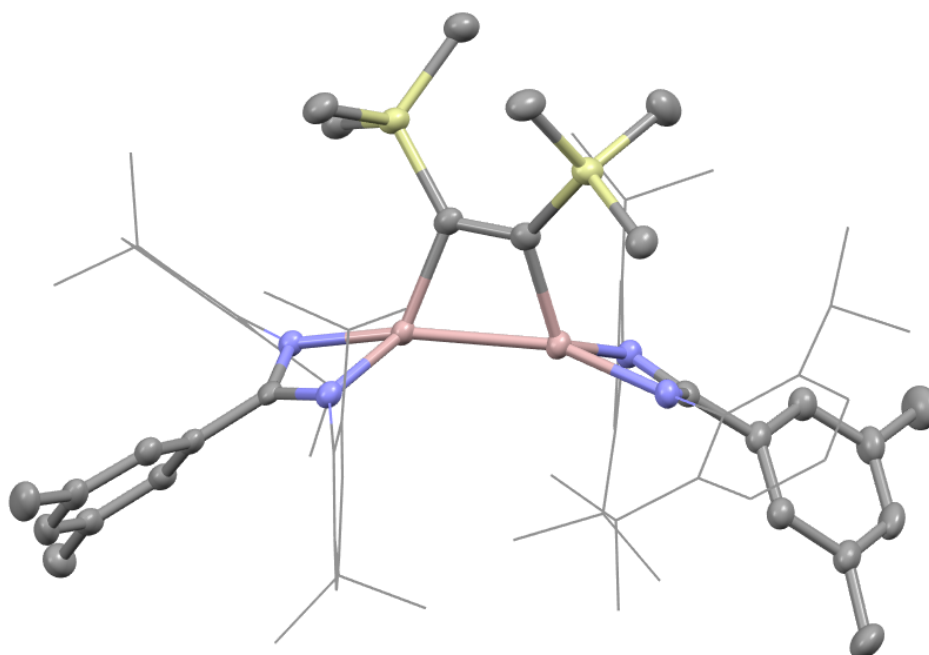


Figure S 32: The solid-state structure of $6^{m\text{-xyl}}$ (Solvent molecules and hydrogen atoms omitted, displacement ellipsoids 50% probability).

Single crystals of $6^{m\text{-xyl}}$ were grown from slow evaporation of a pentane solution. $6^{m\text{-xyl}}$ was found to crystallise in the $P\bar{1}$ space group. The unit cell contained 3 pentane molecules per unit cell, 1 of which was modelled using a solvent mask (SQUEEZE).

$C_{81.5}H_{122}Al_2N_4Si_2$ ($M = 1231.89$ g/mol): triclinic, space group $P\bar{1}$ (no. 2), $a = 12.1557(3)$ Å, $b = 12.6838(3)$ Å, $c = 26.0278(7)$ Å, $\alpha = 96.274(2)^\circ$, $\beta = 96.202(2)^\circ$, $\gamma = 92.214(2)^\circ$, $V = 3960.43(17)$ Å³, $Z = 2$, $T = 100.00(10)$ K, $\mu(\text{Mo K}\alpha) = 0.108$ mm⁻¹, $D_{\text{calc}} = 1.033$ g/cm³, 49617 reflections measured ($5.436^\circ \leq 2\theta \leq 61.998^\circ$), 19497 unique ($R_{\text{int}} = 0.0590$, $R_{\text{sigma}} = 0.0950$) which were used in all calculations. The final R_1 was 0.0635 ($I > 2\sigma(I)$) and wR_2 was 0.1435 (all data). CCDC deposition number 2469916.

Table S 15: Selected bond lengths (Å) for **6^{m-xy}**

Al(1)-Al(2) 2.5462(9)			
Al(1)-N(1) 1.9594(17))	Al(1)-N(2) 1.9866(18)	Al(2)-N(3) 1.9795(17)	Al(2)-N(4) 1.9651(18)
Al(1)-C(64) 2.003(2)	Al(2)-C(65) 2.002(2)		
Si(1)-C(64) 1.872(2)	Si(2)-C(65) 1.871(2)	C(64)-C(65) 1.378(3)	

Table S 16: Selected bond angles and torsions (°) for **6^{m-xy}**

N(1)-Al(1)-N(2) 67.55(7)	N(3)-Al(2)-N(4) 67.27(7)	
Al(1)-C(64)-C(65) 104.8(1)	Al(2)-C(65)-C(64) 105.0(1)	Al(1)-C(64)-C(65)-Al(2) 24.6(2)

Single crystal X-ray data for **9^{m-xy}**

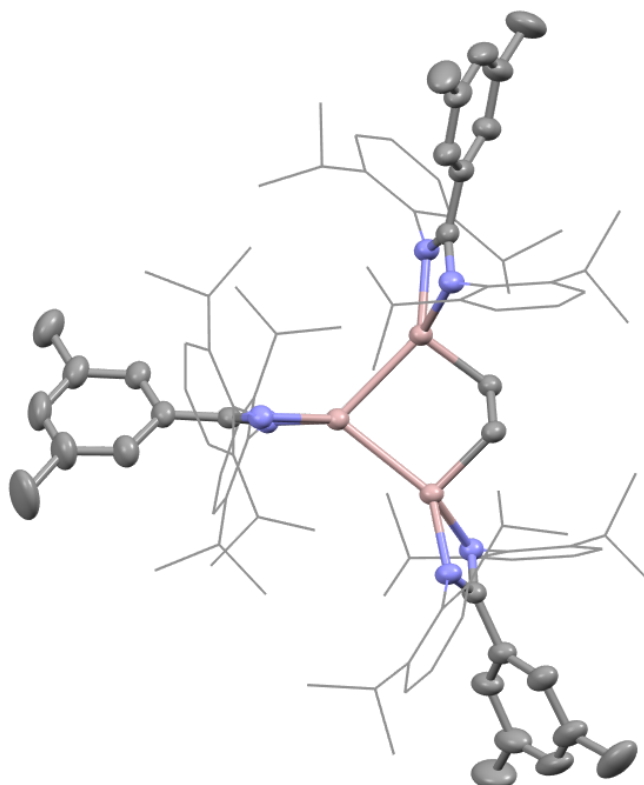


Figure S 33: The solid-state structure of **9^{m-xy}** (Solvent molecules and hydrogen atoms omitted, dipp groups wireframe for clarity, thermal ellipsoids 50% probability).

Single crystals of **9^{m-xyI}** were grown from slow evaporation of a heptane solution. **9^{m-xyI}** was found to crystallise in the $P2_1/n$ space group. The unit cell contained 4 heptane molecules per unit cell, which were modelled using a solvent mask (SQUEEZE).

$C_{108}H_{149}Al_3N_6$ ($M = 1612.26$ g/mol): monoclinic, space group $P2_1/n$ (no. 14), $a = 15.05770(10)$ Å, $b = 44.0378(3)$ Å, $c = 15.49930(10)$ Å, $\beta = 98.5230(10)^\circ$, $V = 10164.21(12)$ Å³, $Z = 4$, $T = 150.03(10)$ K, $\mu(\text{Cu K}\alpha) = 0.689$ mm⁻¹, $D_{\text{calc}} = 1.054$ g/cm³, 276913 reflections measured ($7.026^\circ \leq 2\theta \leq 159.416^\circ$), 21278 unique ($R_{\text{int}} = 0.0742$, $R_{\text{sigma}} = 0.0275$) which were used in all calculations. The final R_1 was 0.0497 ($I > 2\sigma(I)$) and wR_2 was 0.1252 (all data). CCDC deposition number 2469917.

Table S 17: Selected bond lengths and distances (Å) for **9^{m-xyI}**

Al(1)-Al(2)	Al(1)-Al(3)	Al(2)-Al(3)			
2.6651(9)	2.6269(8)	3.5358(6)			
Al(1)-N(1)	Al(1)-N(2)	Al(2)-N(3)	Al(2)-N(4)	Al(3)-N(5)	Al(3)-N(6)
1.955(1)	1.983(2)	1.984(1)	1.976(1)	1.967(1)	1.971(1)
Al(2)-C(100)	Al(3)-C(101)	C(100)-C(101)			
1.984(2)	1.979(2)	1.557(2)			

Table S 18: Selected bond angles and torsions (°) for **9^{m-xyI}**

Al(2)-Al(1)-Al(3)	N(1)-Al(1)-N(2)	N(3)-Al(2)-N(4)	N(5)-Al(3)-N(6)
83.84(3)	67.65(6)	67.51(5)	67.63(6)
Al(2)-C(100)-C(101)	Al(3)-C(101)-C(100)	Al(2)-C(100)-C(101)-Al(3)	
105.49(9)	101.72(9)	81.43(9)	

Single crystal X-ray data for $10^{m\text{-}xy\text{l}}$

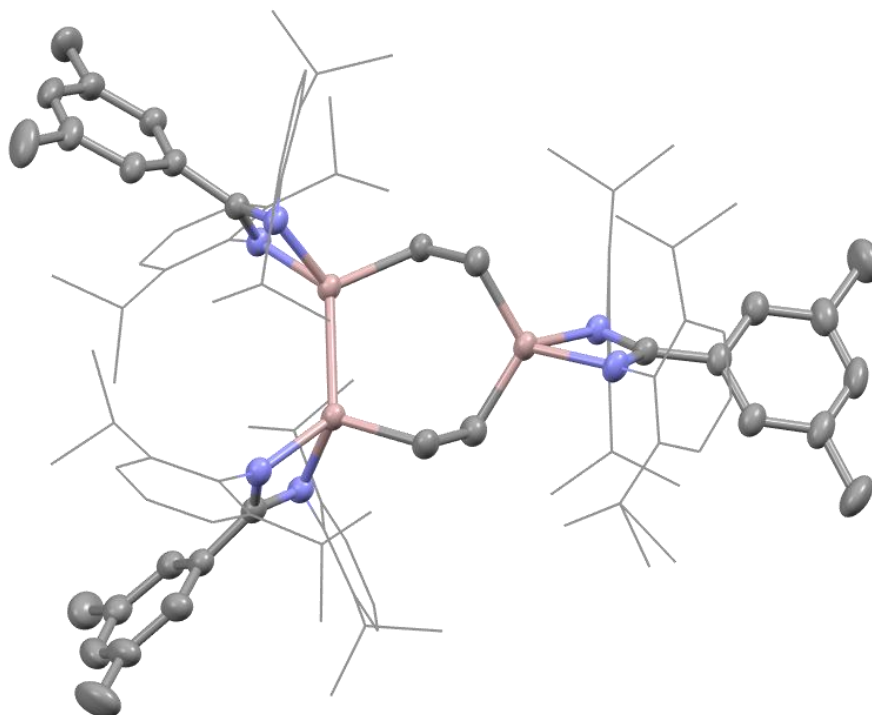


Figure S 34: The solid-state structure of $10^{m\text{-}xy\text{l}}$ (Solvent molecules and hydrogen atoms omitted, dipp groups wireframe for clarity, thermal ellipsoids 50% probability).

Single crystals of $10^{m\text{-}xy\text{l}}$ were grown from slow evaporation of a hexane solution. $10^{m\text{-}xy\text{l}}$ was found to crystallise in the $P\bar{1}$ space group. The unit cell contained 3 hexane molecules per unit cell, which were modelled using a solvent mask (SQUEEZE). C31-C33 and C31-C32 distances were restrained with sigma of 0.02.

$\text{C}_{112}\text{H}_{158}\text{Al}_3\text{N}_6$ ($M=1669.37$ g/mol): triclinic, space group $P\bar{1}$ (no. 2), $a = 12.41140(10)$ Å, $b = 20.3291(2)$ Å, $c = 21.3439(3)$ Å, $\alpha = 82.6960(10)^\circ$, $\beta = 77.6110(10)^\circ$, $\gamma = 88.0250(10)^\circ$, $V = 5217.10(10)$ Å³, $Z = 2$, $T = 150.00(10)$ K, $\mu(\text{Cu K}\alpha) = 0.685$ mm⁻¹, $D_{\text{calc}} = 1.063$ g/cm³, 145252 reflections measured ($6.486^\circ \leq 2\theta \leq 157.376^\circ$), 21690 unique ($R_{\text{int}} = 0.0835$, $R_{\text{sigma}} = 0.0505$) which were used in all calculations. The final R_1 was 0.0459 ($I > 2\sigma(I)$) and wR_2 was 0.136 (all data). CCDC deposition number 2469918.

Table S 19: Selected bond lengths (Å) and distances for **9^{m-xyI}**

Al(1)-Al(2)	Al(1)-Al(3)	Al(2)-Al(3)			
3.9982(6)	4.0162(6)	2.6070(5)			
Al(1)-N(1)	Al(1)-N(2)	Al(2)-N(3)	Al(2)-N(4)	Al(3)-N(5)	Al(3)-N(6)
1.950(1)	1.956(1)	1.987(1)	1.957(1)	1.955(1)	1.978(1)
Al(1)-C(100)	Al(1)-C(102)	Al(2)-C(101)	Al(3)-C(103)		
1.959(1)	1.960(2)	1.977(2)	1.972(2)		
C(101)-C(100)	C(102)-C(103)				
1.558(2)	1.556(2)				

Table S 20: Selected bond angles and torsions(°) for **9^{m-xyI}**

N(1)-Al(1)-N(2)	N(3)-Al(2)-N(4)	N(5)-Al(3)-N(6)	C(100)-Al(1)-C(102)
68.33(5)	67.77(5)	67.77(5)	119.51(6)
C(101)-Al(2)-Al(3)	C(103)-Al(3)-Al(2)	Al(1)-C(100)-C(101)-Al(2)	Al(3)-C(102)-C(103)-Al(4)
113.40(5)	111.06(5)	90.5(1)	102.40(9)

Single crystal X-ray data for **11^{m-xyI}**

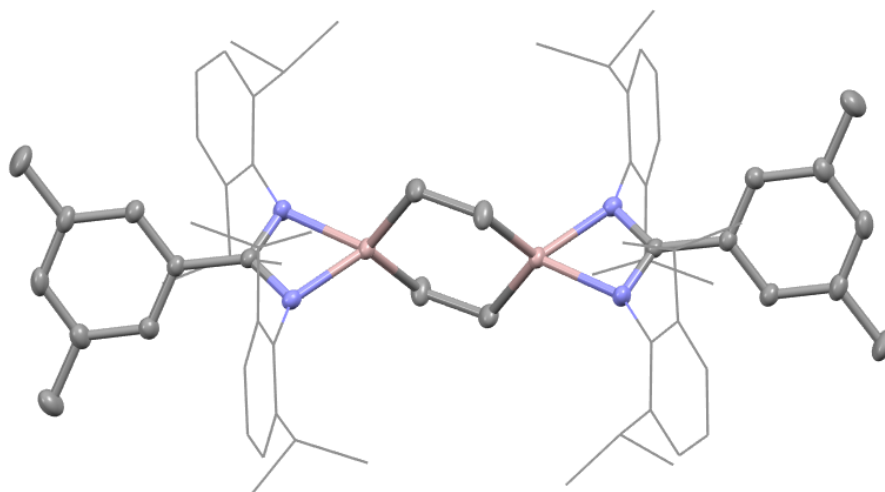


Figure S 35: The solid-state structure of **11^{m-xyI}** (Hydrogen atoms omitted, dipp groups wireframe for clarity, thermal ellipsoids 50% probability).

Single crystals of **11**^{m-xyI} were grown from the slow cooling of a saturated pentane solution. **11**^{m-xyI} was found to crystallise in the $P\bar{1}$ space group, with half a molecule in the asymmetric unit. The unit cell contained 1.33 pentane molecules per unit cell, which were modelled using a solvent mask (SQUEEZE). C_{76.6}H_{109.84}Al₂N₄ (*M* = 1140.68 g/mol): triclinic, space group $P\bar{1}$ (no. 2), *a* = 9.8050(3) Å, *b* = 12.5676(2) Å, *c* = 16.3553(3) Å, α = 99.862(2)°, β = 104.271(2)°, γ = 112.074(2)°, *V* = 1730.11(7) Å³, *Z* = 1, *T* = 100.0(4) K, $\mu(\text{Mo K}\alpha)$ = 0.086 mm⁻¹, *D*_{calc} = 1.095 g/cm³, 77013 reflections measured (4.566° ≤ 2 θ ≤ 70.202°), 15334 unique (*R*_{int} = 0.0534, *R*_{sigma} = 0.0422) which were used in all calculations. The final *R*₁ was 0.0676 (*I* > 2 σ (*I*)) and *wR*₂ was 0.2060 (all data). CCDC deposition number 2469919.

Table S 21: Selected bond lengths and distances (Å) for **11**^{m-xyI}

Al(1)-Al(1')	Al(1)-N(1)	Al(1)-N(2)
3.4711(4)	1.954(1)	1.9501(8)
Al(1)-C(35)	Al(1)-C(34)	C(34)-C(35)
1.967(2)	1.961(2)	1.548(1)

Table S 22: Selected bond angles and torsions (°) for **11**^{m-xyI}

N(1)-Al(1)-N(2)	C(34)-Al(1)-C(35)	Al(1)-C(35)-C(34)-Al(1')
68.44(4)	115.01(6)	-42.2(1)

Single crystal X-ray data for $11^{m\text{-}xyl}\text{-2}$

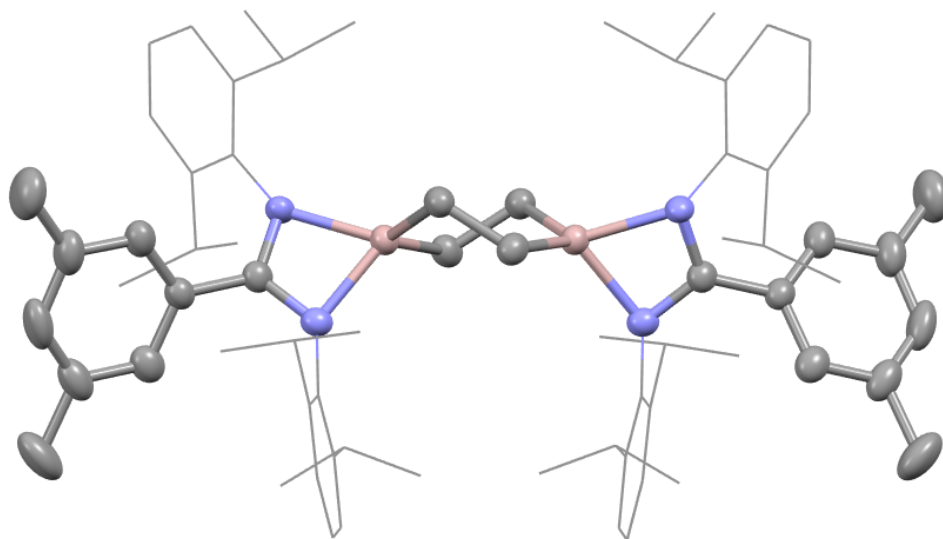


Figure S 36: The solid-state structure of $11^{m\text{-}xyl}\text{-2}$ (Hydrogen atoms omitted, dipp groups wireframe for clarity, thermal ellipsoids 50% probability).

Single crystals of $11^{m\text{-}xyl}\text{-2}$ were obtained from the slow evaporation of a pentane solution. This is preliminary data, where only connectivity was obtained.

$\text{C}_{35}\text{H}_{47}\text{AlN}_2$ ($M = 522.72$ g/mol): monoclinic, space group $C2/c$ (no. 15), $a = 15.8101(5)$ Å, $b = 12.9113(4)$ Å, $c = 32.4070(10)$ Å, $\beta = 96.689(3)^\circ$, $V = 6570.2(4)$ Å³, $Z = 8$, $T = 149.99(10)$ K, $\mu(\text{Cu K}\alpha) = 0.699$ mm⁻¹, $D_{\text{calc}} = 1.057$ g/cm³, 6491 reflections measured ($13.62^\circ \leq 2\theta \leq 113.854^\circ$), 3848 unique ($R_{\text{int}} = 0.0377$, $R_{\text{sigma}} = 0.0644$) which were used in all calculations. The final R_1 was 0.0475 ($I > 2\sigma(I)$) and wR_2 was 0.1268 (all data).

5. Computational analysis

All DFT calculations were performed using the Gaussian 16 software (Revision C.01) as compiled on King's College London's CREATE High Performance Computing (HPC) cluster.^{13,14} Initial coordinates were obtained from the relevant SC-XRD structures. All geometries were optimised without symmetry constraints at the M06-2X-D3 level of theory, including Grimme's atom-pairwise correction to account for dispersion effects. Ahlrichs' def2-TZVP basis set was used for all metal centres and donor atoms directly bound to metal centres. Def2-SVP was placed on the remaining centres (C, H). For all calculations, an ultrafine integration grid corresponding to a pruned grid of 99 radial shells and 590 angular points per shell was employed to ensure highly accurate numerical integration of the electron density. The same procedure was used for literature compounds. In all cases, ground state geometries were confirmed by way of frequency calculation at the same level of theory to indicate the absence of negative eigenvalues in the Hessian matrix. All subsequent single point corrections and analyses were performed at the SMD-M06-2X-D3/def2-TZVP level of theory, using the SMD solvation model by Truhlar, Cramer and Marenich, with solvent parameters corresponding to those of cyclohexane ($\epsilon=2.0165$).¹⁵


Time dependent (TD) DFT calculations were carried out at the SMD-M06-2X-D3/def2-TZVP (cyclohexane, $\epsilon=2.0165$) level of theory, employing the Tamm-Dancoff approximation (TDA). Natural Bond Orbital analysis was conducted using the NBO program (Version 3.1).¹⁶ Quantum Theory of Atoms in Molecules (QTAIM) analysis was conducted using the AIMAll package, from the Gaussian obtained-wavefunction file.¹⁷ Isosurface mapping of the Electron Localization Function (ELF) was performed using the Multiwfn package, employing the high quality grid preset – covering the whole system, about 1,728,000 points in total.^{18,19}

Figures of all structures and isosurface plots were generated with ChemCraft (Version 1.8) and UCSF ChimeraX (Version 1.61).^{20,21}

Functional benchmarking

Table S 23: Functional data table for the parametrisation process of $2^{p\text{-tol}}$

	Al_1-Al_2 (Å)	Al_1-Al_3 (Å)	Al_2-Al_3 (Å)	θAl_1 (°)	θAl_2 (°)	θAl_3 (°)	θNAl_1N (°)	θNAl_2N (°)	θNAl_3N (°)	UV-Vis (nm)
$2^{p\text{-tol}}$	2.6640(12)	2.6603(10)	2.6553(11)	59.83(3)	60.02(3)	60.15(3)	67.22(9)	67.06(10)	67.34(9)	316, 450
	2.6573(10)	2.6309(11)	2.6528(12)	60.22(3)	59.40(3)	60.38(3)	67.49(9)	67.48(10)	67.34(10)	
	2.6621(11)	2.6612(10)	2.6477(10)	59.75(3)	59.83(3)	60.42(3)	67.19(8)	67.27(9)	67.41(9)	
	2.6594(10)	2.6416(11)	2.6436(10)	60.16(3)	59.65(3)	60.19(3)	67.27(8)	67.29(8)	67.43(8)	
B3LYP	2.73576	2.73107	2.73046	59.928	59.95	60.121	66.242	66.245	66.283	532
	2.59856	2.65093	2.60747	59.555	61.221	59.224	67.652	67.845	67.632	570
M06L	2.60192	2.6447	2.59912	59.384	61.127	59.489	68.064	68.4	68.231	656
	2.5901	2.63721	2.59109	59.422	61.194	59.385	68.237	68.532	68.364	660
M062X	2.64889	2.64098	2.62925	59.608	60.047	60.346	67.29	67.513	67.579	332, 428
	2.64029	2.6356	2.62059	59.565	60.128	60.307	67.383	67.64	67.681	335, 429
ωB97X	2.64383	2.64956	2.64781	60.02774	60.09345	59.87881	66.79357	66.81867	66.87371	293, 333
ωB97XD	2.58613	2.63767	2.5958	59.583	61.196	59.221	67.557	67.806	67.616	

 = Dispersion corrected (GD3, unless integrated)

Given the complexity of the electronic structure, ensuring functional best fit was a priority before conducting in depth analysis. The fitting of four common functionals: B3LYP, ω B97XD, M06-L and M06-2x was tested against experimental geometry values obtained from two separate single crystal structures (four units) and UV-Vis spectroscopic parameters.

The M06-2x-D3 functional was selected for the remainder of the analysis work based on its excellent adherence to the crystallographically determined geometries and mapping of the key TD-DFT transition bands seen *via* UV-Vis spectroscopy. All other functionals failed to accurately determine reasonable transition wavelengths and resolve both experimentally observed bands.

Time dependent-DFT

Table S 24: Key TD-DFT transition bands of **2^{p-tol}**, transitions with $f < 0.2$ have been excluded.

Key TD-DFT Bands					
Excited State 6:					
Ground	Excited	E (eV)	λ (nm)	f	S ²
HOMO-1	LUMO	2.8875	429.39	0.2854	0.000
	LUMO+1				
	LUMO+2				
	LUMO+3				
HOMO	LUMO+1	2.8875	429.39	0.2854	0.000
	LUMO+2				
Excited State 7:					
HOMO-1	LUMO +2	2.9171	425.03	0.2763	0.000
	LUMO +3				
HOMO	LUMO				
	LUMO +1				
	LUMO +2				
	LUMO +3				
Excited State 9:					
HOMO	LUMO+6	3.6415	340.48	0.2750	0.000
	LUMO+7				
	LUMO+8				
	LUMO+19				
Excited State 10:					
HOMO-1	LUMO+6	3.6861	336.35	0.3116	0.000
	LUMO+7				
	LUMO+8				
	LUMO+18				
	LUMO+19				

Table S 25: Key TD-DFT transition bands of **2^{m-xyI}**, transitions with $f < 0.2$ have been excluded.

Key TD-DFT Bands									
Excited State 6:									
Ground	Excited	E (eV)	λ (nm)	f	S ²				
HOMO-1	LUMO	2.8936	428.47	0.2724	0.000				
	LUMO+1								
	LUMO+2								
	LUMO+3								
HOMO	LUMO+1	2.8936	428.47	0.2724	0.000				
	LUMO+2								
Excited State 7:									
HOMO-1	LUMO +1	2.9241	424.01	0.2639	0.000				
	LUMO +2								
	LUMO +3								
HOMO	LUMO					2.9241	424.01	0.2639	0.000
	LUMO +1								
	LUMO +2								
	LUMO +3								
Excited State 9:									
HOMO	LUMO+4	3.6415	340.47	0.2800	0.000				
	LUMO+5								
	LUMO+7								
	LUMO+8								
	LUMO+14								
	LUMO+19								
Excited State 10:									
HOMO-1	LUMO+4	3.6866	336.31	0.3127	0.000				
	LUMO+5								
	LUMO+7								
	LUMO+8								
	LUMO+19								

Electron localisation function

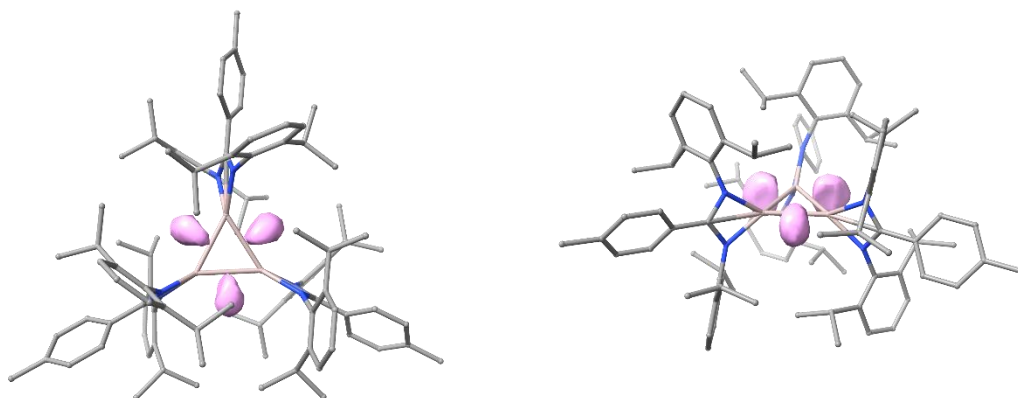


Figure S 37: Isosurfaces for the ELF of $2^{p\text{-tol}}$ (Isovalue: 0.92), highlighting the localisation of the Al-Al bond density to lie outside the interatomic plane

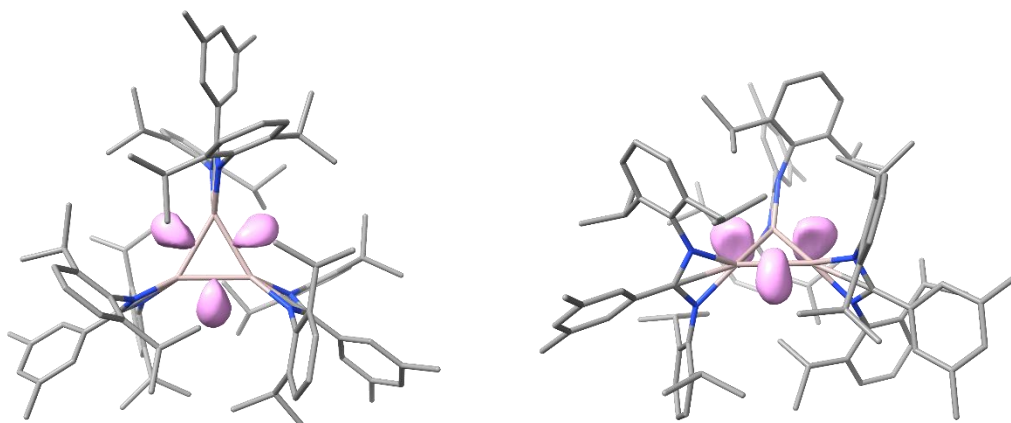


Figure S 38: Isosurfaces for the ELF of $2^{m\text{-xyI}}$ (Isovalue: 0.92), highlighting the localisation of the Al-Al bond density to lie outside the interatomic plane.

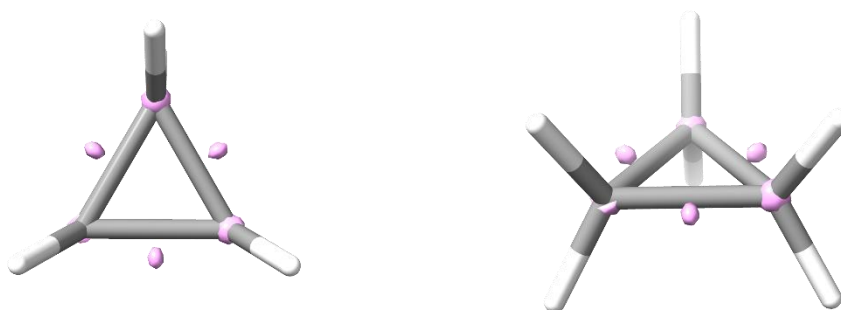


Figure S 39: Isosurfaces for the ELF of cyclopropane (Isovalue: 0.92), indicated much smaller accumulation of electron density outside the C-C plane compared to $2^{m\text{-xyI/p-tol}}$.

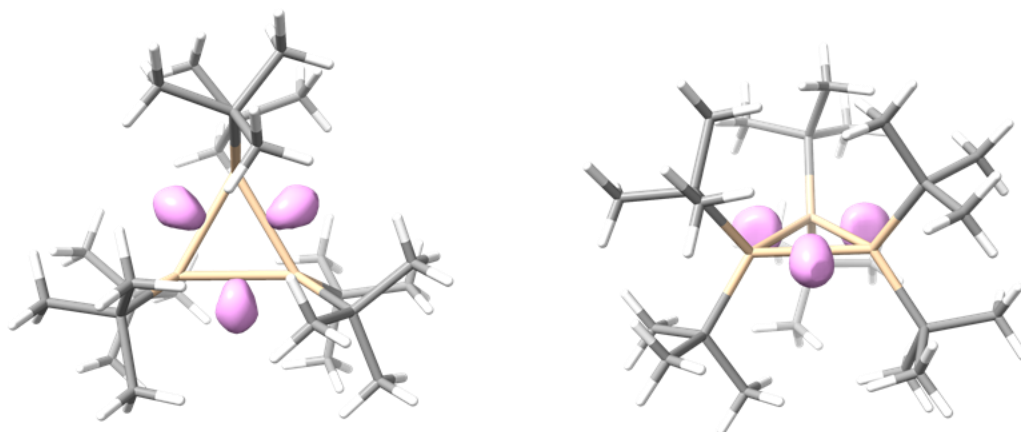


Figure S 40: Isosurfaces for the ELF of for cyclotrisilane (Isovalue: 0.92), indicating an accumulation of electron density outside the C-C plane similar to **2**^{m-xy/p-tol}.

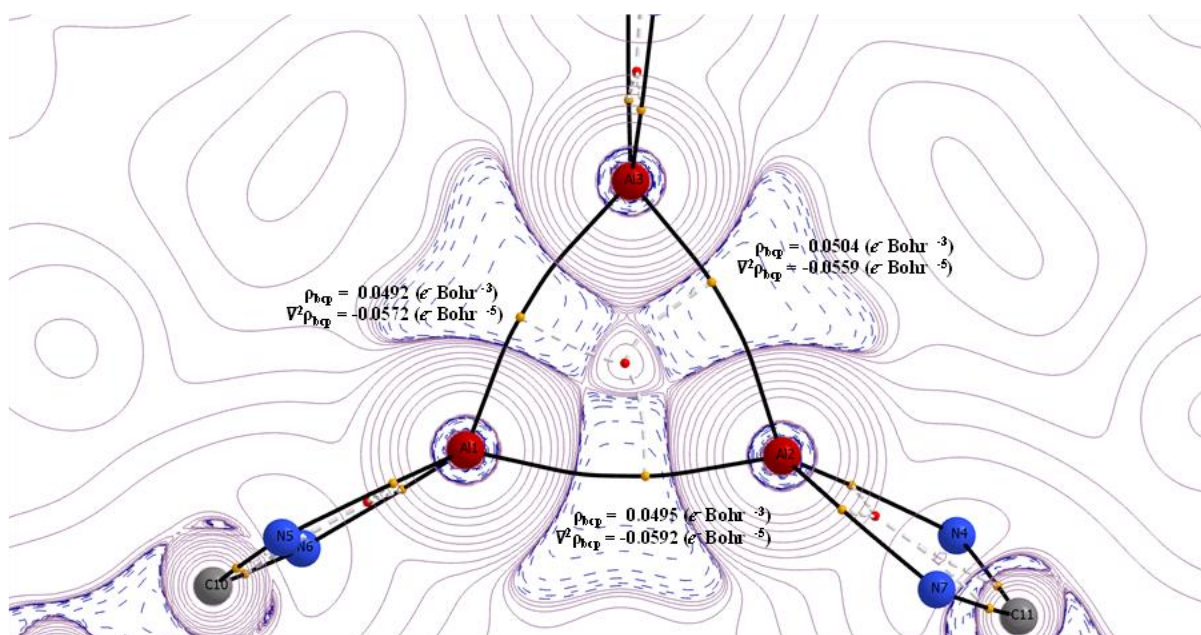


Figure S 41: QTAIM topology plot for the Laplacian of the electron density ($\nabla^2\rho$) of $2^{p\text{-tol}}$, highlighting areas of charge concentration (blue) and depletion (pink). The values of electron density (ρ) and $\nabla^2\rho$ are indicated at each bcp.

Table S 26: Data table for the QTAIM analysis of $2^{p\text{-tol}}$, indicating the electronic parameters found at the bcps as well as strain indicators (BPL-GBL_I) and rcp properties. Cremer and Kraka energy density parameters (V,G,K,H) are also presented.

	Al ₁ -Al ₂	Al ₁ -Al ₃	Al ₂ -Al ₃
ρ_{bcp} ($e^- \text{ Bohr}^{-3}$)	0.0492	0.0495	0.0504
$\nabla^2\rho_{\text{bcp}}$ ($e^- \text{ Bohr}^{-5}$)	-0.0572	-0.0592	-0.0559
BPL	5.0561	5.0477	5.0183
GBL_I	4.9899	4.9806	4.9521
BPL-GBL_I	0.0662	0.0671	0.0662
V	-0.0242	-0.0234	-0.0273
G	0.0050	0.0043	0.0067
K	0.0192	0.0191	0.0206
H	-0.0192	-0.0191	-0.0206
ρ_{rcp} ($e^- \text{ Bohr}^{-3}$)		0.0352	
$\nabla^2\rho_{\text{rcp}}$ ($e^- \text{ Bohr}^{-5}$)		0.0108	

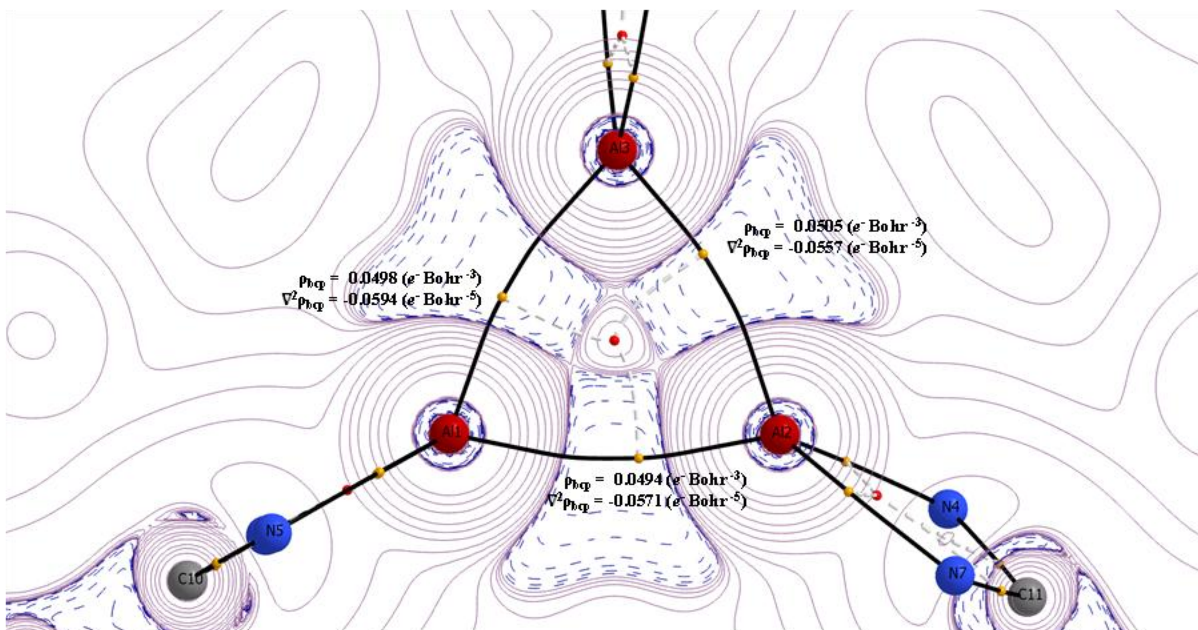


Figure S 42: QTAIM topology plot for the Laplacian of the electron density ($\nabla^2\rho$) of 2^{m-xyI} , highlighting areas of charge concentration (blue) and depletion (pink). The values of electron density (ρ) and $\nabla^2\rho$ are indicated at each bcp.

Table S 27: Data table for the QTAIM analysis of 2^{m-xyI} , indicating the electronic parameters found at the bcps as well as strain indicators (BPL-GBL_I) and rcp properties. Cremer and Kraka energy density parameters (V,G,K,H) are also presented.

	Al ₁ -Al ₂	Al ₁ -Al ₃	Al ₂ -Al ₃
ρ_{bcp} ($e^- \text{ Bohr}^{-3}$)	0.0494	0.0498	0.0505
$\nabla^2\rho_{bcp}$ ($e^- \text{ Bohr}^{-5}$)	-0.0571	-0.0594	-0.0557
BPL	5.0492	5.0388	5.0127
GBL_I	4.9832	4.9719	4.9465
BPL-GBL_I	0.0661	0.0669	0.0662
V	-0.0246	-0.0241	-0.0276
G	0.0052	0.0046	0.0068
K	0.0194	0.0195	0.0208
H	-0.0194	-0.0195	-0.0208
ρ_{rcp} ($e^- \text{ Bohr}^{-3}$)		0.0354	
$\nabla^2\rho_{rcp}$ ($e^- \text{ Bohr}^{-5}$)		0.0105	

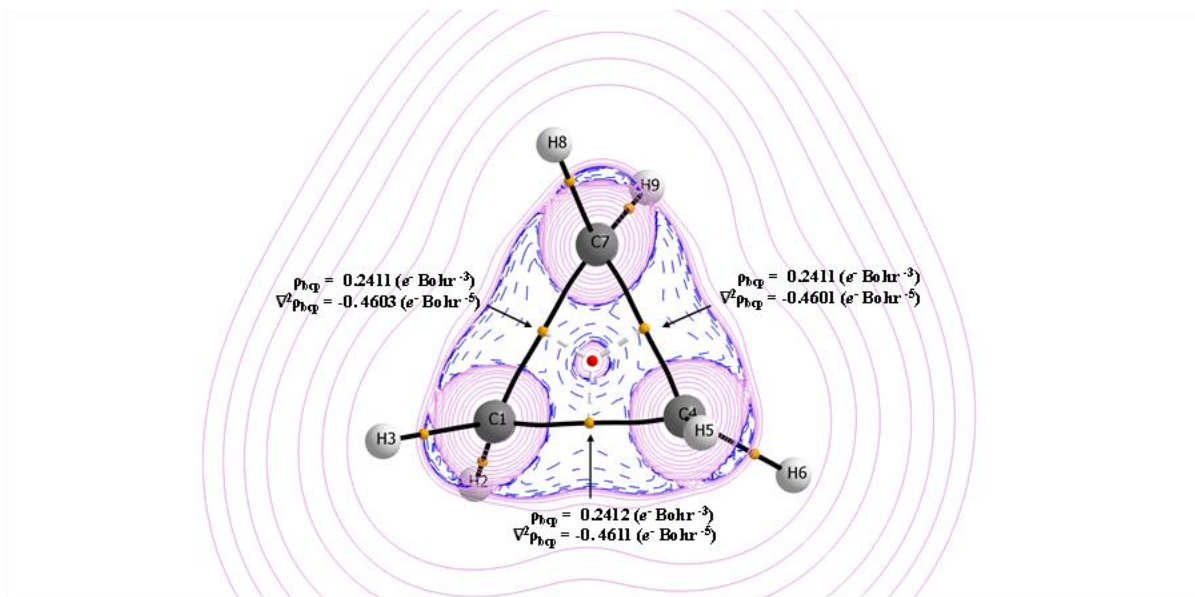


Figure S 43: QTAIM topology plot for the Laplacian of the electron density ($\nabla^2\rho$) of cyclopropane, highlighting areas of charge concentration (blue) and depletion (pink). The values of electron density (ρ) and $\nabla^2\rho$ are indicated at each bcp.

Table S 28: Data table for the QTAIM analysis of cyclopropane, indicating the electronic parameters found at the bcps as well as strain indicators (BPL-GBL_I) and rcp properties. Cremer and Kraka energy density parameters (V,G,K,H) are also presented.

	C ₁ -C ₄	C ₁ -C ₇	C ₄ -C ₇
ρ_{bcp} (e ⁻ Bohr ⁻³)	0.2412	0.2411	0.2411
$\nabla^2\rho_{\text{bcp}}$ (e ⁻ Bohr ⁻⁵)	-0.4611	-0.4603	-0.4601
BPL	2.8373	2.8378	2.8379
GBL_I	2.8307	2.8312	2.8313
BPL-GBL_I	0.0066	0.0066	0.0066
V	-0.3081	-0.3079	-0.3078
G	0.0964	0.0964	0.0964
K	0.2117	0.2115	0.2114
H	-0.2117	-0.2115	-0.2114
ρ_{rcp} (e ⁻ Bohr ⁻³)		0.2044	
$\nabla^2\rho_{\text{rcp}}$ (e ⁻ Bohr ⁻⁵)		0.0703	

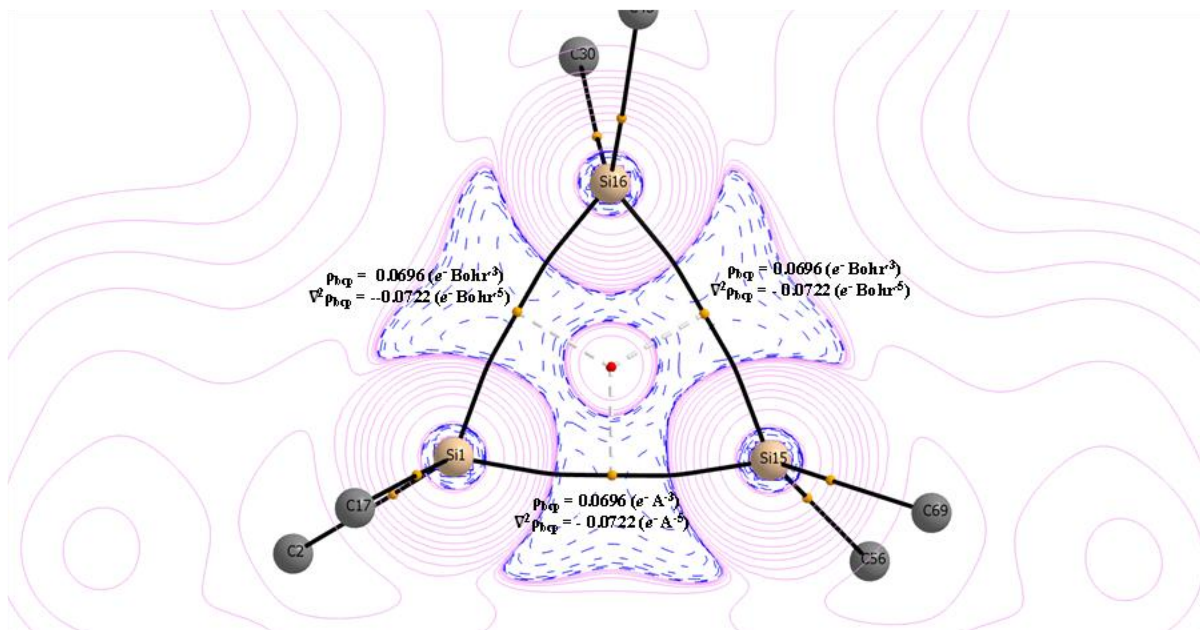


Figure S 44: QTAIM topology plot for the Laplacian of the electron density ($\nabla^2\rho$) of cyclotrisilane, highlighting areas of charge concentration (blue) and depletion (pink). The values of electron density (ρ) and $\nabla^2\rho$ are indicated at each bcp.

Table S 29: Data table for the QTAIM analysis of cyclotrisilane, indicating the electronic parameters found at the bcps as well as strain indicators (BPL-GBL_I) and rcp properties. Cremer and Kraka energy density parameters (V,G,K,H) are also presented.

	Si ₁ -Si ₁₅	Si ₁ -Si ₁₆	Si ₁₅ -Si ₁₆
ρ_{bcp} (e ⁻ Bohr ⁻³)	0.0696	0.0696	0.0696
$\nabla^2\rho_{\text{bcp}}$ (e ⁻ Bohr ⁻⁵)	-0.0722	-0.0722	-0.0723
BPL	4.7829	4.7829	4.7828
GBL_I	4.7444	4.7444	4.7444
BPL-GBL_I	0.0385	0.0385	0.0385
V	-0.0349	-0.0349	-0.0349
G	0.0084	0.0084	0.0084
K	0.0265	0.0265	0.0265
H	-0.0265	-0.0265	-0.0265
ρ_{rcp} (e ⁻ Bohr ⁻³)		0.0476	
$\nabla^2\rho_{\text{rcp}}$ (e ⁻ Bohr ⁻⁵)		0.0378	

Canonical molecular orbitals

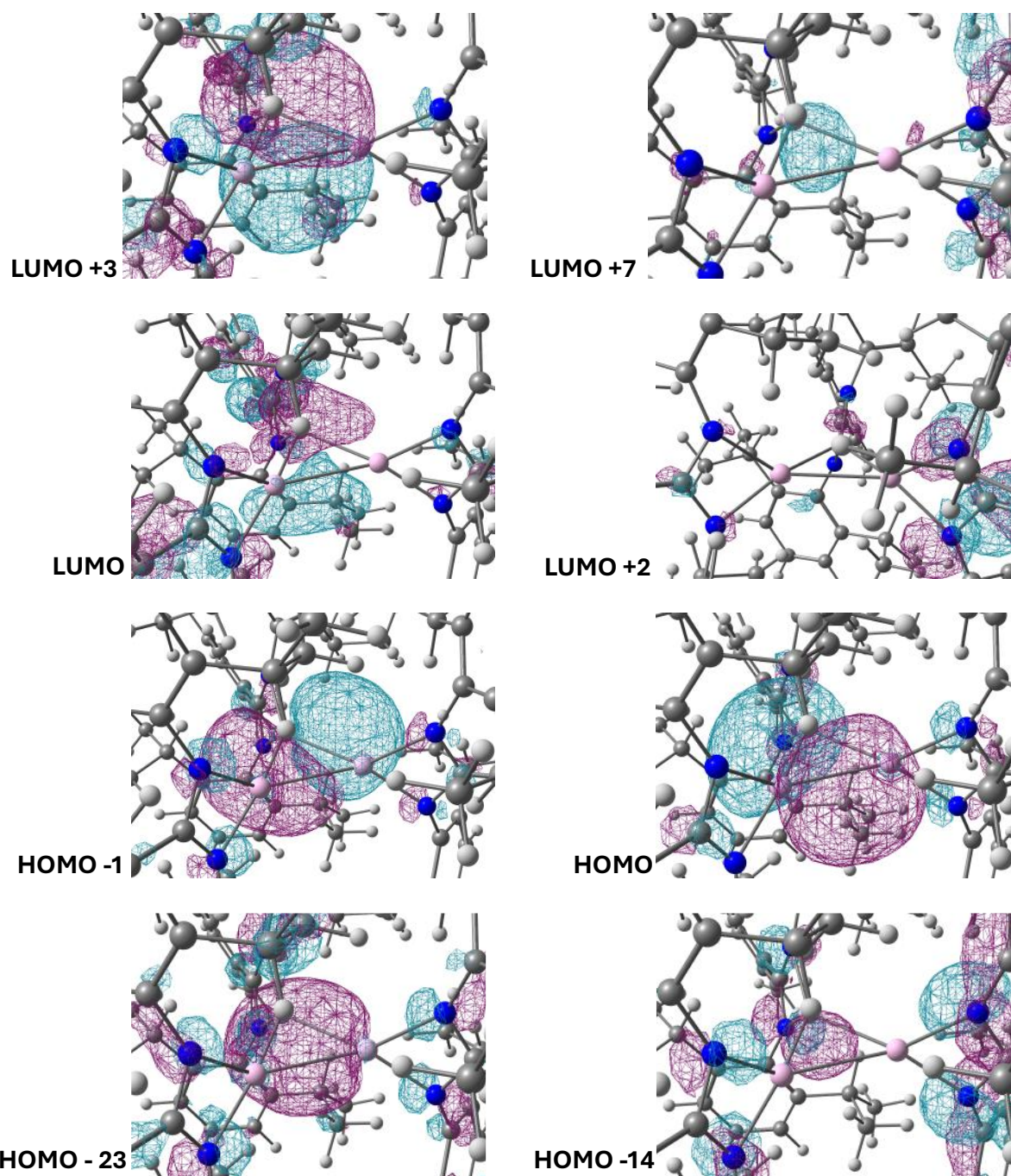


Figure S 45: DFT calculated canonical molecular orbitals of $2^{p\text{-tol}}$. Specifically, orbitals involving areas of density localised around the Al_3 core, highlighting the presence of a low-lying radial sigma bonding combination (HOMO-23) as well as two effectively degenerate HOMO orbitals contributing to the overall sigma bonding skeleton of the cyclotrialumane.

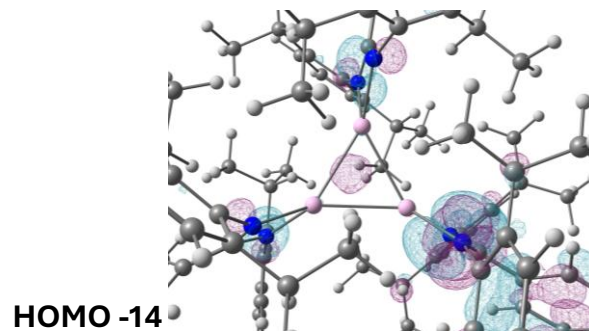
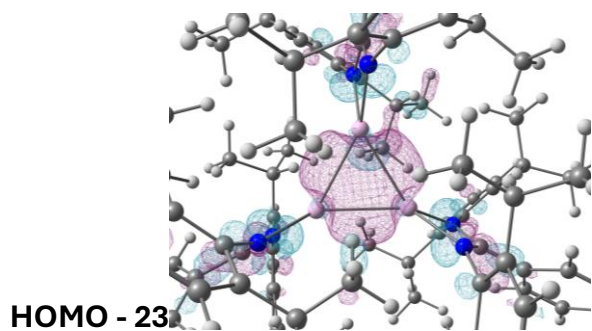
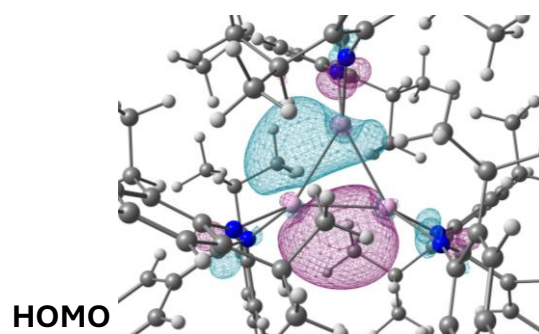
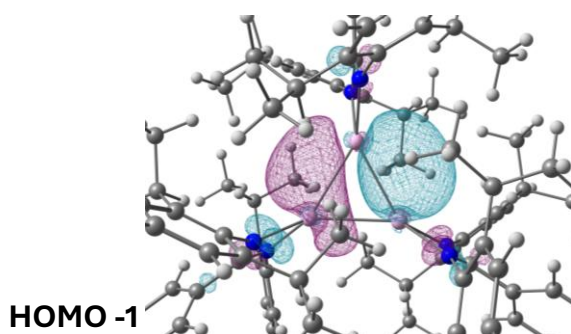
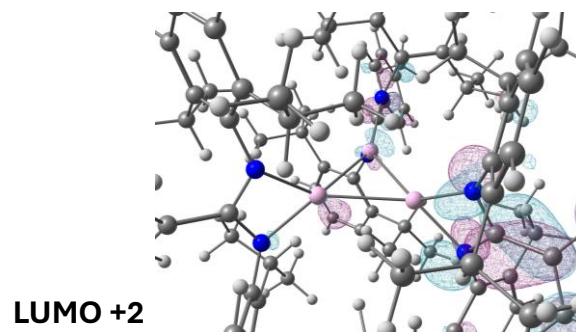
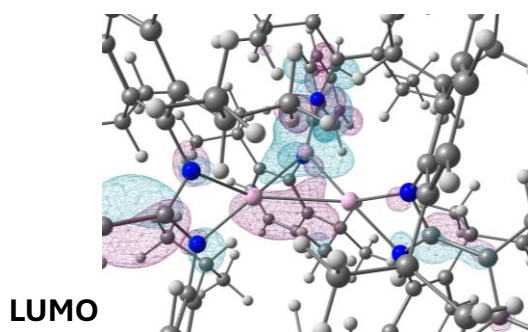
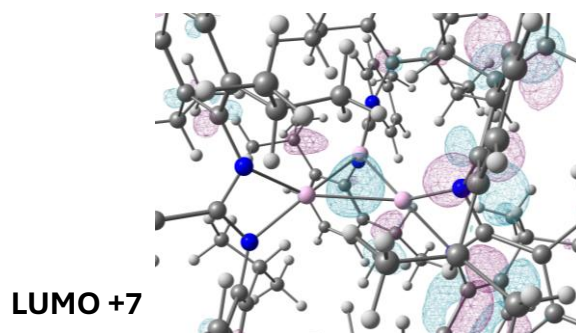
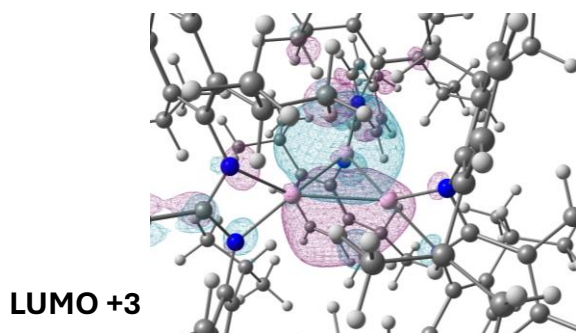


Figure S 46: DFT calculated canonical molecular orbitals of $\mathbf{2}^{m\text{-}xy\text{-}l}$. Specifically, orbitals involving areas of density localised around the Al_3 core, highlighting the presence of a low-lying radial sigma bonding combination (379) as well as two effectively degenerate HOMO orbitals (401+402) contributing to the overall sigma bonding skeleton of the cyclotrialumane.

Natural bonding orbitals

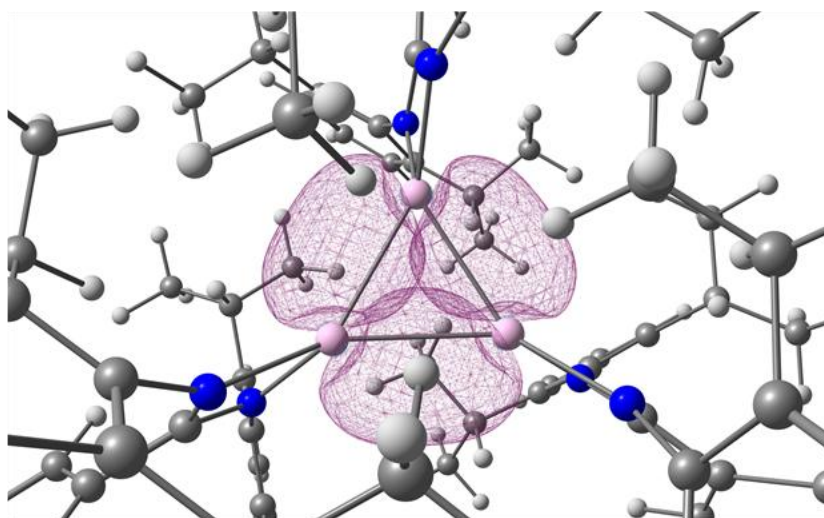


Figure S 47: Natural bonding orbitals of the Al_3 core of $2^{p\text{-tol}}$.

Table S 30: The respective calculated occupancies of the natural bonding orbitals of the Al_3 core of $2^{p\text{-tol}}$.

Lewis Quality			
97.60%			
Bond	WBI	NBO Occupancy	Bond Orbital Composition
$\text{Al}_1\text{-Al}_2$	0.9658	1.831 (50.69% Al_1)	Al_1 [50.69%]: s(38.45%), p(60.87%), d(0.67%); Al_2 [49.31%]: s(36.55%), p(62.77%), d(0.66%)
$\text{Al}_1\text{-Al}_3$	0.9697	1.836 (50.77% Al_3)	Al_1 [49.23%]: s(37.34%), p(62.01%), d(0.64%); Al_3 [50.77%]: s(37.85%), p(61.45%), d(0.69%)
$\text{Al}_2\text{-Al}_3$	0.9741	1.839 (50.92% Al_2)	Al_2 [50.93%]: s(38.78%), p(60.63%), d(0.57%); Al_3 [49.08%]: s(37.27%), p(62.04%), d(0.68%)

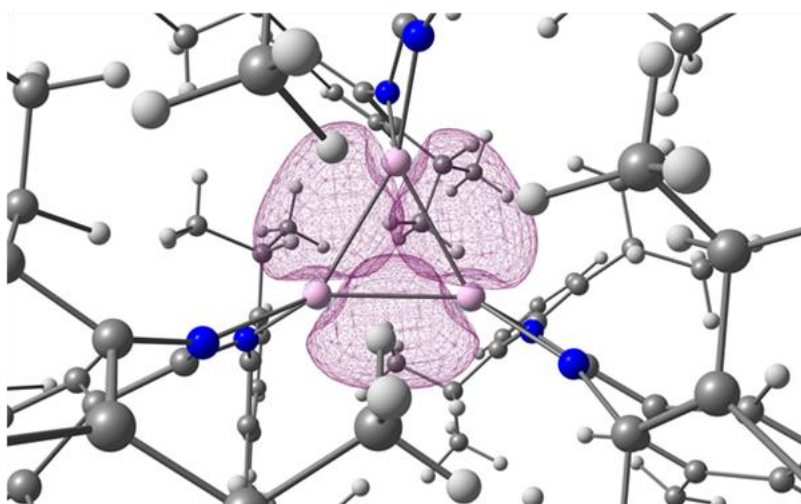


Figure S 48: Natural bonding orbitals of the Al_3 core of $2^{m\text{-xyI}}$.

Table S 31: The respective calculated occupancies of the natural bonding orbitals of the Al₃ core of 2^{m-xy}.

Lewis Quality			
97.65%			
Bond	WBI	NBO Occupancy	Bond Orbital Composition
Al ₁ -Al ₂	0.9663	1.832 (50.64% Al ₁)	Al1 [50.64%]: s(38.31%), p(61.01%), d(0.67%); Al2 [49.36%]: s(36.62%), p(62.71%), d(0.65%)
Al ₁ -Al ₃	0.9705	1.837 (50.69% Al ₃)	Al1 [49.31%]: s(37.38%), p(61.97%), d(0.65%); Al3 [50.69%]: s(37.82%), p(61.48%), d(0.69%)
Al ₂ -Al ₃	0.9744	1.839 (50.87% Al ₂)	Al2 [50.87%]: s(38.67%), p(60.75%), d(0.57%); Al3 [49.13%]: s(37.25%), p(62.07%), d(0.67%)

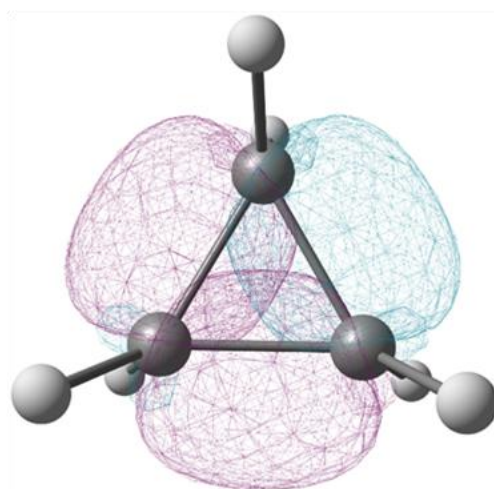


Figure S 49: Natural bonding orbitals of the C₃ core of cyclopropane.

Table S 32: The respective calculated occupancies of the natural bonding orbitals of the C₃ core of cyclopropane.

Lewis Quality			
99.34%			
Bond	WBI	NBO Occupancy	Bond Orbital Composition
C ₁ -C ₂	1.0000	1.969 (50% C ₁ -C ₂)	C1 [50%]: s(21.96%), p(77.79%), d(0.24%); C2 [50%]: s(21.95%), p(77.80%), d(0.24%)
C ₁ -C ₃	0.9999	1.969 (50% C ₁ -C ₃)	C1 [50%]: s(21.92%), p(77.82%), d(0.24%); C3 [50%]: s(21.95%), p(77.80%), d(0.24%)
C ₂ -C ₃	0.9999	1.969 (50% C ₂ -C ₃)	C2 [50%]: s(21.93%), p(77.81%), d(0.24%); C3 [50%]: s(21.92%), p(77.82%), d(0.24%)

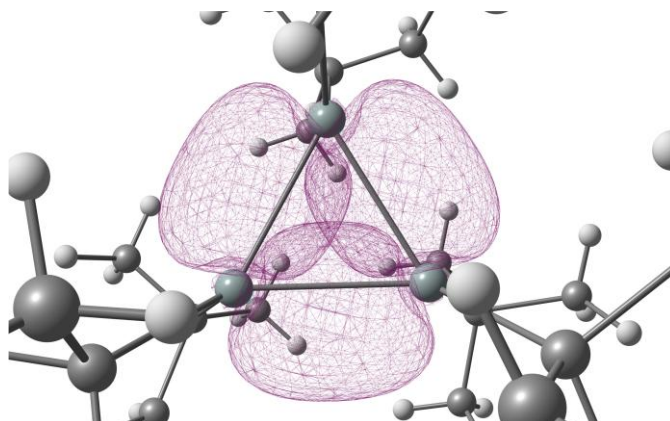


Figure S 50: Natural bonding orbitals of cyclotrisilane.

Table S 33: The respective calculated occupancies of the natural bonding orbitals of cyclotrisilane.

Lewis Quality			
99.28%			
Bond	WBI	NBO Occupancy	Bond Orbital Composition
Si₁-Si₂	0.9367	1.90739 (50% Si ₁ -Si ₂)	Si1 [50%]: s(20.29%), p(79.10%), d(0.60%); Si2 [50%]: s(20.28%), p(79.10%), d(0.60%)
Si₁-Si₃	0.9367	1.90739 (50% Si ₁ -Si ₃)	Si1 [50%]: s(20.29%), p(79.10%), d(0.60%); Si3 [50%]: s(20.28%), p(79.10%), d(0.60%)
Si₂-Si₃	0.9367	1.90738 (50% Si ₂ -Si ₃)	Si2 [50%]: s(20.28%), p(79.10%), d(0.60%); Si3 [50%]: s(20.68%), p(79.10%), d(0.60%)

Second order perturbation theory

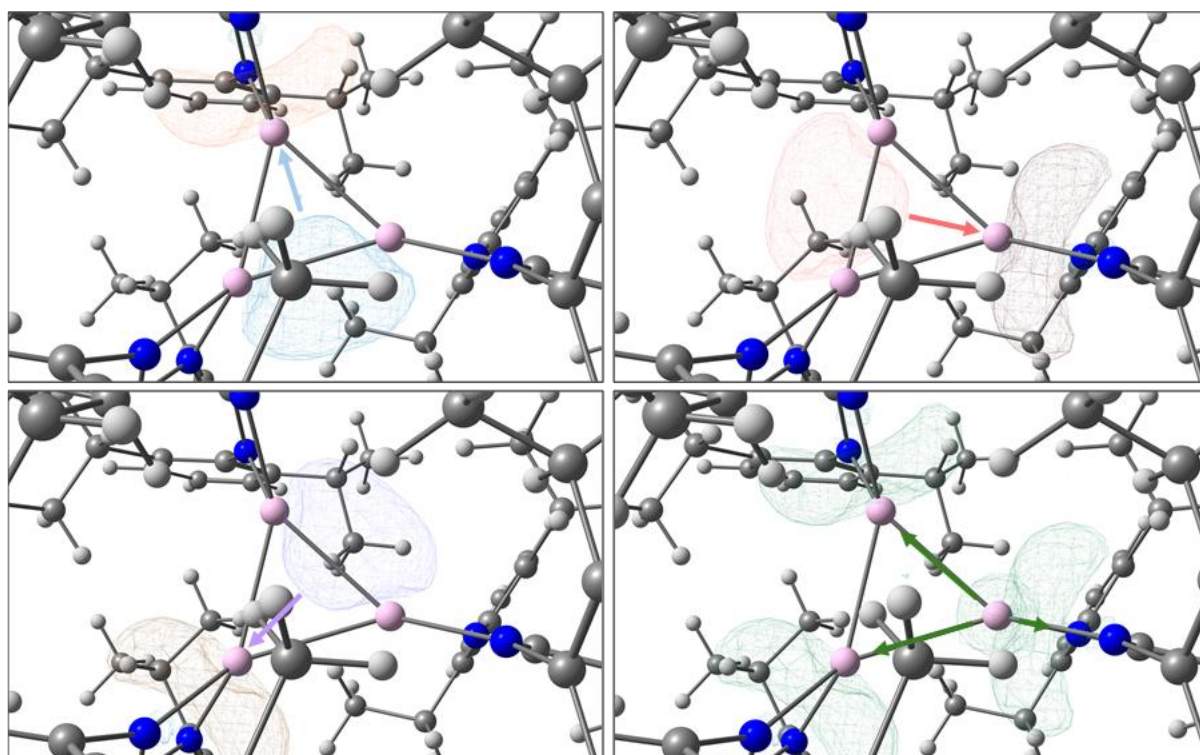


Figure S 51: Donor-acceptor interactions of $2^{p\text{-tol}}$ calculated via second order perturbation theory analysis for interactions of $E(2) > 5.00$ kcal/mol. For simplicity, only one of three interactions involving donations directly from an Al centre (shown in green) is highlighted. Two more symmetric interactions from the remaining Al_2 and Al_3 are observed.

Table S 34: Tabulated donor-acceptor interactions of $2^{p\text{-tol}}$ calculated via second order perturbation theory analysis for interactions of $E(2) > 5.00$ kcal/mol. For simplicity, only one of three interactions involving donations directly from an Al centre (shown in green) is highlighted. Two more symmetric interactions from the remaining Al_2 and Al_3 are observed.

Donor NBO	Acceptor NBO	E(2) kcal/mol
BD Al_1-Al_2	LP* Al_3	36.75
BD Al_1-Al_3	LP* Al_2	36.74
BD Al_2-Al_3	LP* Al_1	36.23
CR(2) Al_1	LP* Al_1	10.36
CR(2) Al_1	LP* Al_2	5.90
CR(2) Al_1	LP* Al_3	6.25

6. Multinuclear NMR data

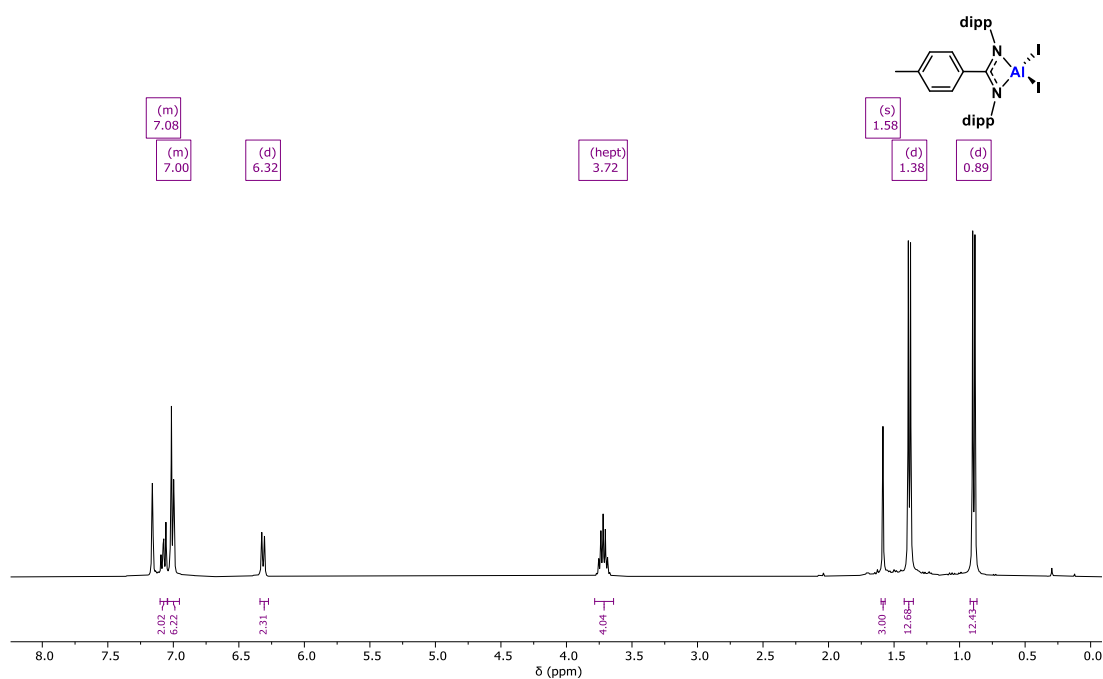


Figure S 52: ¹H NMR (400 MHz) spectrum of **1^{P-tol}** in benzene-*d*₆

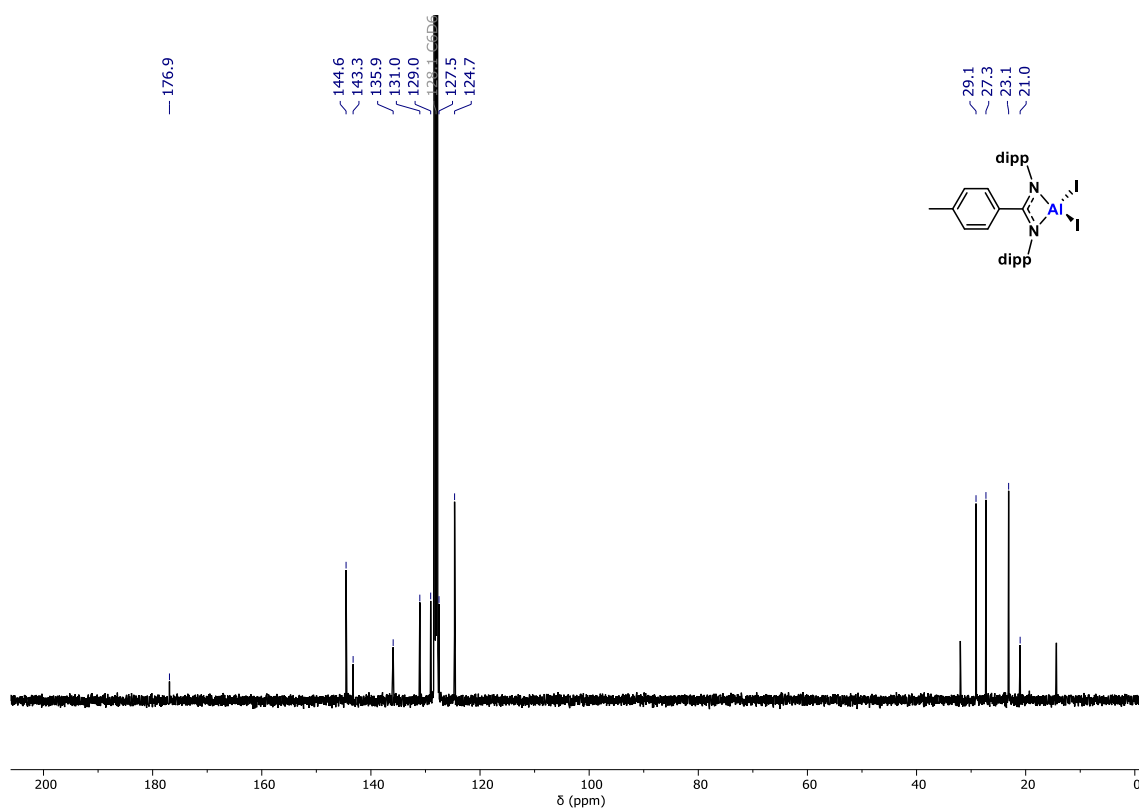


Figure S 53: ¹³C{¹H} NMR (101 MHz) spectrum of **1^{P-tol}** in benzene-*d*₆

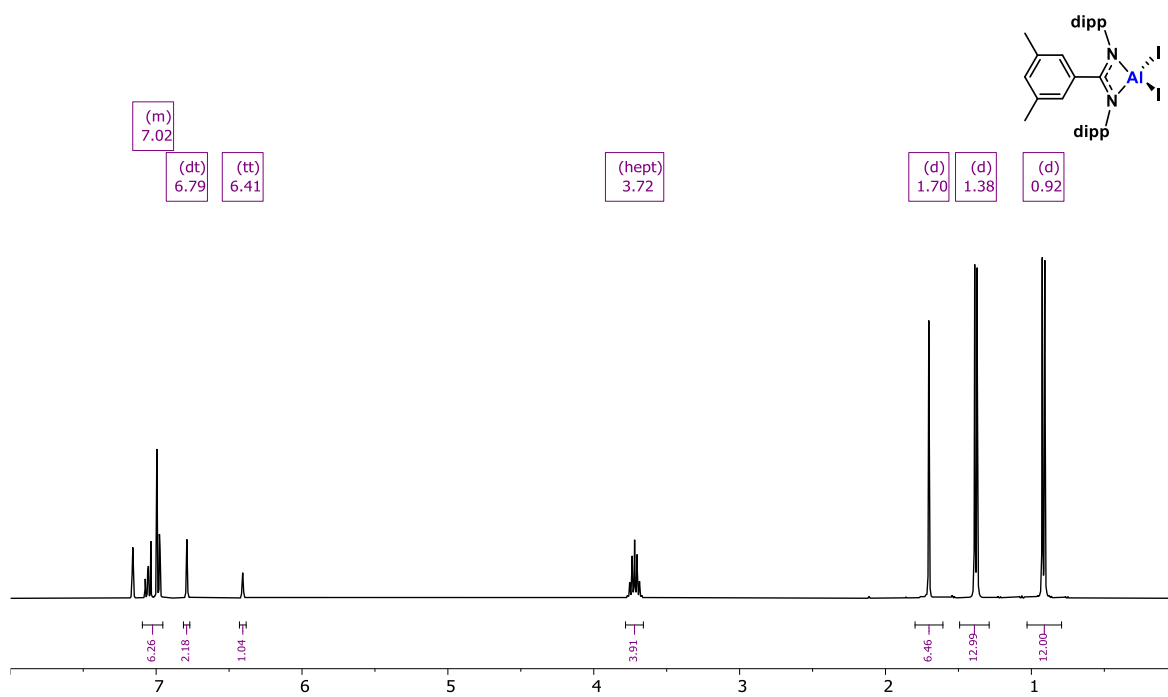


Figure S 54: ^1H NMR (400 MHz) spectrum of $\mathbf{1}^{m\text{-}xy\text{I}}$ in benzene- d_6

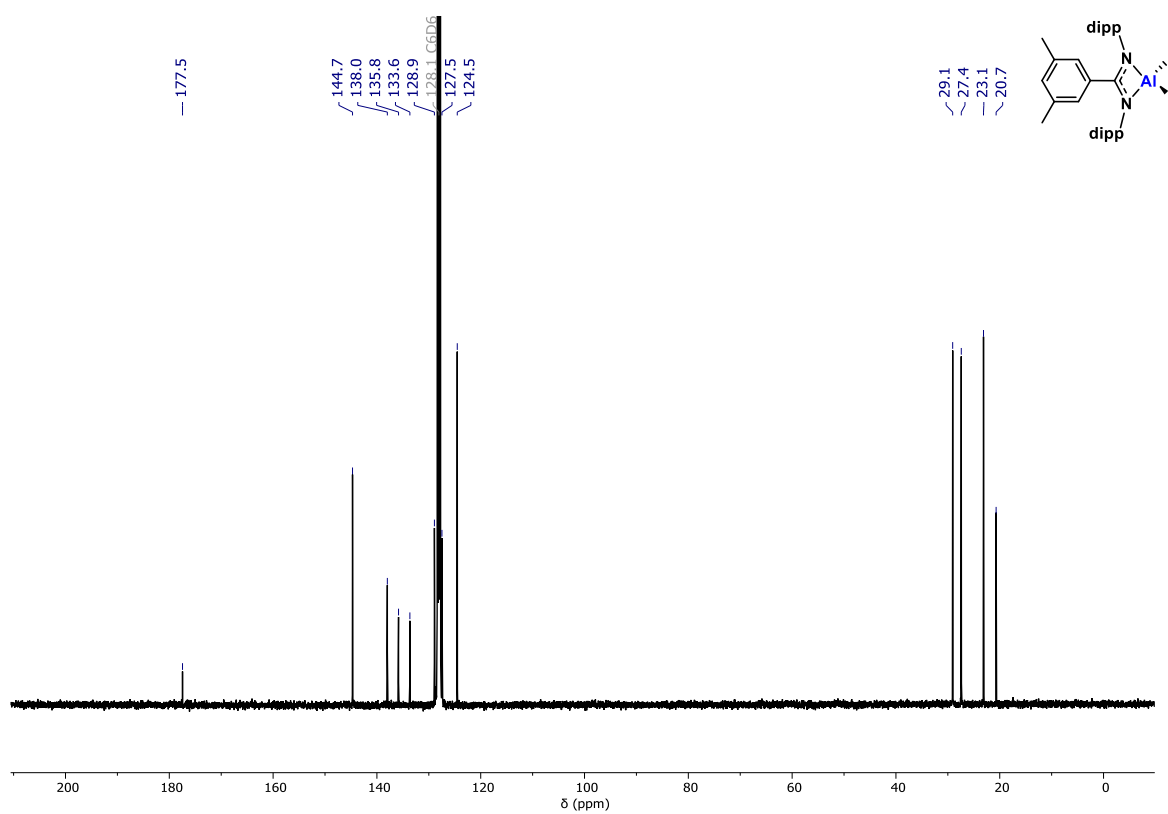


Figure S 55: $^{13}\text{C}\{^1\text{H}\}$ NMR (101 MHz) spectrum of $\mathbf{1}^{m\text{-}xy\text{I}}$ in benzene- d_6

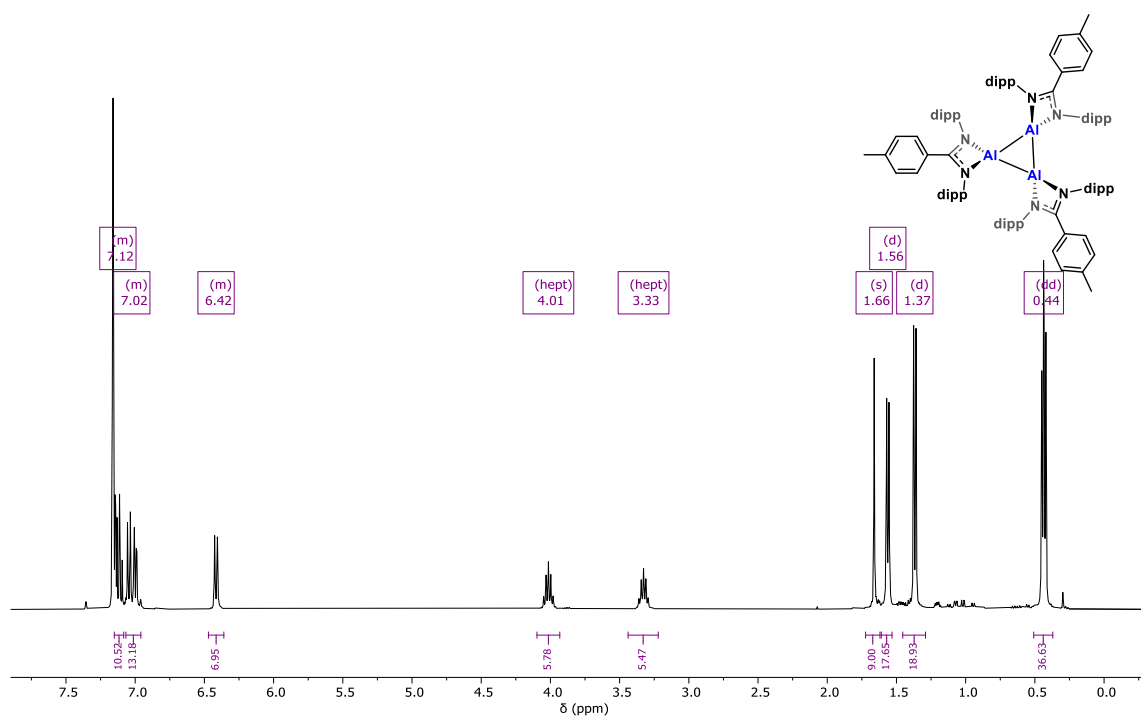


Figure S 56: ¹H NMR (400 MHz) spectrum of **2^{p-tol}** in benzene-d₆

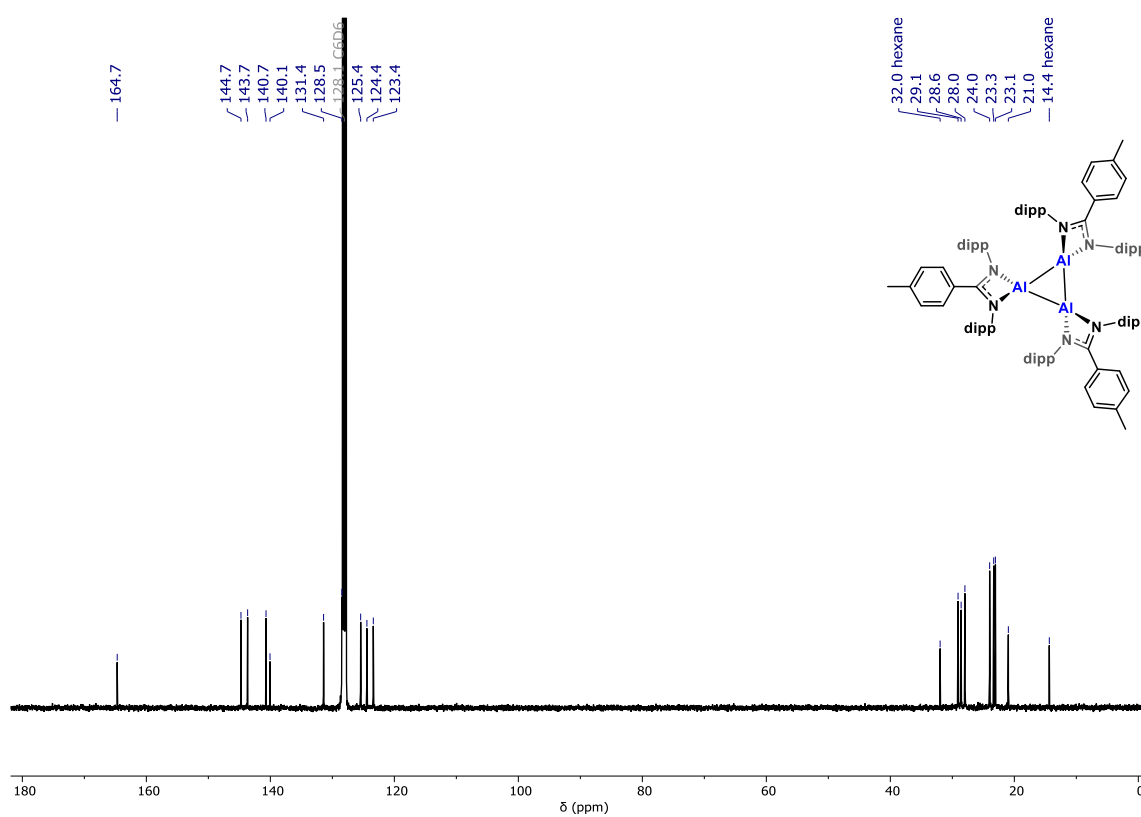


Figure S 57: ¹³C{¹H} NMR (101 MHz) spectrum of **2^{p-tol}** in benzene-d₆

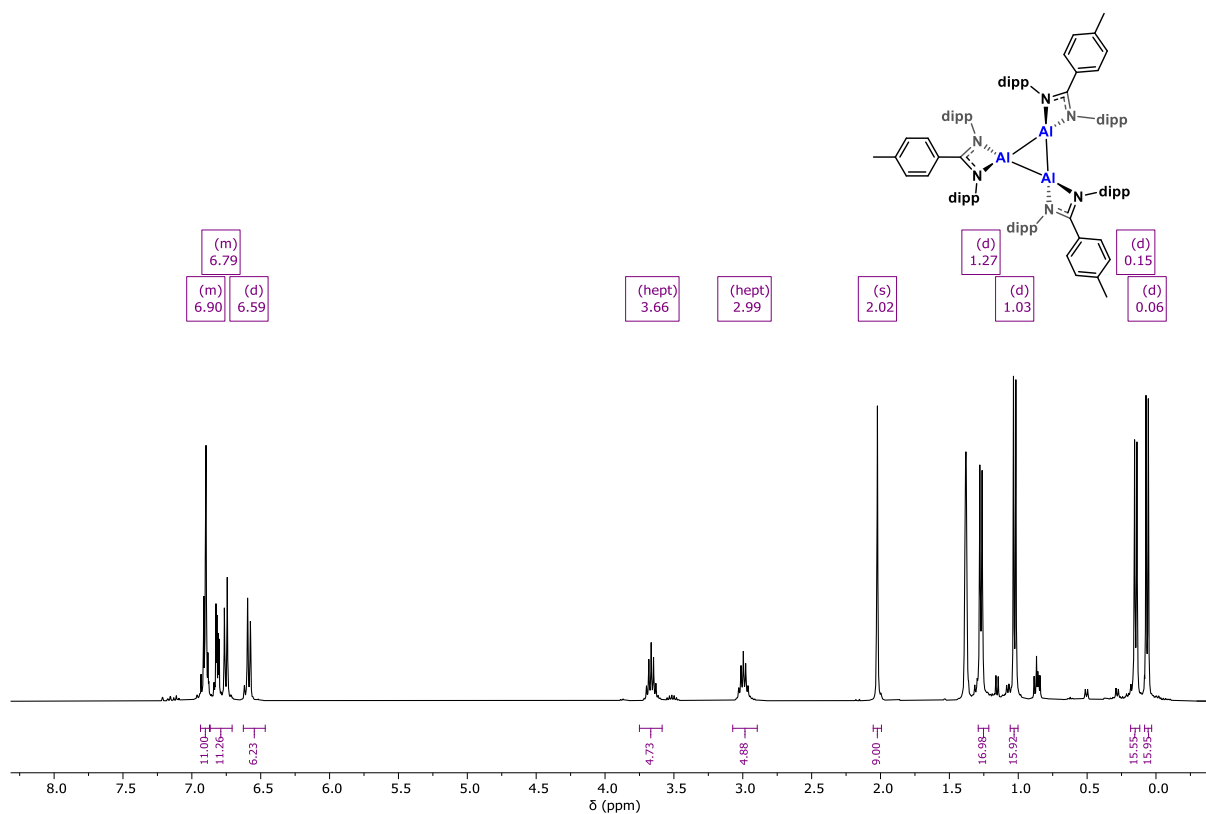


Figure S 58: ¹H NMR (400 MHz) spectrum of **2^{p-tol}** in cyclohexane-*d*₁₂

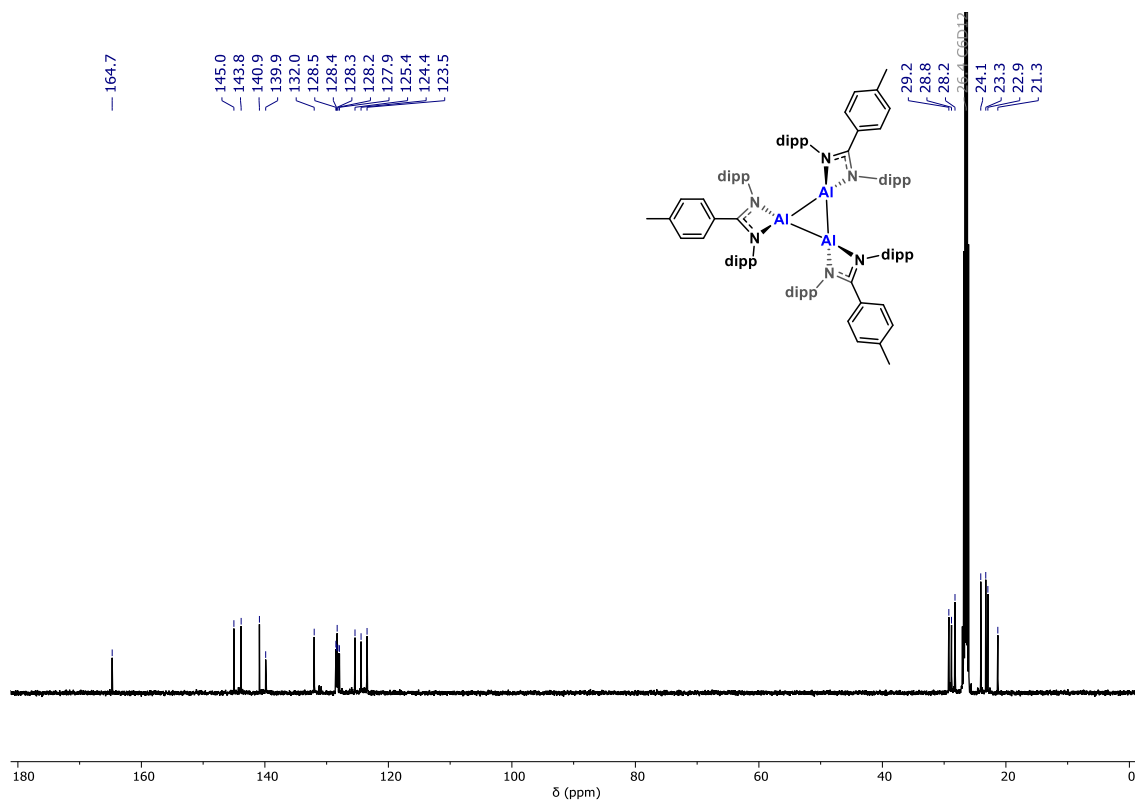


Figure S 59: ¹³C{¹H} NMR (101 MHz) spectrum of **2^{p-tol}** in cyclohexane-*d*₁₂

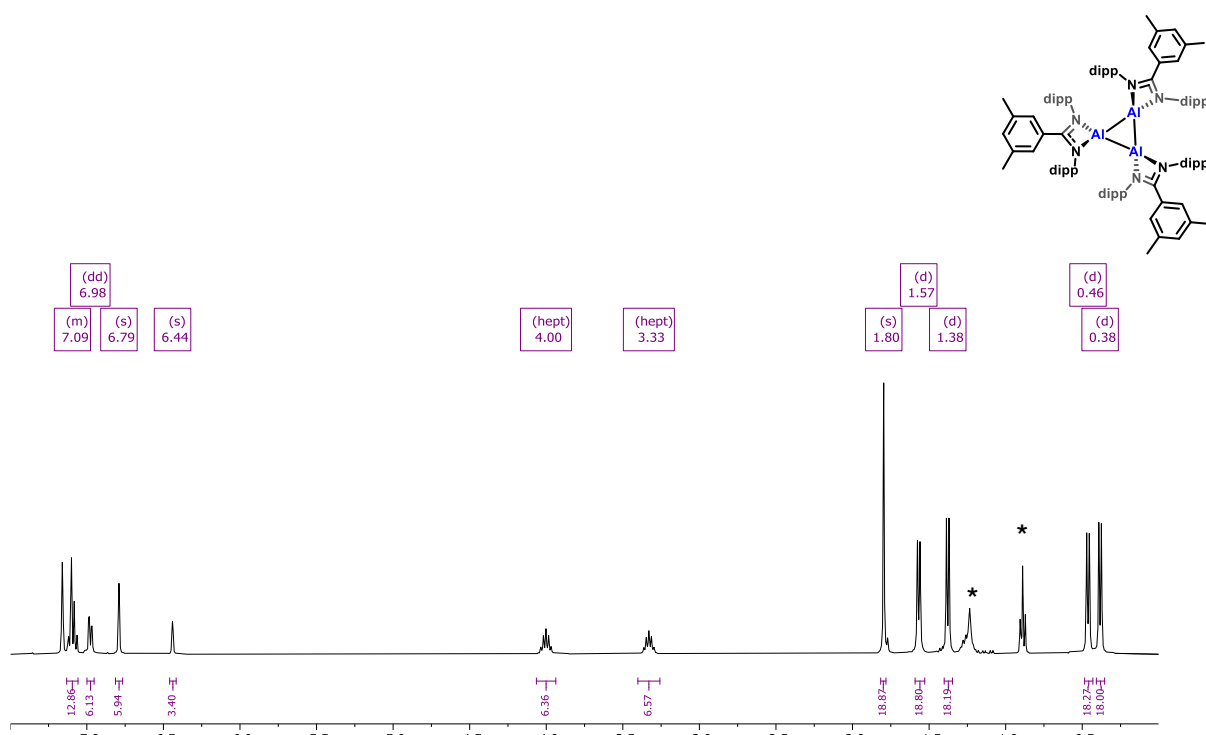


Figure S 60: ¹H NMR (400 MHz) spectrum of **2^m-xyI** in benzene-d₆ (*residual hexane)

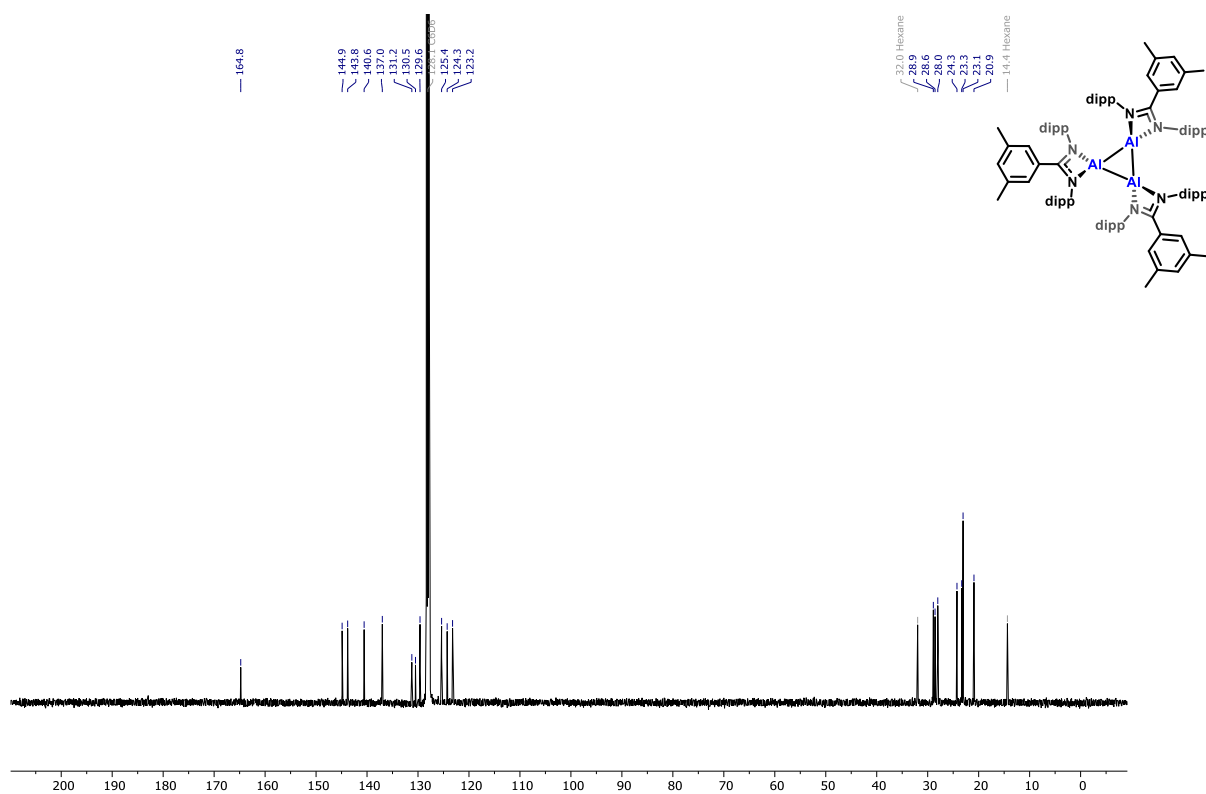


Figure S 61: ¹³C{¹H} NMR (101 MHz) spectrum of **2^m-xyI** in benzene-d₆

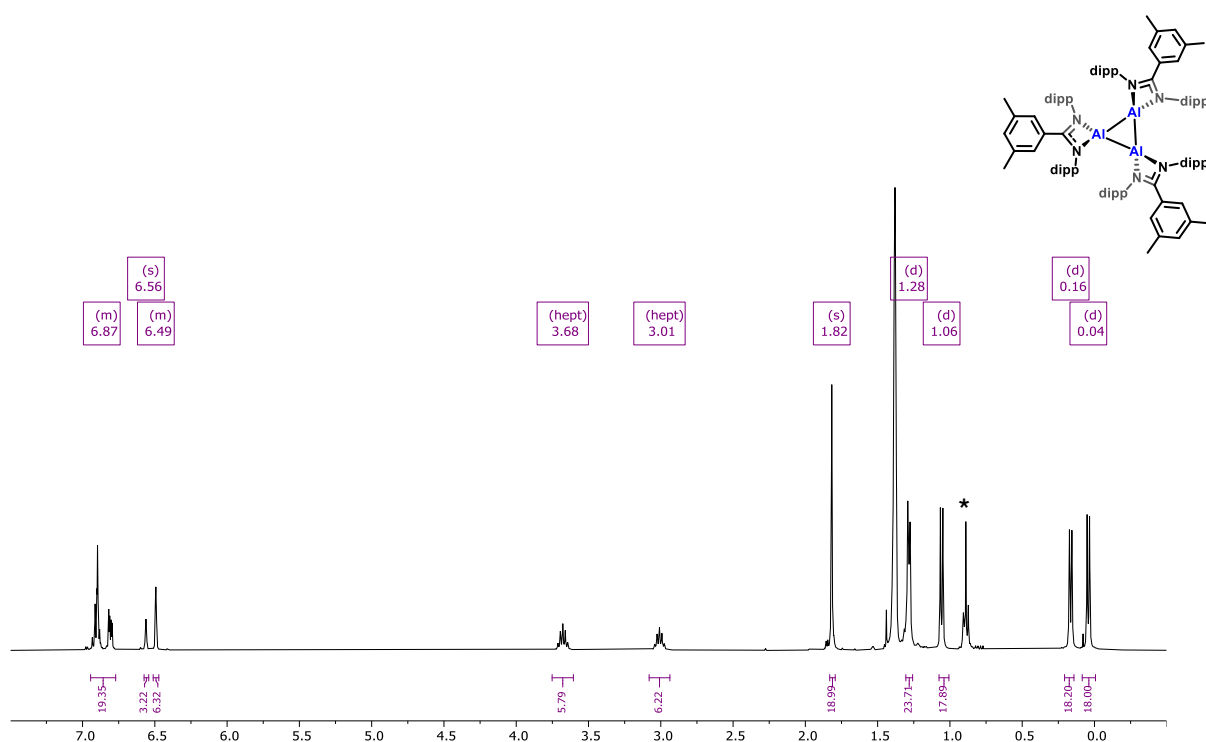


Figure S 62: ¹H NMR (400 MHz) spectrum of **2^{m-xyI}** in cyclohexane-*d*₁₂ (*residual hexane)

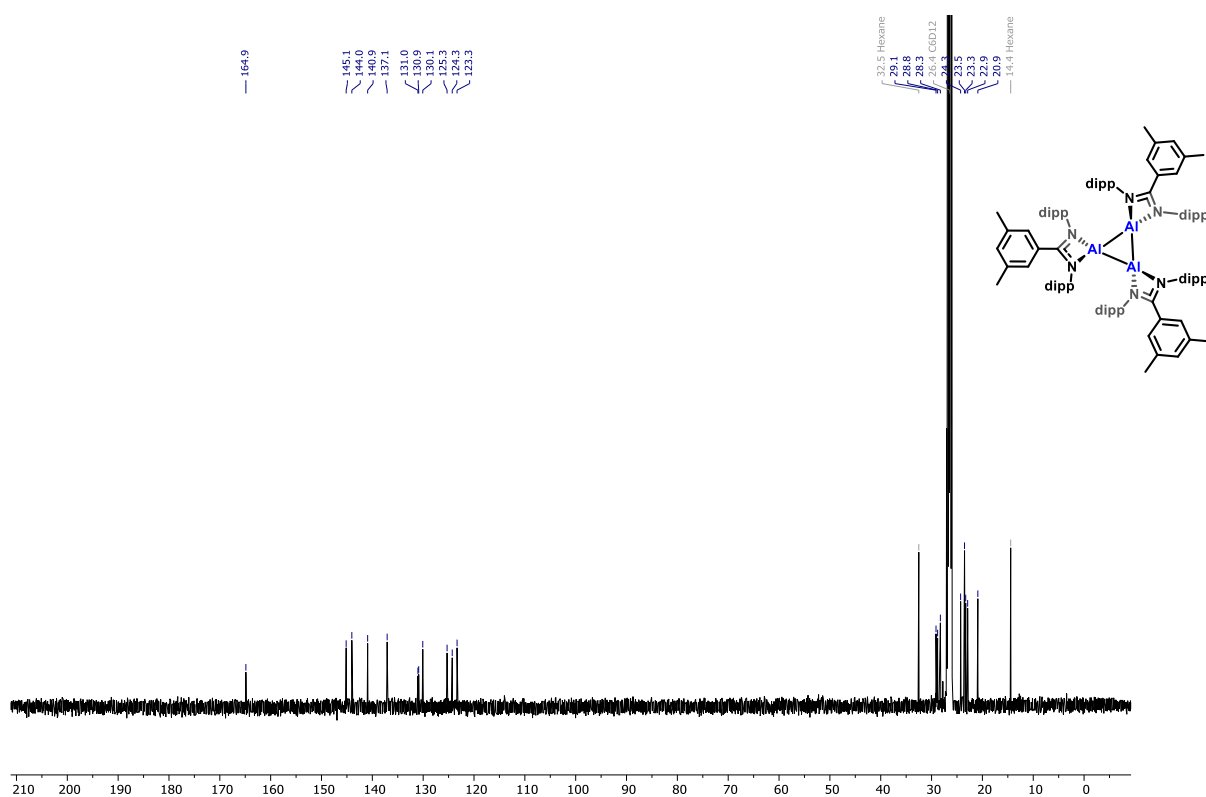


Figure S 63: ¹³C{¹H} NMR (101 MHz) spectrum of **2^{m-xyI}** in cyclohexane-*d*₁₂

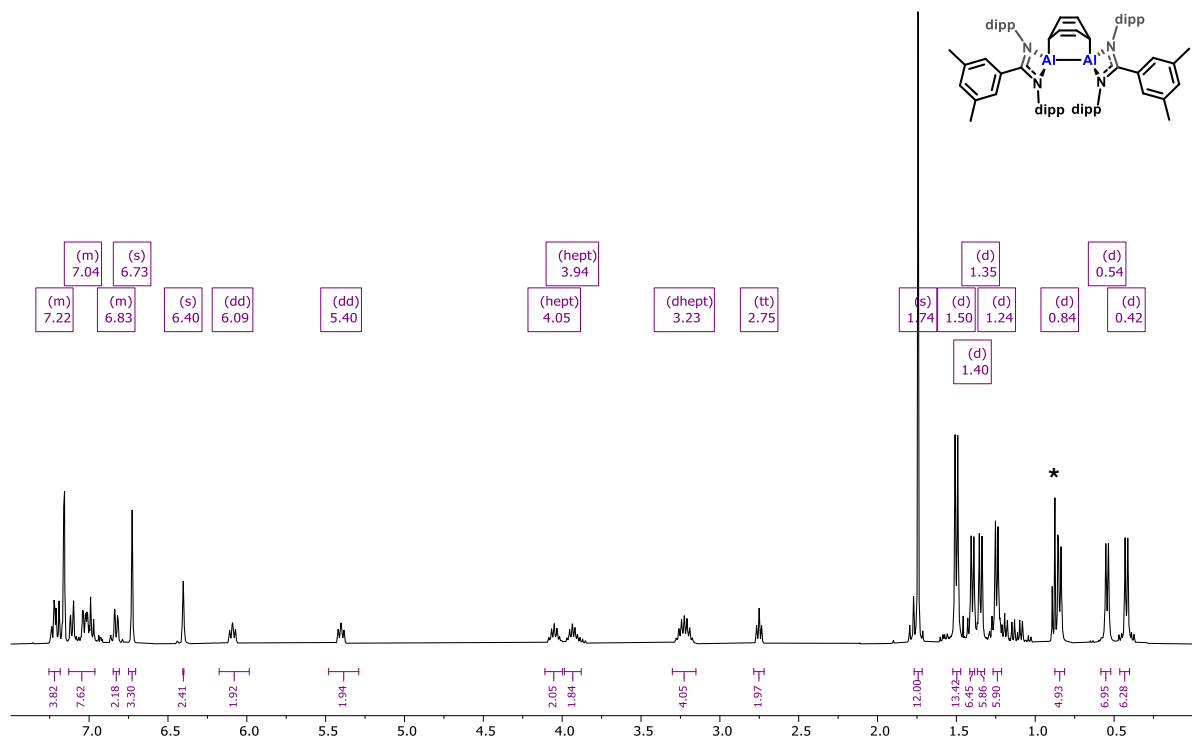


Figure S 64: ^1H NMR (400 MHz) spectrum of **3^{m-xyI}** in benzene- d_6 (* residual hexane)

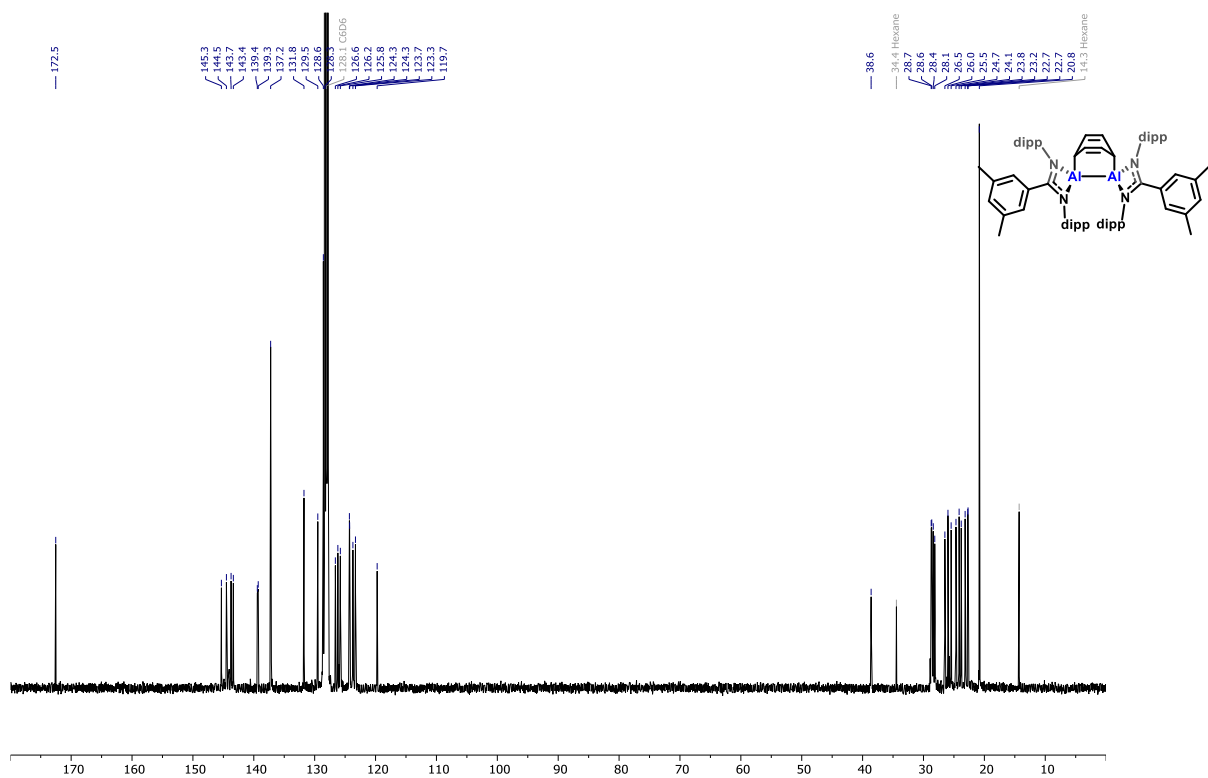


Figure S 65: $^{13}\text{C}\{^1\text{H}\}$ NMR (101 MHz) spectrum of **3^{m-xyI}** in benzene- d_6

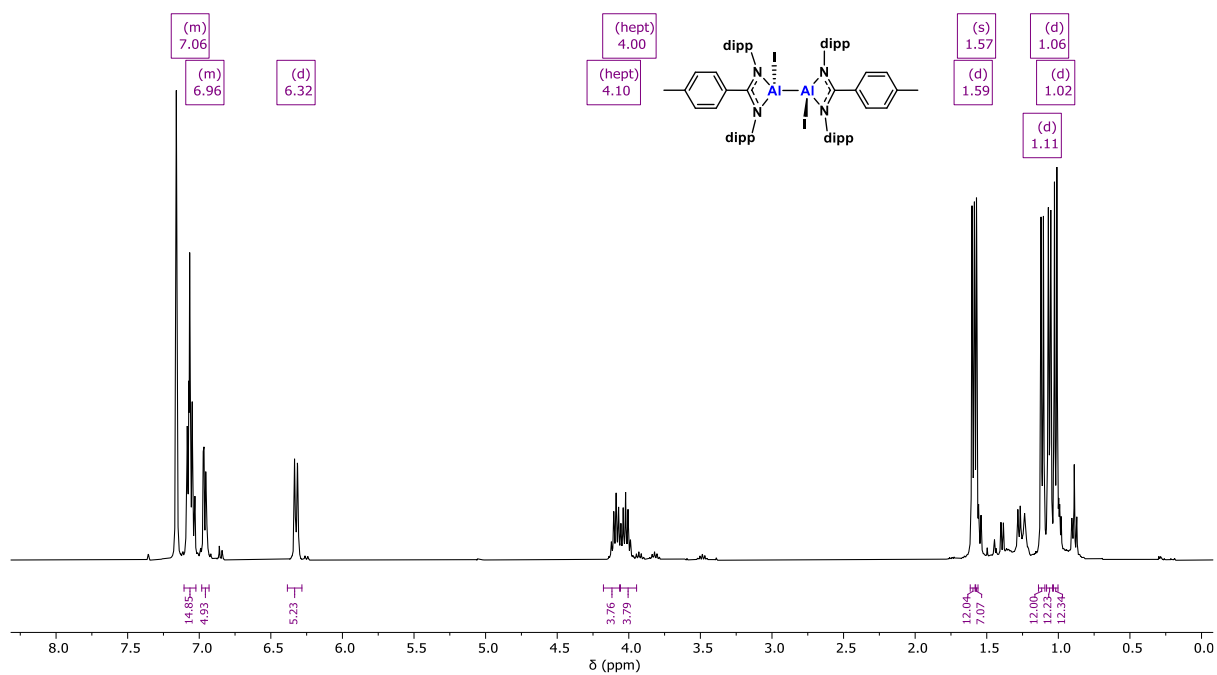


Figure S 66: ¹H NMR (400 MHz) spectrum of **5^{p-tol}** in benzene-*d*₆

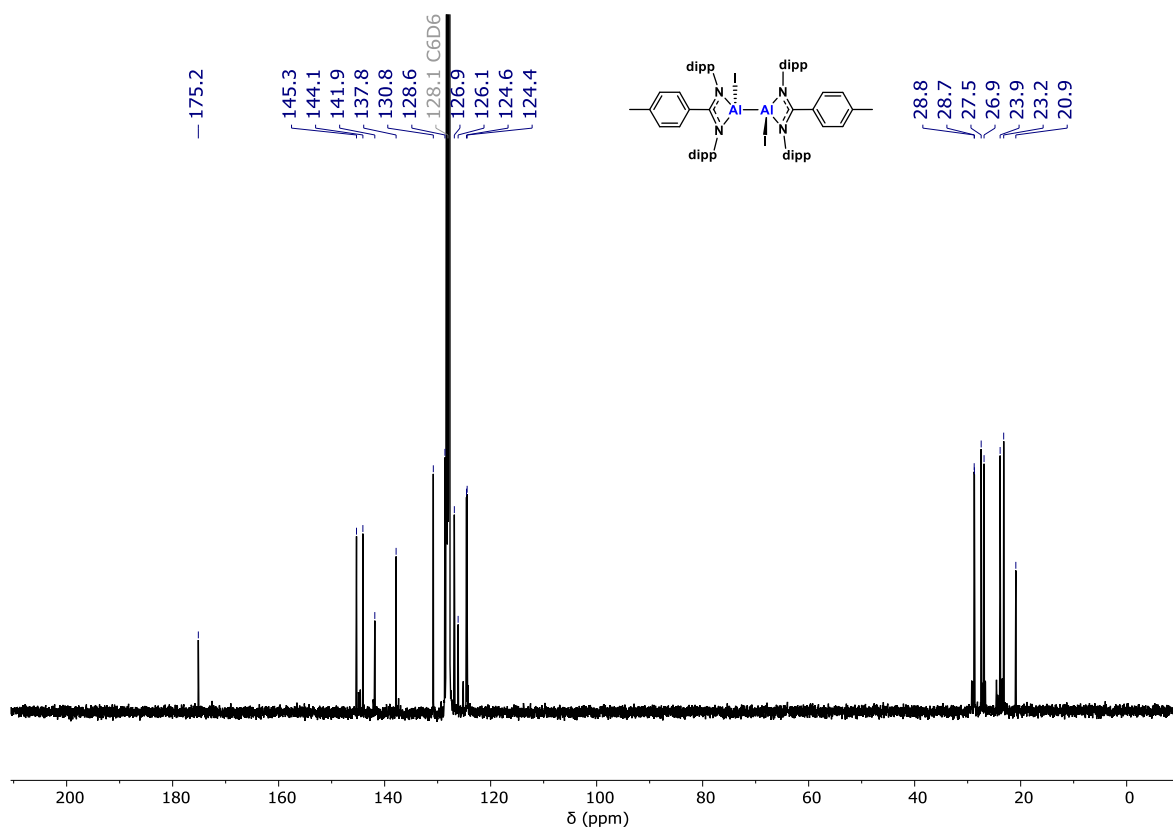


Figure S 67: ¹³C{¹H} NMR (101 MHz) spectrum of **5^{p-tol}** in benzene-*d*₆

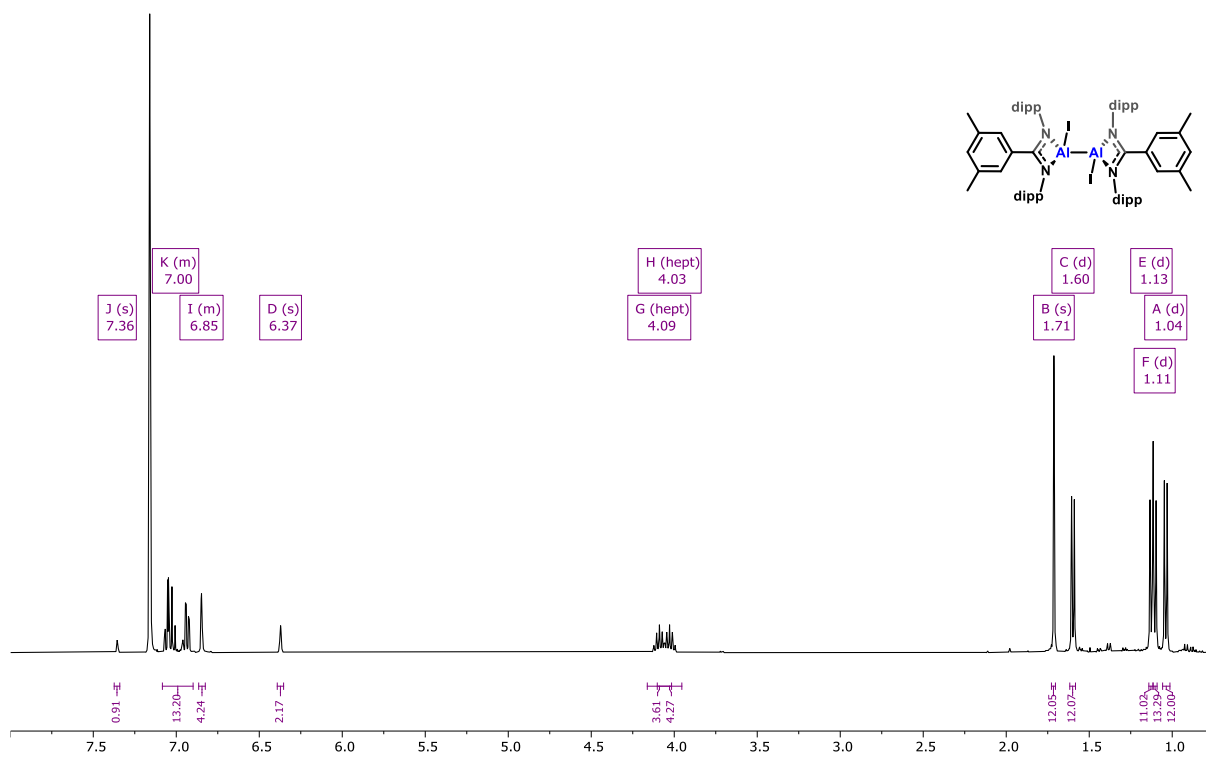


Figure S 68: ^1H NMR (400 MHz) spectrum of $5^{\text{m-xyI}}$ in benzene- d_6

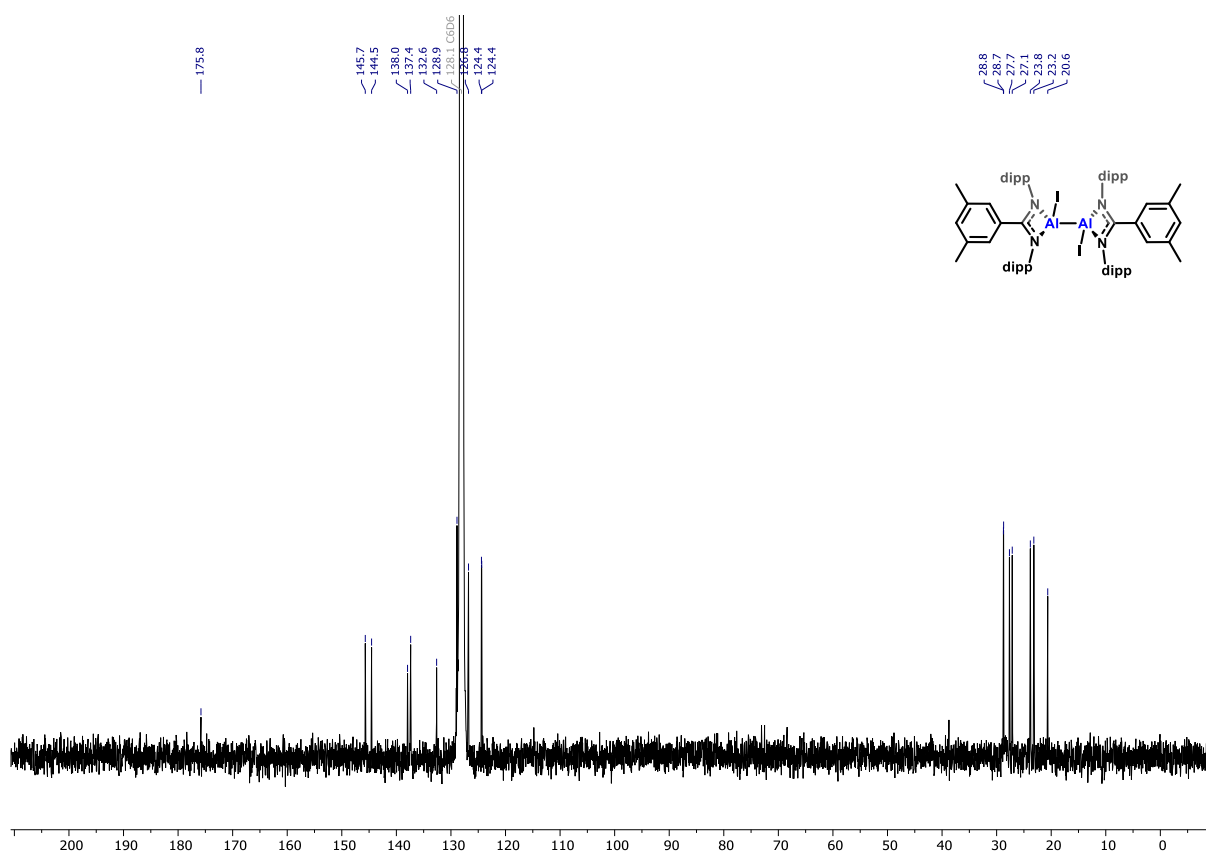


Figure S 69: $^{13}\text{C}\{^1\text{H}\}$ NMR (101 MHz) spectrum of $5^{\text{m-xyI}}$ in benzene- d_6

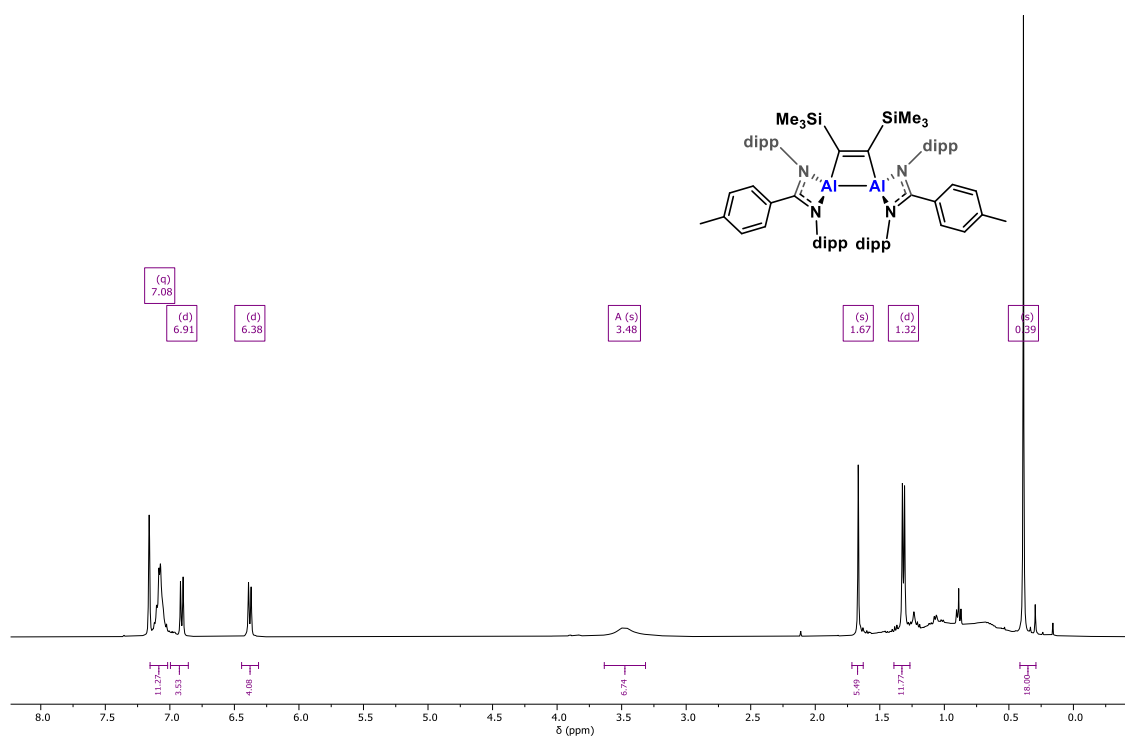


Figure S 70: ¹H NMR (400 MHz) spectrum of **6^{p-tol}** in benzene-*d*₆

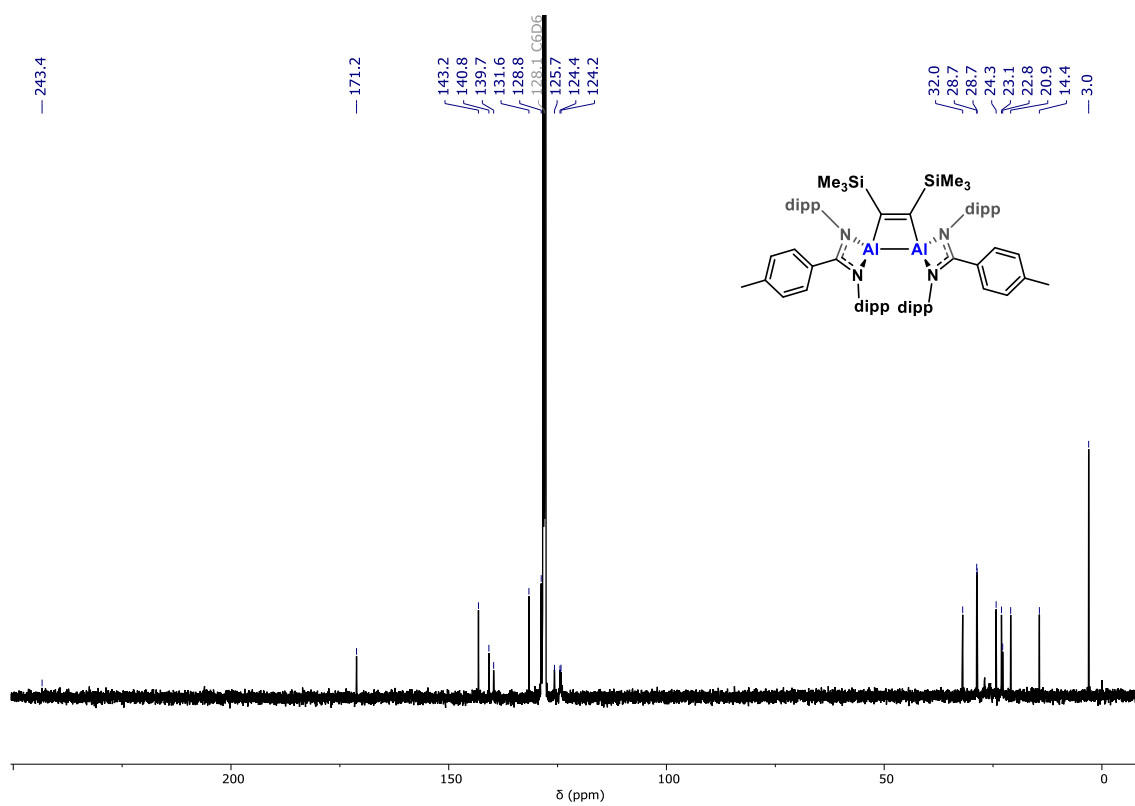


Figure S 71: ¹³C{¹H} NMR (101 MHz) spectrum of **6^{p-tol}** in benzene-*d*₆

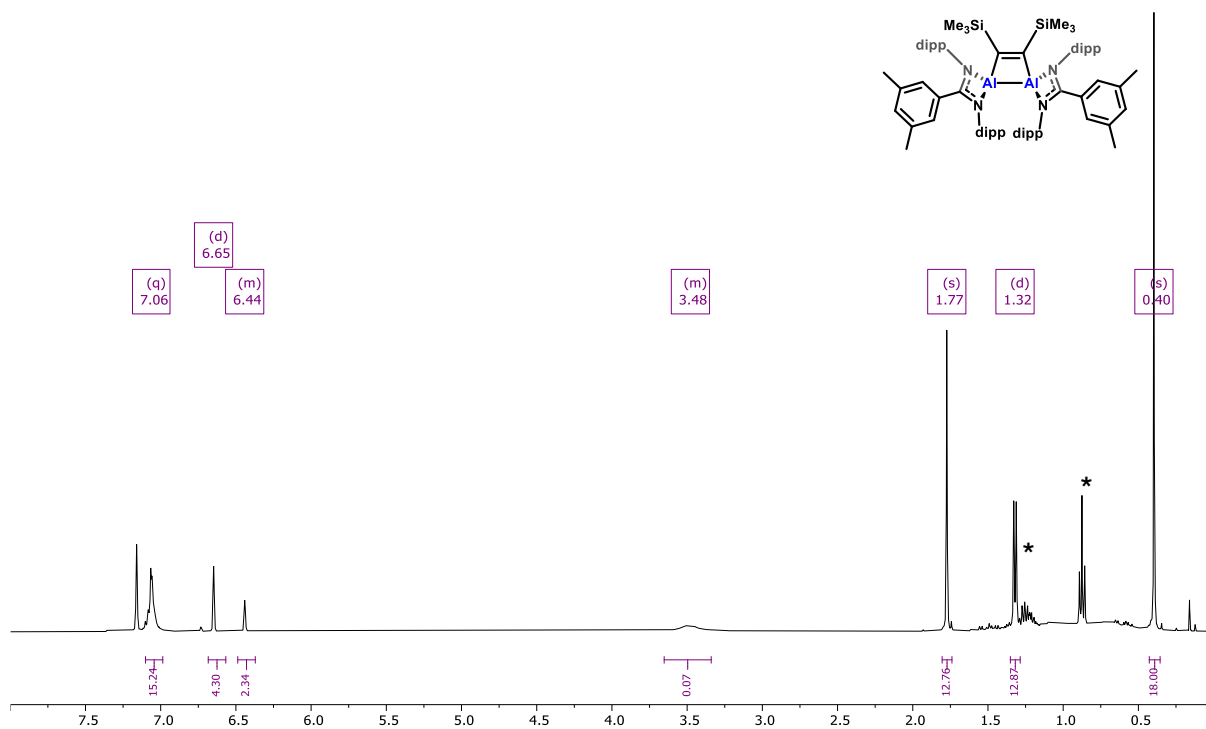


Figure S 72: ¹H NMR (400 MHz) spectrum (298 K) of **6^m-xyI** in benzene-d₆ (* residual pentane)

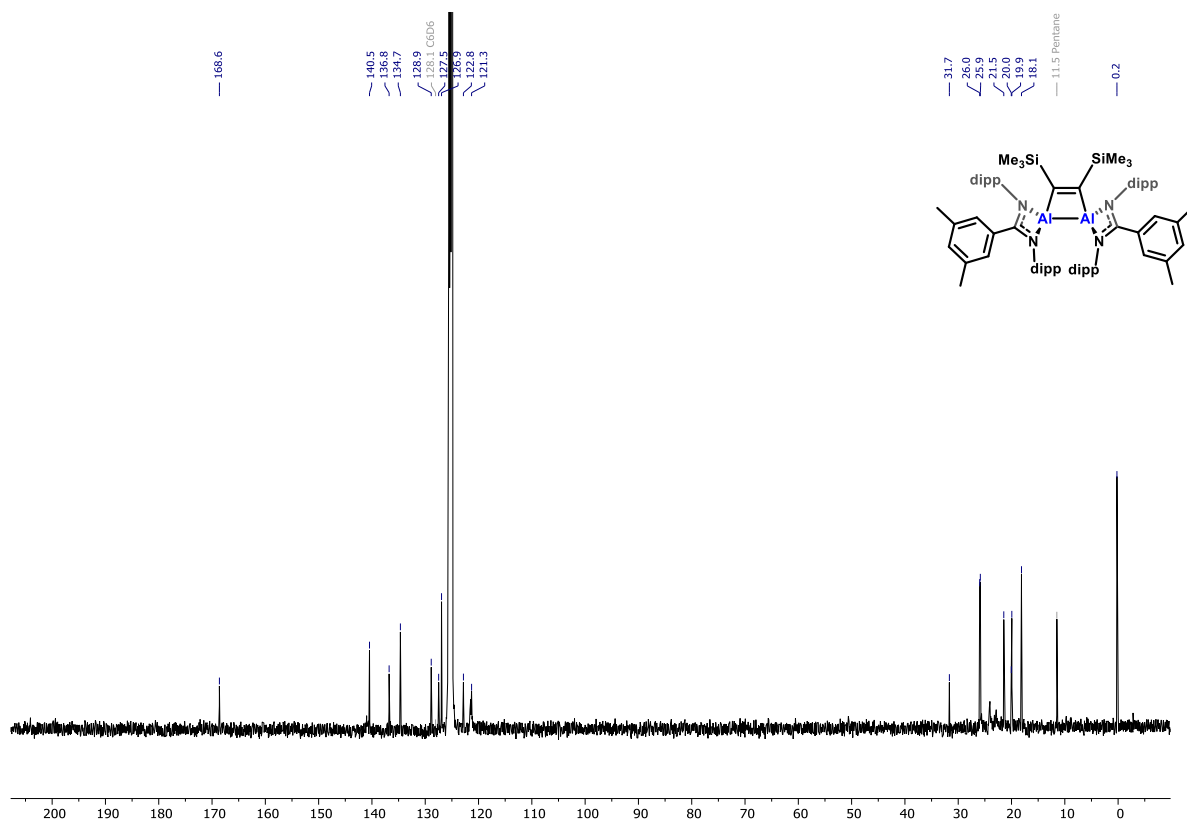


Figure S 73: ¹³C{¹H} NMR (101 MHz) spectrum (298 K) of **6^m-xyI** in benzene-d₆

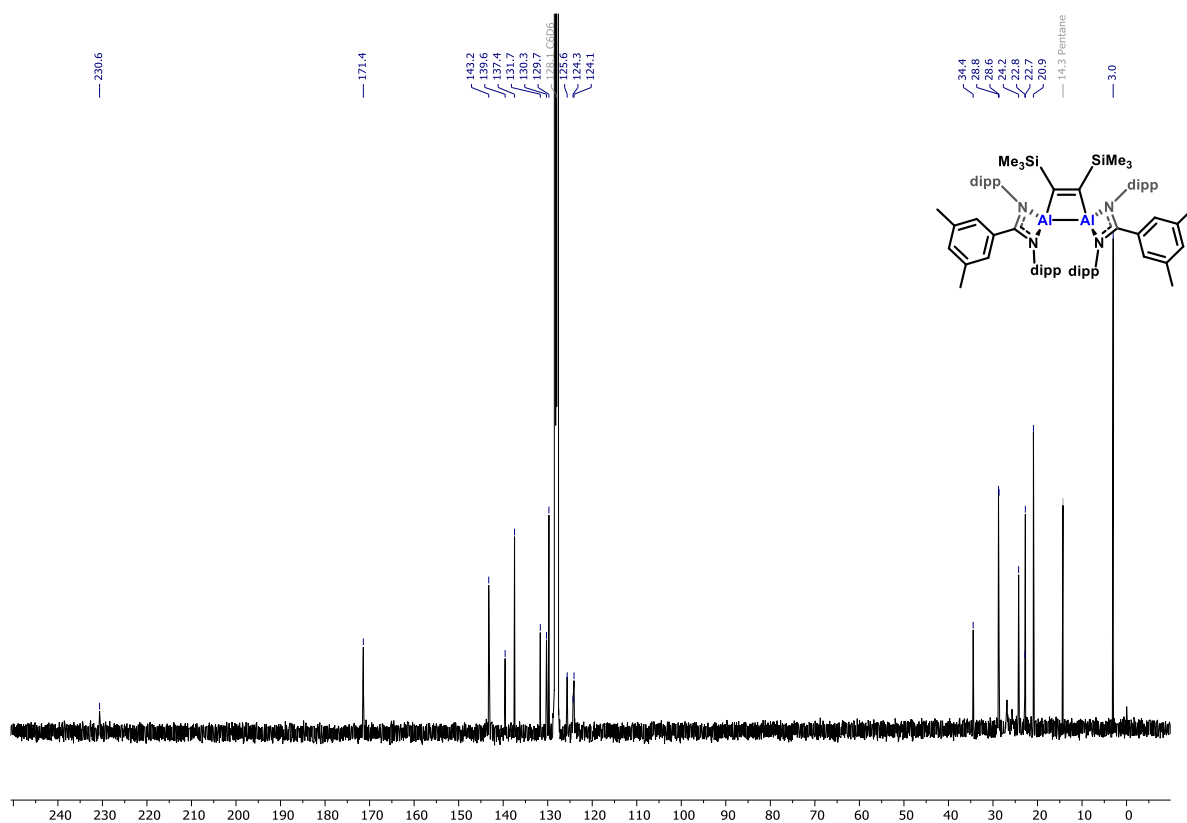


Figure S 74: wide $^{13}\text{C}\{^1\text{H}\}$ NMR (101 MHz) spectrum (298 K) of **6^{m-xyI}** in benzene- d_6

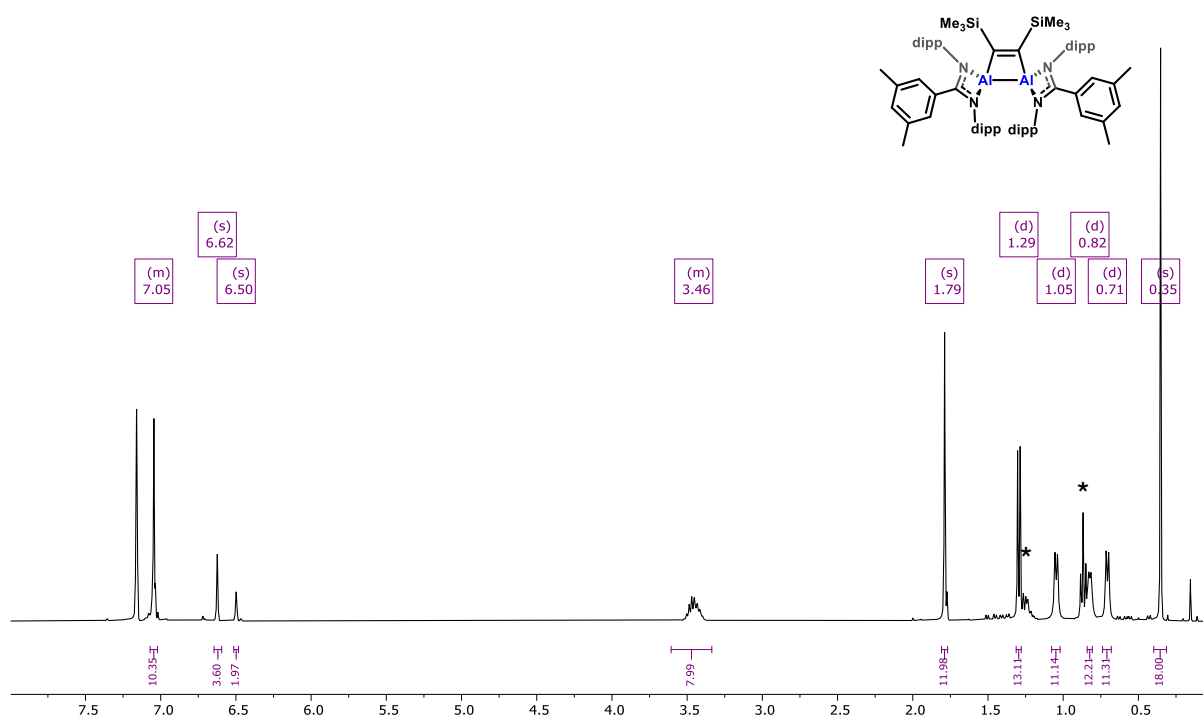


Figure S 75: ^1H NMR (400 MHz) spectrum (353 K) of **6^{m-xyI}** in benzene- d_6 (* residual pentane)

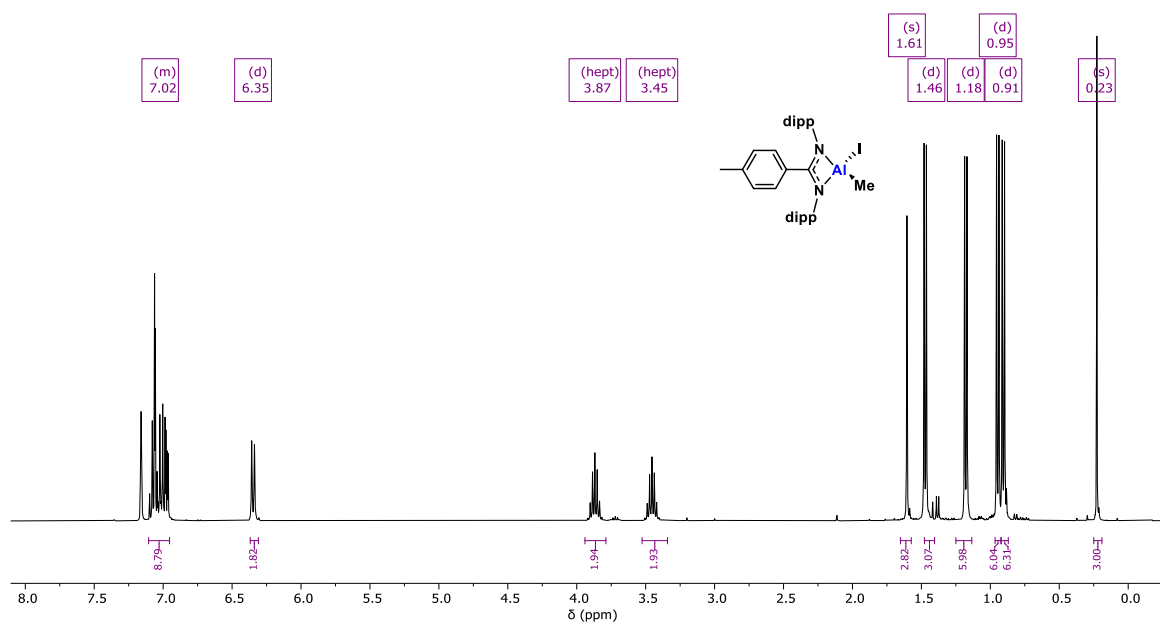


Figure S 76: ¹H NMR (400 MHz) spectrum of **7p-tol** in benzene-d₆

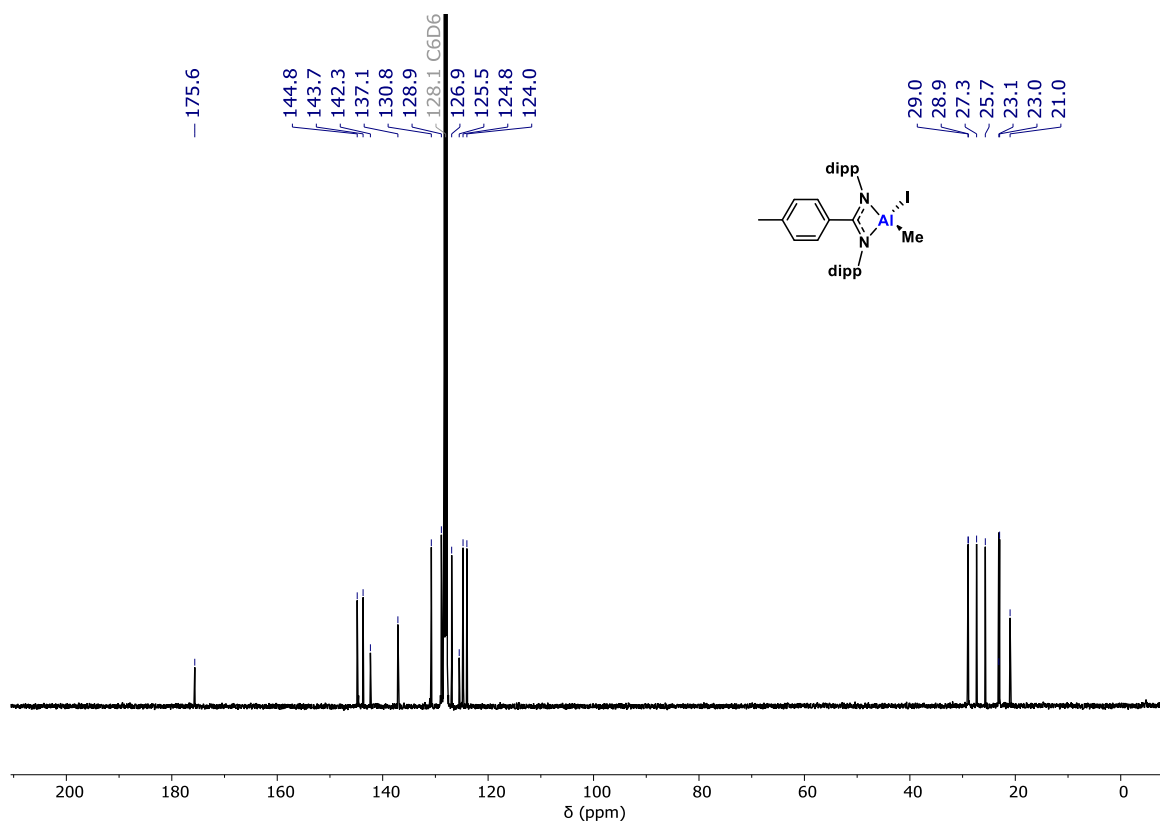


Figure S 77: ¹³C{¹H} NMR (101 MHz) spectrum of **7p-tol** in benzene-d₆

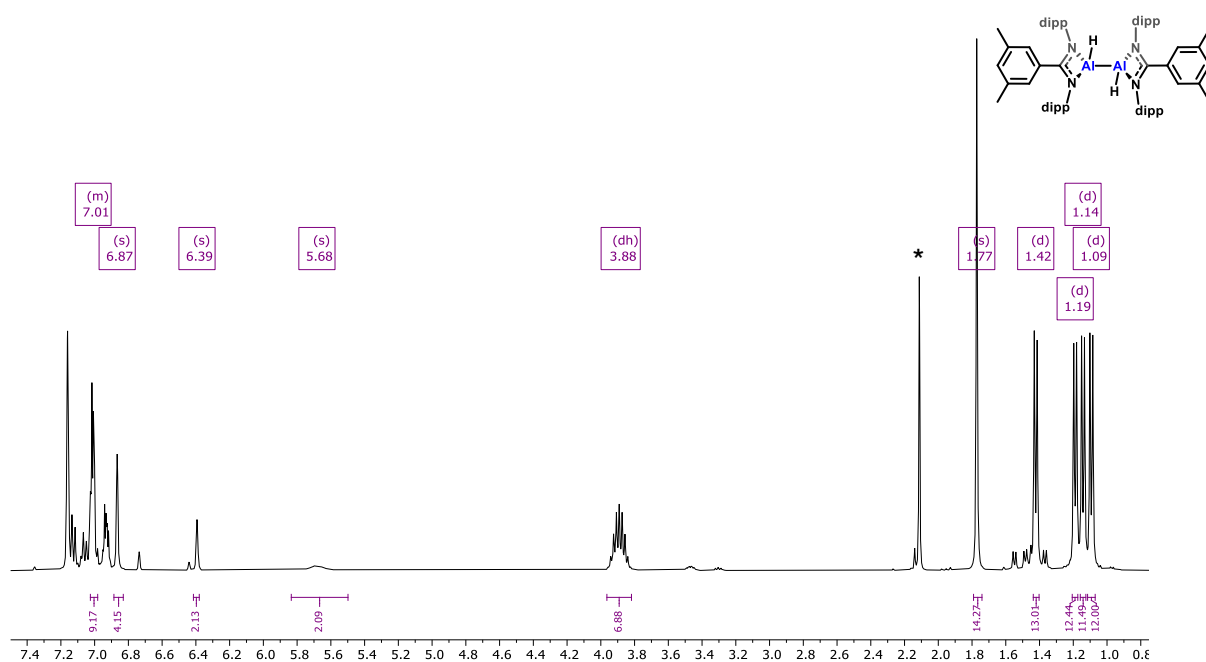


Figure S 78: ¹H NMR (400 MHz) spectrum of 8^{m-xyI} in benzene-d₆ (* residual toluene)

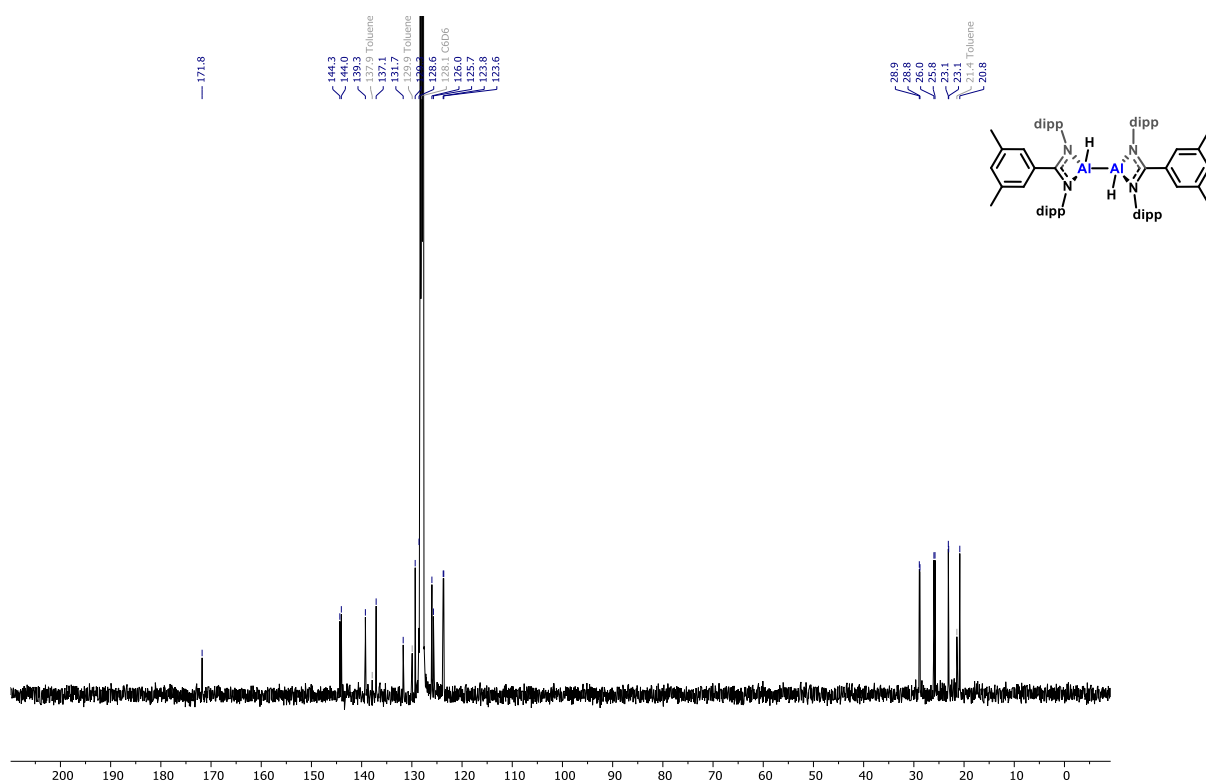


Figure S 79: ¹³C{¹H} NMR (101 MHz) spectrum of 8^{m-xyI} in benzene-d₆

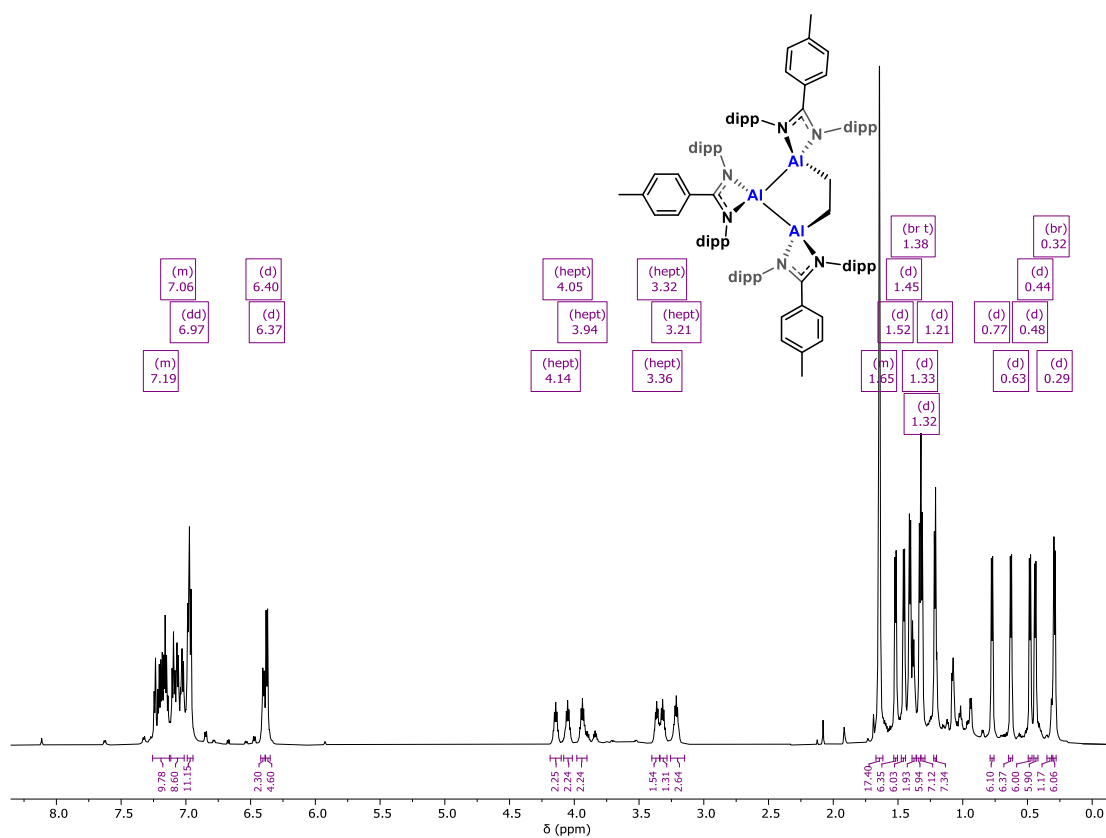


Figure S 80: ¹H NMR (700 MHz) spectrum of **9^{p-tol}** in benzene-*d*₆

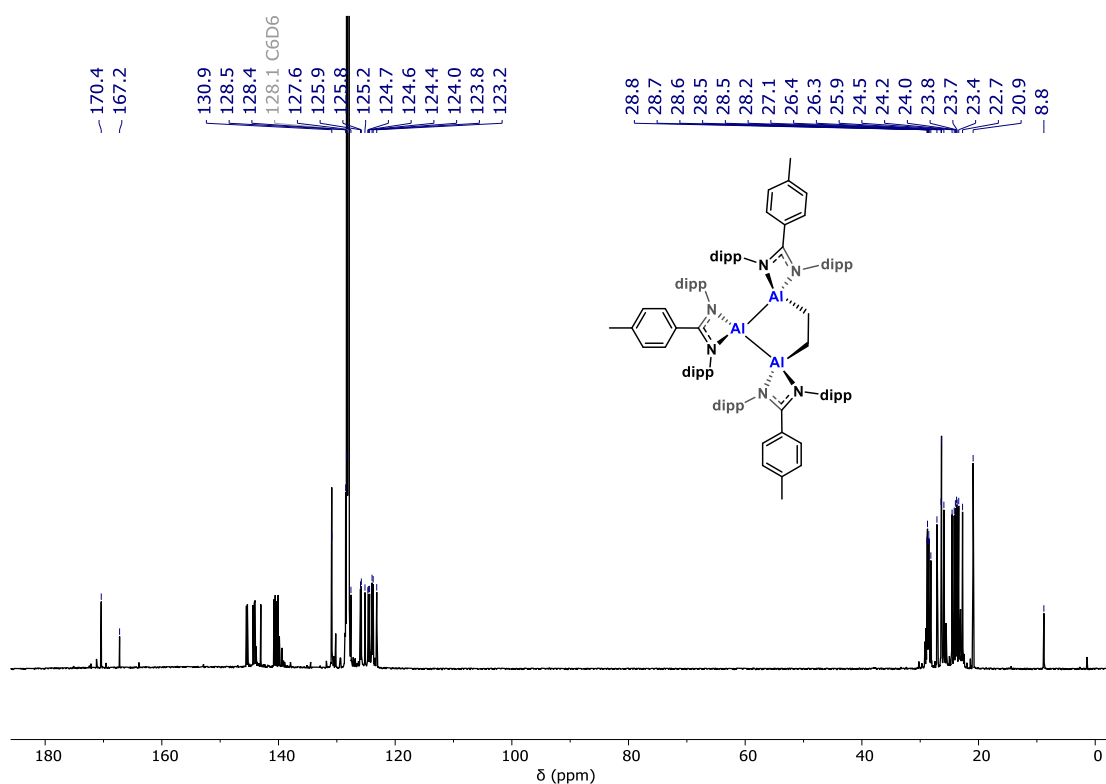


Figure S 81: ¹³C{¹H} NMR (176 MHz) spectrum **9^{p-tol}** in benzene-*d*₆

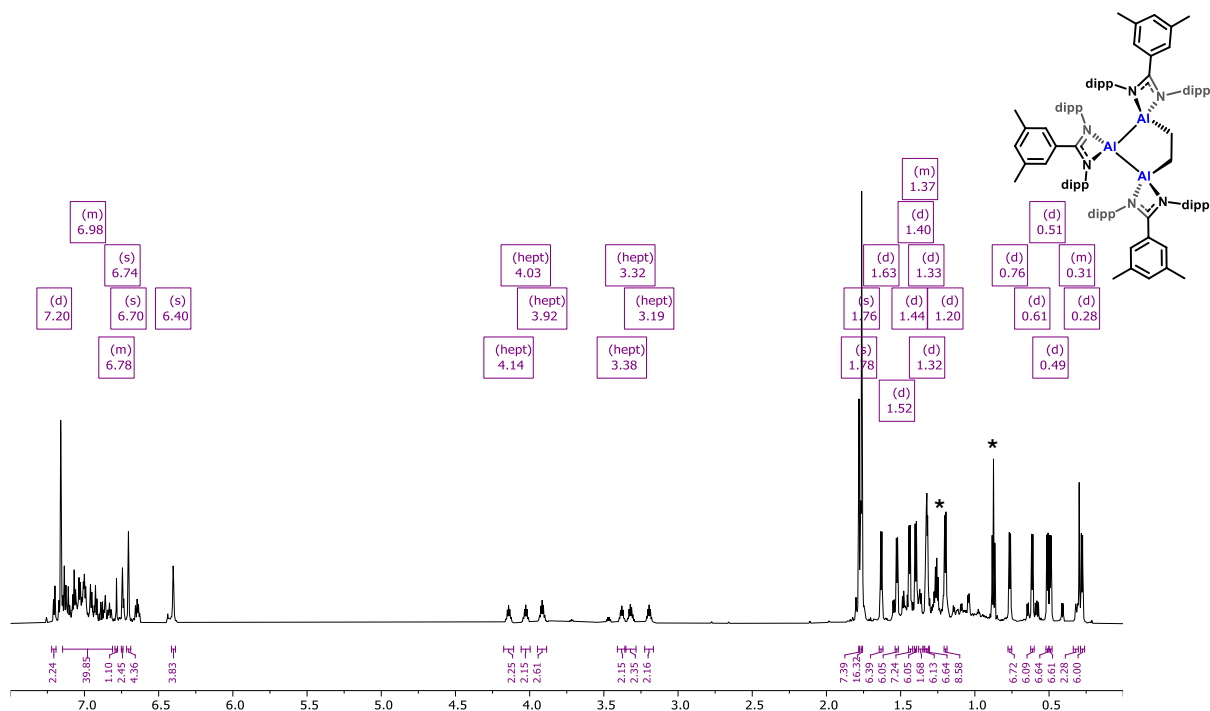


Figure S 82: ¹H NMR (800 MHz) spectrum of **9^{m-xyI}** in benzene-d₆ (* residual pentane)

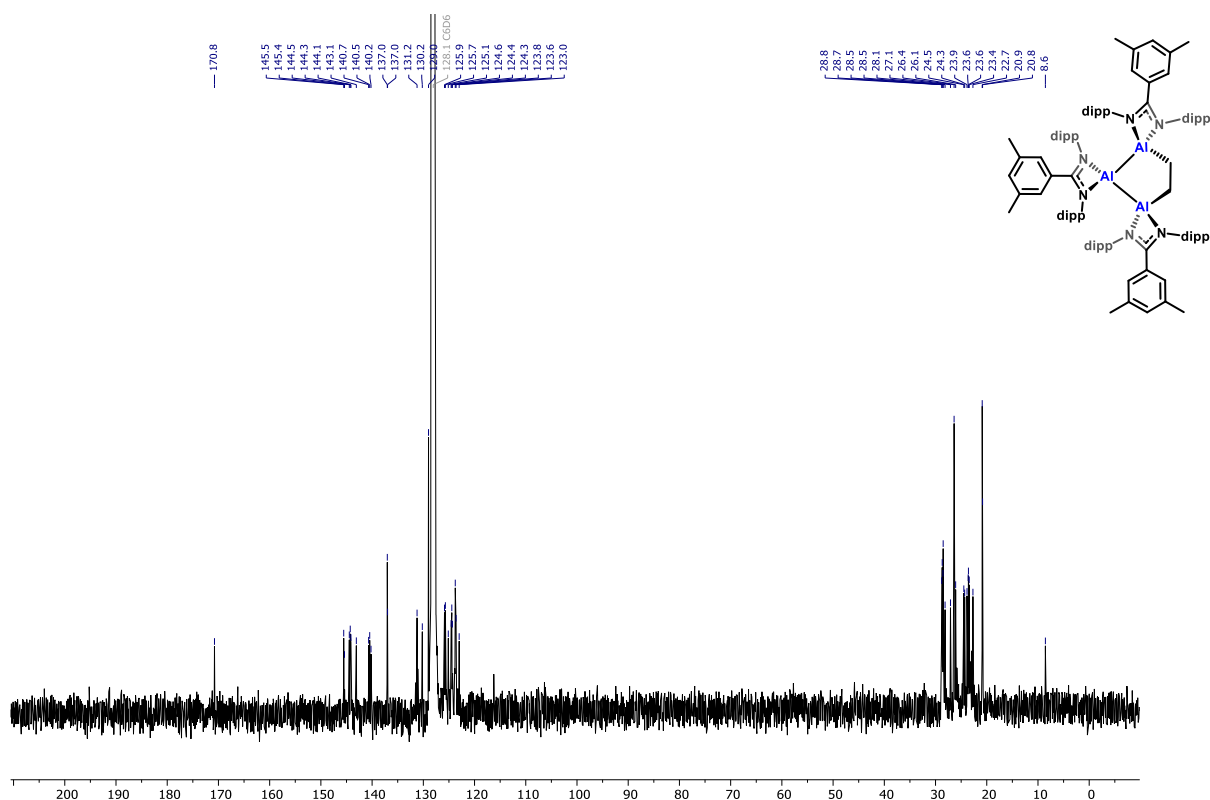


Figure S 83: ¹³C{¹H} (201 MHz) NMR spectrum of **9^{m-xyI}** in benzene-d₆

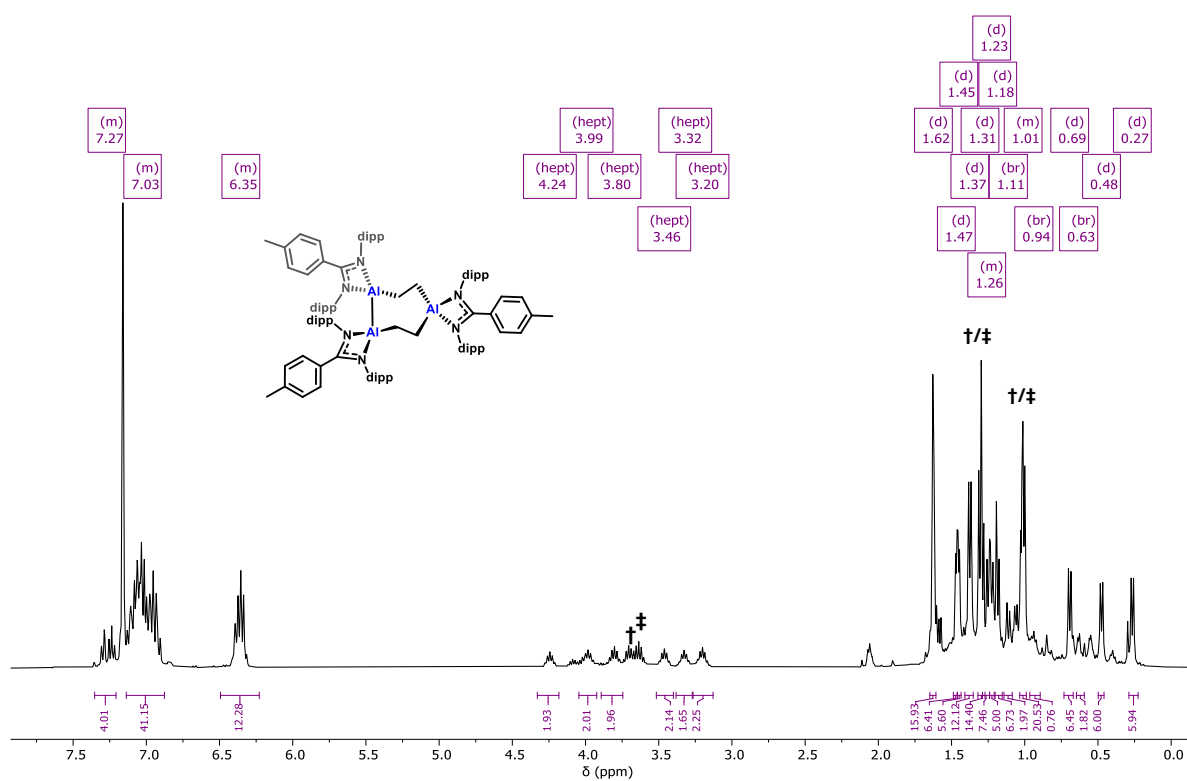


Figure S 84: ¹H NMR (400 MHz) spectrum of **10^{p-tol}** in benzene-*d*₆ (+ **11^{p-tol}**, ± **12^{p-tol}**)

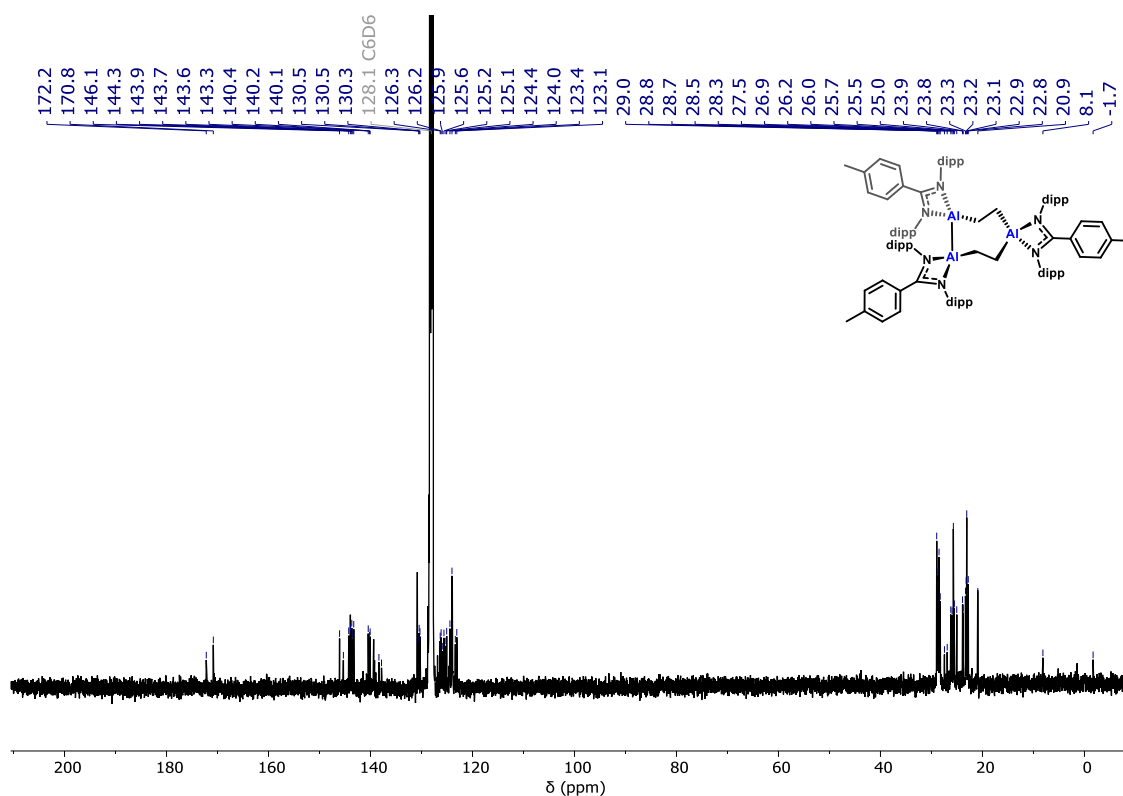


Figure S 85: ¹³C{¹H} NMR (101 MHz) spectrum of **10^{p-tol}** in benzene-*d*₆

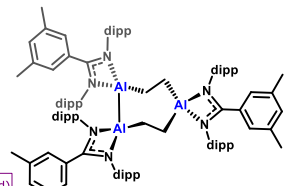


Figure S 87: $^{13}\text{C}\{^1\text{H}\}$ (201 MHz) NMR spectrum of **10^{m-xy}** in benzene- d_6

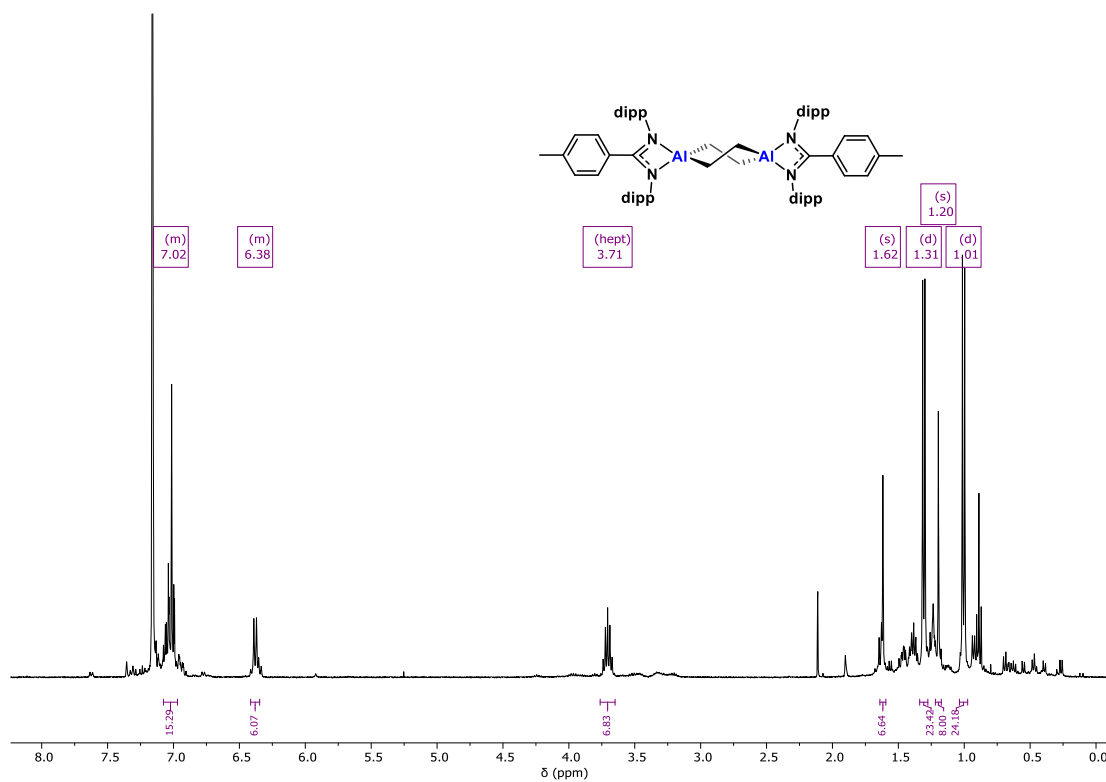


Figure S 88: ^1H NMR (400 MHz) spectrum of **11^{p-tol}** in benzene- d_6

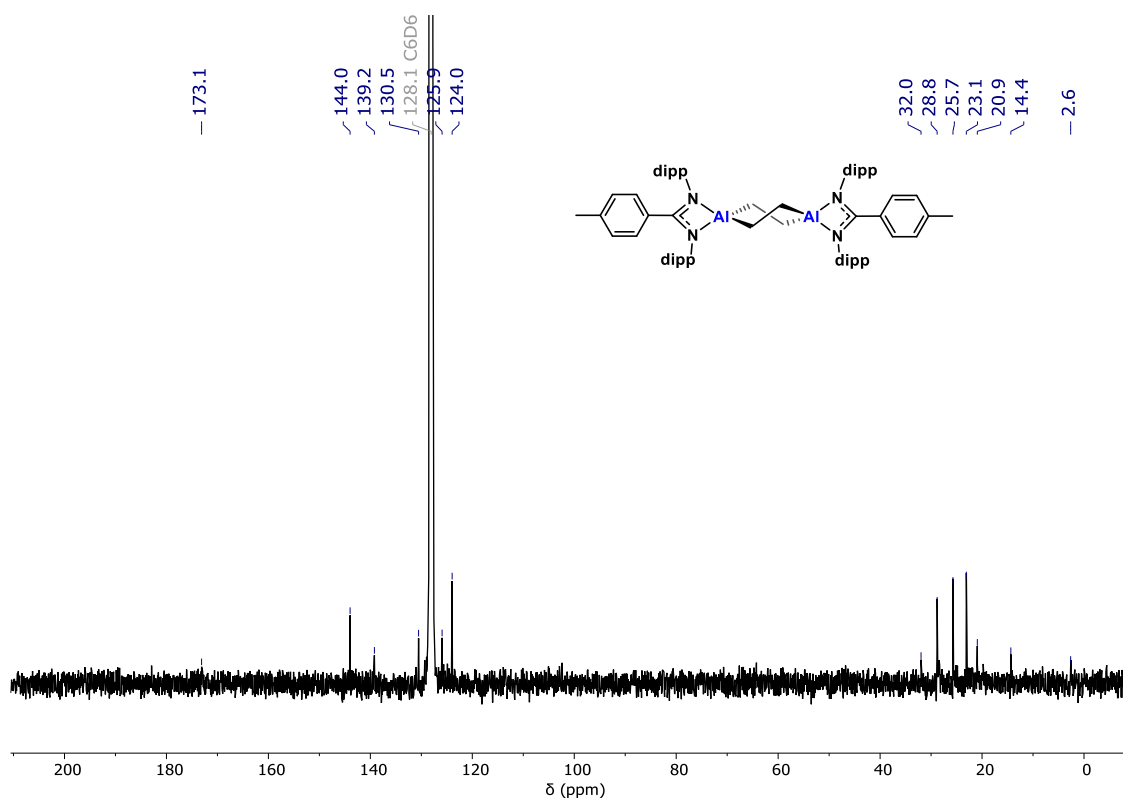


Figure S 89: $^{13}\text{C}\{^1\text{H}\}$ NMR (101 MHz) spectrum of **11^{p-tol}** in benzene- d_6

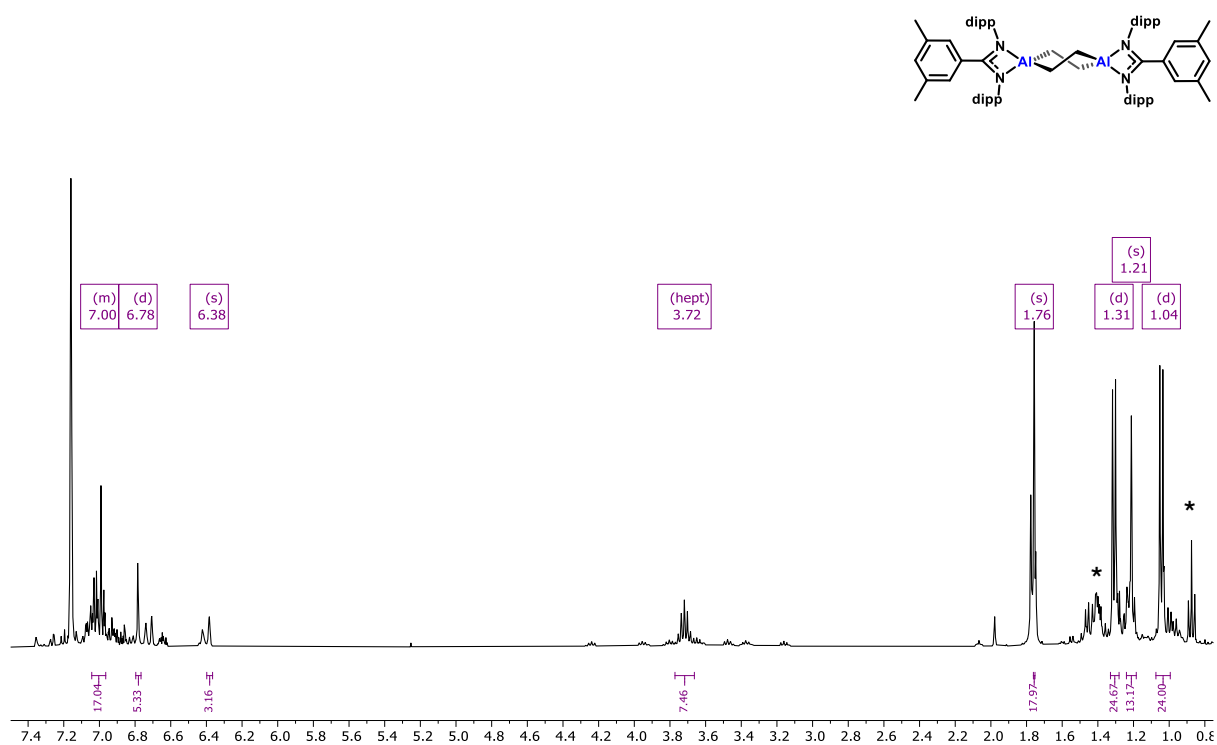


Figure S 90: ¹H NMR (400 MHz) spectrum of **11^{m-xyI}** in benzene-*d*₆ (* residual pentane, note substantial residual **10^{m-xyI}**)

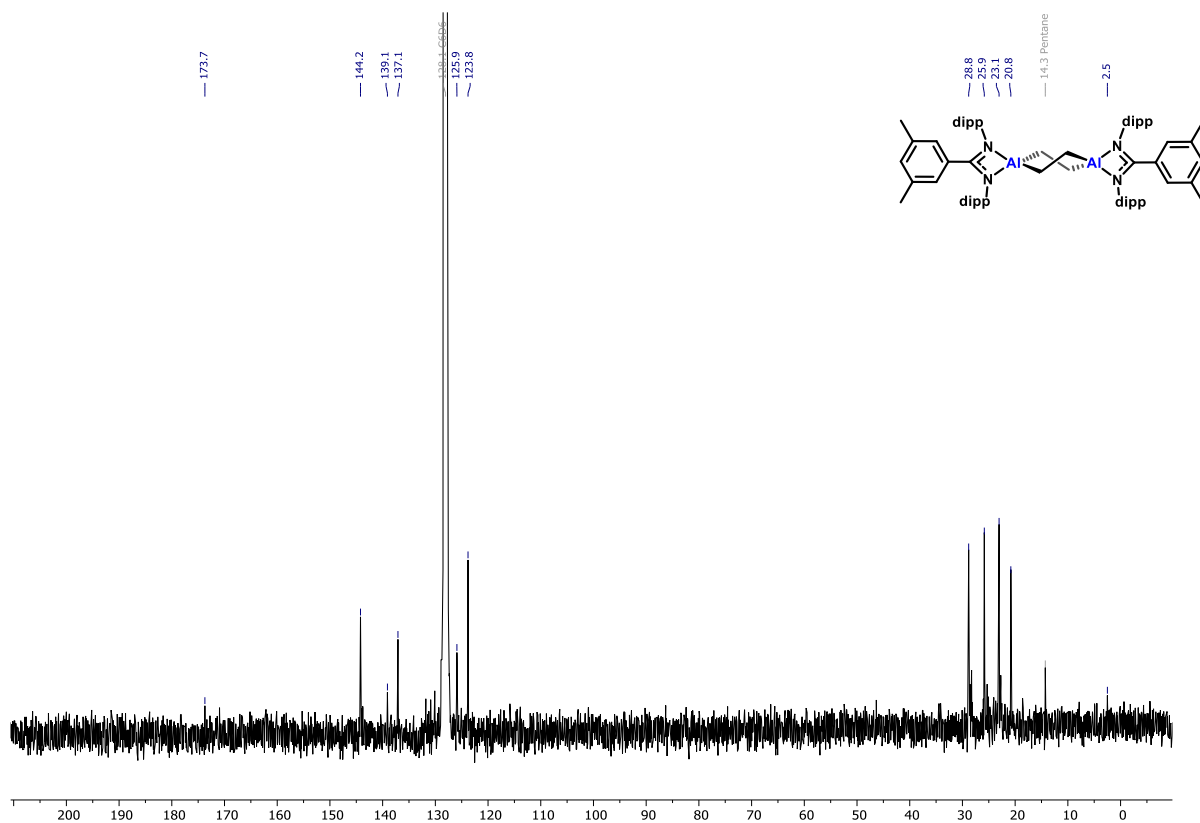


Figure S 91: ¹³C{¹H} NMR (101 MHz) spectrum of **11^{m-xyI}** in benzene-*d*₆

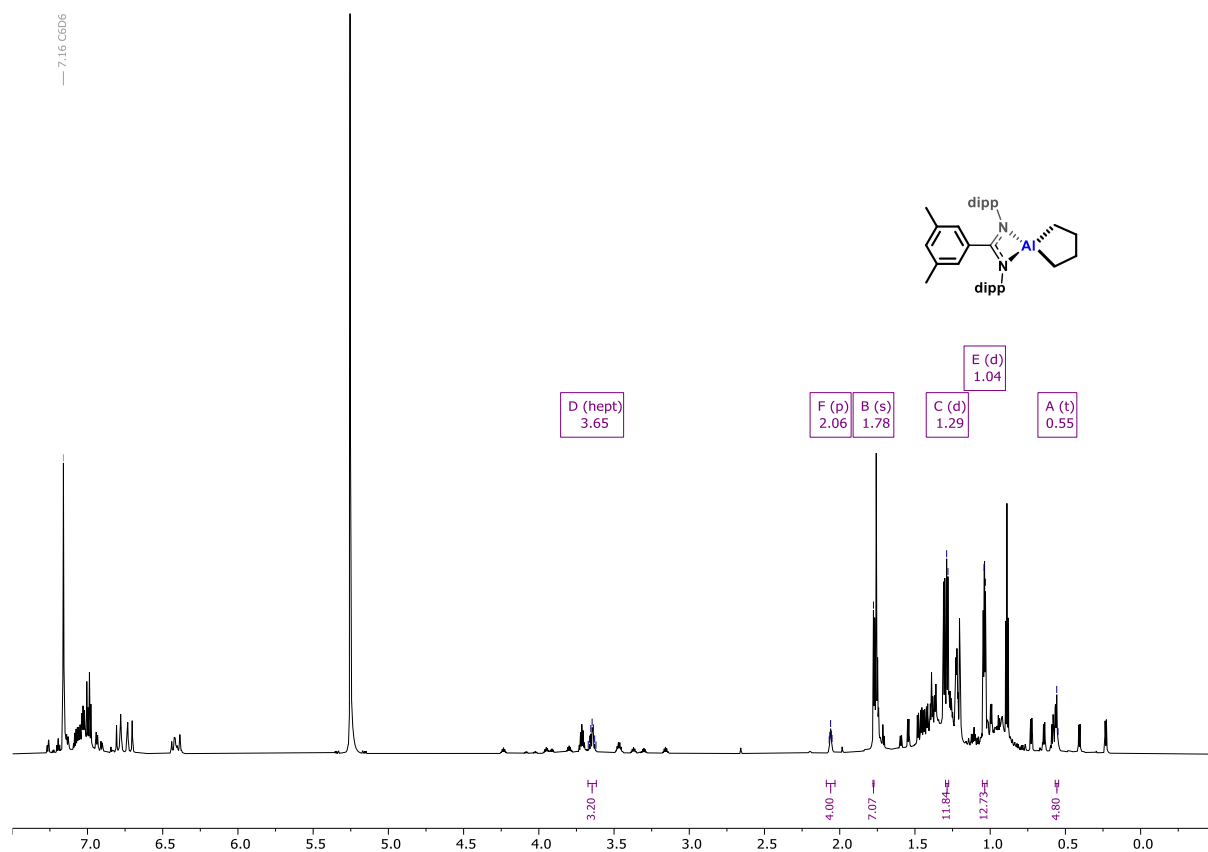


Figure S 92: ^1H NMR (800 MHz) spectrum of a mixture of **10**, **11** and **12^{m-xyI}** in benzene- d_6 , with the resonances for **12^{m-xyI}** picked out, with ethene gas present

7. References

1. Hobson, K., Carmalt, C. J. & Bakewell, C. Aluminum Amidinates: Insights into Alkyne Hydroboration. *Inorg. Chem.* **60**, 10958–10969 (2021).
2. Cui, C. *et al.* Synthesis and Structure of a Monomeric Aluminum(I) Compound [HC(CMeNAr)₂Al] (Ar=2,6-*i*Pr₂C₆H₃): A Stable Aluminum Analogue of a Carbene. *Angew. Chem. Int. Ed.* **39**, 4274–4276 (2000).
3. Bonyhady, S. J. *et al.* Synthesis of a stable adduct of dialane(4) (Al₂H₄) via hydrogenation of a magnesium(I) dimer. *Nat. Chem.* **2**, 865–869 (2010).
4. Bonyhady, S. J. *et al.* β -Diketiminato-Stabilized Magnesium(I) Dimers and Magnesium(II) Hydride Complexes: Synthesis, Characterization, Adduct Formation, and Reactivity Studies. *Chem. Eur. J.* **16**, 938–955 (2010).
5. Boeré, R. T., Cole, M. L. & Junk, P. C. The syntheses and structures of some main group complexes of the sterically hindered N,N'-bis(2,6-diisopropylphenyl)-4-toluidinate ligand. *New J. Chem.* **29**, 128–134 (2005).
6. Cherepanova, V. A., Gordeev, E. G. & Ananikov, V. P. Magnetic Stirring May Cause Irreproducible Results in Chemical Reactions. *JACS Au* (2025) doi:10.1021/jacsau.5c00412.
7. Bakewell, C., Hobson, K. & Carmalt, C. J. Exploring Equilibria between Aluminium(I) and Aluminium(III): The Formation of Dihydroalanes, Masked Dialumenes and Aluminium(I) Species. *Angew. Chem. Int. Ed.* **61**, e202205901 (2022).
8. Squire, I., Tritto, M., Morell, J. & Bakewell, C. Probing the reactivity of a transient Al(I) species with substituted arenes. *Chem. Commun.* **60**, 12908–12911 (2024).
9. Rigaku Oxford Diffraction, (2025), CrysAlisPro Software system, version 171.44.85, Rigaku Corporation, Wroclaw, Poland.
10. Sheldrick, G. M. SHELXT – Integrated space-group and crystal-structure determination. *Acta Crystallogr. A* **71**, 3–8 (2015).
11. Sheldrick, G. M. Crystal structure refinement with SHELXL. *Acta Crystallogr. C* **71**, 3–8 (2015).
12. Dolomanov, O. V., Bourhis, L. J., Gildea, R. J., Howard, J. A. K. & Puschmann, H. OLEX2: a complete structure solution, refinement and analysis program. *J. Appl. Cryst.* **42**, 339–341 (2009).
13. King's College London e-Research team. King's Computational Research, Engineering and Technology Environment (CREATE). (2022) doi:10.18742/RNVF-M076.
14. Gaussian 16, Revision C.01, Frisch, M. J.; Trucks, G. W.; Schlegel, H. B.; Scuseria, G. E.; Robb, M. A.; Cheeseman, J. R.; Scalmani, G.; Barone, V.; Petersson, G. A.; Nakatsuji, H.; Li, X.; Caricato, M.; Marenich, A. V.; Bloino, J.; Janesko, B. G.; Gomperts, R.; Mennucci, B.; Hratchian, H. P.; Ortiz, J. V.; Izmaylov, A. F.; Sonnenberg, J. L.; Williams-Young, D.; Ding, F.; Lipparini, F.; Egidi, F.; Goings, J.; Peng, B.; Petrone, A.; Henderson, T.; Ranasinghe, D.; Zakrzewski, V. G.; Gao, J.; Rega, N.; Zheng, G.; Liang, W.; Hada, M.; Ehara, M.; Toyota, K.; Fukuda, R.; Hasegawa, J.; Ishida, M.; Nakajima, T.; Honda, Y.; Kitao, O.; Nakai, H.; Vreven, T.; Throssell, K.; Montgomery, J. A., Jr.; Peralta, J. E.; Ogliaro, F.; Bearpark, M. J.; Heyd, J. J.; Brothers, E. N.; Kudin, K. N.; Staroverov, V. N.; Keith, T. A.; Kobayashi, R.; Normand, J.; Raghavachari, K.; Rendell, A. P.; Burant, J. C.; Iyengar, S. S.; Tomasi, J.; Cossi, M.; Millam, J. M.; Klene, M.; Adamo, C.; Cammi, R.; Ochterski, J. W.; Martin, R. L.; Morokuma, K.; Farkas, O.; Foresman, J. B.; Fox, D. J. Gaussian, Inc., Wallingford CT, 2016.
15. Marenich, A. V., Cramer, C. J. & Truhlar, D. G. Universal Solvation Model Based on Solute Electron Density and on a Continuum Model of the Solvent Defined by the Bulk Dielectric Constant and Atomic Surface Tensions. *J. Phys. Chem. B* **113**, 6378–6396 (2009).

16. F. Weinhold, E. D. G., J. K. Badenhoop, A. E. Reed, J. E. Carpenter, J. A. Bohmann, C. M. Morales, P. Karafiloglou, C. R. Landis. NBO. Theoretical Chemistry Institute, University of Wisconsin, Madison (2018).
17. AIMAll (Version 19.10.12), Todd A. Keith, TK Gristmill Software, Overland Park KS, USA, 2019 (aim.tkgristmill.com).
18. Lu, T. & Chen, F. Multiwfn: A multifunctional wavefunction analyzer. *J. Comput. Chem.* **33**, 580–592 (2012).
19. Lu, T. A comprehensive electron wavefunction analysis toolbox for chemists, Multiwfn. *J. Chem. Phys.* **161**, 082503 (2024).
20. Chemcraft - graphical software for visualization of quantum chemistry computations. Version 1.8, build 682. <https://www.chemcraftprog.com>.
21. Pettersen, E. F. *et al.* UCSF Chimera--a visualization system for exploratory research and analysis. *J. Comput. Chem.* **25**, 1605–1612 (2004).